Marine Physical Laboratory

AD-A245 562

(2)

Trip Report - June 1989 Swallow Float Deployment with RUM

G. L. D'Spain, W. S. Hodgkiss, and G. L. Edmonds

DTIC
ELECTE
FEB 0 3 1992
S D
D

MPL Technical Memorandum 424
December 1990

Approved for public release; distribution unlimited.

University of California, San Diego
Scripps Institution of Oceanography

92-02507

029

REPORT DOCUMENTATION PAGE

Form Approved OMB No. 0704-0188

Public reporting burden for this collection of information is estimated to average 1 hour per response, including the time for reviewing instructions, searching existing data sources, gathering and maintaining the data needed, and completing and reviewing the collection of information. Send comments regarding this burden estimate or any other aspect of this collection of information, including suggestions for reducing this burden, to Washington Headquarters Services, Directorate for Information Operations and Reports, 1215 Jefferson Davis Highway, Suite 1204, Arlington, VA 22202-4302, and to the Office of Management and Budget, Paperwork Reduction Project (0704-0188), Washington, DC 20503

1. Agency Use Only (Leave Blank).	2. Report Date. December 1990	3. Report Type and Dates Covered. technical memorandum

4. Title and Subtitle.

Trip Report - June 1989 Swallow Float Deployment with RUM

5. Funding Numbers.

N00014-88-K-2040

6. Author(s).

G. L. D'Spain, W. S. Hodgkiss and G. L. Edmonds

Project No.
Task No.

7. Performing Monitoring Agency Names(s) and Address(es).

University of California, San Diego
Marine Physical Laboratory
Scripps Institution of Oceanography
San Diego, California 92152

8. Performing Organization Report Number.

MPL-U-92/90

MPL TM-424

9. Sponsoring/Monitoring Agency Name(s) and Address(es).

Director of Research
Naval Research Laboratory
Washington, D.C. 0C320

10. Sponsoring/Monitoring Agency Report Number.

11. Supplementary Notes.

12a. Distribution/Availability Statement.

Approved for public release; distribution is unlimited.

12b. Distribution Code.

13. Abstract (Maximum 200 words).

The deployment of the three Marine Physical Laboratory's Swallow floats using the Remote Underwater Manipulator (RUM) was conducted in June, 1989 in the deep northeast Pacific Ocean at 32.4 N, 120.7 W. Representative data collected by the two properly-functioning Swallow floats, one with an external, triaxial geophone package resting on the ocean bottom and the other equippd with an infrasonic hydrophone and bottom-tethered by a 0.5-meter line, are presented in this report.

14. Subject Terms.

Swallow float, ambient noise, particle velocity , data acquisition system

15. Number of Pages. 80

16. Price Code.

17. Security Classification of Report.	18. Security Classification of This Page.	19. Security Classification of Abstract..	20. Limitation of Abstract.
Unclassified	Unclassified	Unclassified	None

Trip Report - June 1989 Swallow Float Deployment with RUM

G. L. D'Spain, W. S. Hodgkiss, and G. L. Edmonds

Marine Physical Laboratory
Scripps Institution of Oceanography
San Diego, CA 92152

ABSTRACT

The deployment of three of the Marine Physical Laboratory's Swallow floats using the Remote Underwater Manipulator (RUM) was conducted in June, 1989 in the deep northeast Pacific Ocean at 32.4° N, 120.7° W. Representative data collected by the two properly-functioning Swallow floats, one with an external, triaxial geophone package resting on the ocean bottom and the other equipped with an infrasonic hydrophone and bottom-tethered by a 0.5-meter line, are presented in this report.

Introduction

An experiment designed to compare the ambient sound field levels just above, on, and just below the ocean-sediment interface was conducted by the Marine Physical Laboratory in June, 1989. To make these measurements, an attempt was made to deploy four modified Swallow floats on the ocean bottom using the Remote Underwater Manipulator (RUM). Two of the floats were successfully deployed on 3-4 June, 1989, and recorded full data tapes. The experimental site was located at 32° 23′ N, 120° 44′ W in 3800-meter deep water. A summary of the Swallow float data collected in the experiment are presented herein.

The Swallow floats are designed to be neutrally buoyant, freely drifting, very low frequency (0.5-20 Hz) pressure and particle velocity sensors. They usually contain within a 0.432 m diameter glass shell three orthogonally-oriented geophones to measure infrasonic particle velocity, a magnetic compass, and the necessary hardware to record up to 19 hours of data. They are also usually equipped with an infrasonic ceramic hydrophone and an 8 kHz acoustic localization system.

However, four of the Swallow floats, with ID numbers 1, 2, 3, and 5, (serial numbers 1, 2, 12, and 13) were modified for this experiment. Instead of being freely drifting, each of the floats was connected in a different way to the ocean bottom. Floats 3 and 5 were equipped with only infrasonic hydrophones and were tethered to the bottom by 0.5-meter and 10-meter lines, respectively. Floats 1 and 2 were equipped with only the three-component geophone assemblies which were external to the floats' glass spheres. Their geophones were connected to the float recording hardware by cables composed of seven #18 stranded wires within a neoprene insulation. Each of the stranded wires was connected through one of the glass sphere's seven penetrators; two wires/penetrators were required for each of the three geophone components and one for ground. No penetrators were available these floats' 8 kHz hydrophones; therefore, no localization data could be collected by these floats. Float 1's geophone package was designed to be placed upon the ocean-sediment interface. It was enclosed in a pressure casing and mounted on a 1/4-inch by 10-inch (0.64 cm by 25.4 cm) polyvinylchloride (pvc) disk on which the orientation of the horizontal geophones was marked. This mounting guaranteed that the geophone package, which was placed on the sediment by RUM, would be upright. Float 2's geophone package was secured within a cage composed of metal tubing terminated with water nozzles. Using water flow driven through the metal tubing and nozzles by a pump on RUM, this geophone package could then be jetted into the sediment.

On the fifth attempt at deployment (the first four attempts were truncated due to minor RUM malfunctions), RUM successfully carried floats 1, 3, and 5 to the bottom and deployed them on the sediment. Float 1, with its external geophone package resting on the sediment, and float 3, equipped with an infrasonic hydrophone and tethered to the bottom by a 0.5-meter line, recorded full data tapes. The deployment configuration for these two floats is shown in Figure 1. Float 2, whose geophones were designed to be jetted into the sediment, was not deployed due to a malfunction of RUM's sonar and an inability to maneuver its cameras. Withoug its sonar and camera maneuverability, RUM would have much difficulty in relocating this float for recovery. The other floats could be recovered without help from RUM. Float 5, with the 10-meter tether, inexplicably stopped functioning after recording only two hours of data (from records 640 to 836). In addition to deploying the three floats during this trip to the bottom, RUM also successfully collected a sediment box core as part of another experiment.

A final modification was made to the geophone electronic data acquisition system on float 1; the fixed gain was decreased by 12 dB from 95 dB to 83 dB. The spectral levels reported in Section VII take this change in system gain into account. The fixed gain in the hydrophone electronic data acquisition systems on floats 3 and 5 remained at 80 dB, the same as in previous deployments.

After deploying the Swallow floats, RUM was recovered on board the R/V New Horizon and the ship then left the deployment area. During the ship's transit away from the area, and also during its return, seal bombs were detonated in order to provide broadband sources for the Swallow floats. Figure 2 is a plan view of the Swallow float deployment location, indicated by the triangle, and the seal bomb deployment locations, indicated by the exclamation marks. The following table lists the times and locations of the seal bomb detonations.

Accesion For
NTIS CRA&I
DTIC TAB
Unannounced
Justification
By
Distribution /
Availability Codes
Dist | Avail and/or Special
A-1

Seal Bomb Number	Swallow Float Record Number	Time on 4 June (local time)	Location (Loran-C)
1	1661	04:57:00	32° 22.69′ N, 120° 43.35′ W
2	1662	04:57:42	32° 22.69′ N, 120° 43.35′ W
3	1693	05:20:56	32° 20.90′ N, 120° 34.30′ W
4	1694	05:21:43	32° 20.90′ N, 120° 34.30′ W
5	1942	08:28:23	32° 20.40′ N, 120° 38.70′ W
6	1960	08:41:36	32° 19.90′ N, 120° 41.00′ W
7	1997	09:09:02	32° 21.00′ N, 120° 44.20′ W

An average sound speed profile for the deployment area, derived from historical National Oceanographic Data Center (NODC) temperature and salinity data [1] and an empirical equation relating sound speed to temperature and salinity [2], is shown in Figure 3. The NODC data were collected in the area, 31-34° N, 120-125° W.

Swallow Float Log Summary

Note: All times are in local Pacific Daylight Time. To obtain standard Greenwich Mean Time, add 7 hours.

3 June 1989

08:11	Synchronize floats for the fourth time. Standing by for RUM deployment in the next four hours.
12:30	Remove float 2 from RUM. This float, equipped with the buriable geophone package, will not be deployed since the sonar and the camera mobility on RUM are not functional, making it difficult for RUM to relocate the float for retrieval. However, RUM will attempt to bury float 2's geophone cage in the sediment.
15:25	RUM, with Swallow floats 1, 3, and 5, is put in the water.
19:03 (rec 869)	RUM touches down on ocean bottom.
21:00 (rec 1025)	RUM grips the geophone cage thrust bar and attempts to push it into the sediment. However, the cage slips out and falls on the bottom. Begin to take sediment box core.
21:30 (rec 1065)	RUM's VARIAC (variable AC) fails due to excessive voltage. Therefore, begin to retrieve RUM from the bottom.
21:50 (rec 1092)	RUM's VARIAC system has inexplicably recovered so that RUM's ascent from the bottom is halted.
21:57,(rec 1101)	RUM begins to descend back to the bottom.
22:23 (rec 1136)	RUM arrives on the ocean bottom. Begin to obtain box core.
23:15 (rec 1205)	Box core is tripped in the sediment.
23:29 (rec 1224)	Box core is now on board RUM.
23:36 (rec 1233)	Begin to deploy float 5.

4 June 1989

00:22 (rec 1294)	Float 5 is deployed. Begin to deploy float 3.
00:50 (rec 1332)	Float 3 is deployed. Begin to deploy float 1.
01:38 (rec 1396)	The connector end of float 1's geophone package, which is aligned with the + y geophone axis, is aligned with the front of RUM, whose heading is 192° true, and

deployed.

01:49 (rec 1410)	Store RUM's manipulator in preparation for retrieval.
01:56 (rec 1420)	RUM is moving forward along the bottom, away from the Swallow floats.
01:60 (rec 1425)	RUM is now ascending.
04:20 (rec 1612)	RUM is now on board the R/V New Horizon.
04:29 (rec 1624)	The ship position is 32° 23.42′ N, 120° 44.50′ W.
04:57 (rec 1661)	The first seal bomb is deployed at time 04:57:00 and location 32° 22.69′ N, 120° 43.35′ W.
04:58 (rec 1662)	The second seal bomb is deployed at time 04:57:42 and location 32° 22.69′ N, 120° 43.35′ W.
05:21 (rec 1693)	The third seal bomb is deployed at time 05:20:56 and location 32° 20.90′ N, 120° 34.30′ W.
05:22 (rec 1694)	The fourth seal bomb is deployed at time 05:21:43 and location 32° 20.90′ N, 120° 34.30′ W.
08:28 (rec 1942)	The fifth seal bomb is deployed at time 08:28:23 and location 32° 20.40′ N, 120° 38.70′ W.
08:36 (rec 1953)	The New Horizon is traveling at 10.25 knots. At this speed, the diesel shafts are rotating at 270 rpm. The ship has twin screws with 3 blades per screw. The reduction gear ratio is 3.9 to 1.
08:42 (rec 1960)	The sixth seal bomb is deployed at time 08:41:36 and location 32° 19.90′ N, 120° 41.00′ W.
09:09 (rec 1997)	The seventh seal bomb is deployed at time 09:09:02 and location 32° 21.00′ N, 120° 44.20′ W.
09:30 (rec 2025)	Float 1 is detected on the surface, about 9 hours earlier than expected.
09:45 (rec 2045)	Float 1 is recovered and its program is still running.
13:01	The New Horizon has been station-keeping about 100 meters south of floats 3 and 5 most of the morning. Repairs of RUM are being made. The station-keeping has been under program control for the last hour and a half. During 12 kHz station-keeping, it is not possible to transpond off the Swallow floats.
14:00	Launch RUM for tow tests.
21:40	Release float 3.
21:42	Release float 5.

5 June 1989

01:55	Recover float 5. An "HL" message appears on its LED display.
02:05	Recover float 3. Its program is still running. Prepare to return to port.

I. General Indication of Data Quality

The results of screening the float data tapes for the proper location of resynchronization characters and the proper sum of byte values in a group prior to a checksum are shown in Figure I.1. Both floats 1 and 3 recorded full data tapes with only 0.1 per cent bad records. However, these excellent screening results were obtained only after solving the problem of the glitch occurring in the 81st acoustic subrecord of many records. This problem is described in Section V of the August, 1988 Swallow float trip report [3]. Its solution required an adjustment to the signal strength output by the float cassette reader.

The last table entry under floats 1 and 3 shows a record with zero bytes. A zero byte record is written at the end of the data tape indicating the total number of internal records recorded by that float. Float 5 stopped recording data prematurely after record 836 and no zero byte record was written.

II. The 8 kHz Surface and Bottom Bounce Data

Figures II.1 and II.2 show the arrival times, converted to depth, of the self-generated 8 kHz acoustic location pings recorded by floats 3 and 5. (Recall that float 1 was not equipped with an 8 kHz localization hydrophone). The sampling interval in this plot is 12 records, or 9 minutes. Float 5 stopped recording data after record 836 so that the discussion below focuses on float 3's data.

The first 400 records or so were written while the float was on board RUM as it descended to the bottom. During this time, the float's 8 kHz localization hydrophone was placed in the bottom of a plastic container on top of which the float was strapped. Therefore, the localization ping energy was confined within the container. Around record 1075 (21:36 local time, 3 June), two sets of detections, one at zero depth and the other starting at about 3700 meters, were recorded just after the time when RUM began its ascent to the surface after reaching the bottom and suffering a VARIAC failure (re Swallow Float Log Summary). Detections of surface reflections were again recorded starting at record 1426 (02:00, 4 June), about the time RUM began its ascent to the ocean surface after deploying floats 1, 3, and 5 on the bottom. The surface reflections became detectable after this time probably because of the decrease in the background noise level. The float depth indicated by these data is 3825 meters.

III. Battery Voltage, Float Heading, and AGC Level

Figures III.1, III.2, and III.3 display the battery voltage, compass heading, and AGC gain for floats 1, 3, and 5, respectively. The value of each of these quantities for every 45 sec record is plotted. As can be seen by the flat nature of the battery-output plots, the deployment time for the floats is certainly not constrained by power-supply requirements.

The compass heading for the three floats during RUM's descent (records 640 to 868) shows large variations. This is due to the rotation of RUM during descent. Once on the bottom (after record 868), the compass headings for both floats 1 and 3 remain constant, even after RUM began to ascend to the surface because of an apparent VARIAC failure, until record 1135. The jump in heading around record 1135 occurs just as RUM returned to the bottom a second time. The compass headings for both floats again remained constant until they were deployed; float 3 at record 1309 (00:33, 4 June) and float 1 at record 1350 (01:03, 4 June). During these periods of constant heading, the compasses on both floats may have been stuck; the Swallow float compass can only withstand a 3° tilt from vertical. The compass on float 1 was also stuck at 0° heading between record 1400 (the time when RUM began deployment of the external geophone package) and record 1800 (the time when float 1 prematurely released from the bottom and began ascending to the surface). After deployment, float 3's heading changed very little during the remainder of the deployment. Note that since float 1's geophone was external to the glass sphere and float 3 was equipped with only an omni-directional infrasonic hydrophone, both sets of compass readings are of little consequence to the infrasonic acoustic data.

The automatic gain control (AGC) settings for both of the floats (in the bottom plots in Figures III.1 through III.3) show a decrease from an initialized value of 14 dB over the first 28 records. The AGC can only change by approximately 1/2-dB increments between each record. The AGC level for float 1 remained at 0 dB gain until RUM lifted off the bottom at record 1426 (02:00, 4 June). It then increased to 23 dB and fluctuated around this value until the float released from the bottom after record 1800. The large increase to 36 dB in float 3's AGC gain, starting at record 868 when RUM first arrived on the bottom, was due to the saturation and resulting loss in sensitivity in the hydrophone data acquisition system. Float 3's AGC gain also increased to 15 dB after about record 1315, the time when the float was deployed by RUM. It remained around 15 dB while RUM was on the bottom. The decrease in AGC gain at record 1420 and subsequent increase at record 1428 is associated with RUM moving away from the floats, and then lifting

off the bottom. Float 3's AGC level then increased to 23 dB and remained at about that level for the remainder of the recording period.

IV. Root Mean Square Pressure and Particle Velocity

Plots of the root mean square (rms) particle velocity recorded by float 1 and the rms pressure recorded by floats 3 and 5 are presented in Figures IV.1a through IV.1h, Figures IV.2a through IV.2h, and Figures IV.3a and IV.3b, respectively. Five seconds of data, or 250 points, are averaged together, yielding nine rms data points per record. The reduction of 12 dB in fixed gain in float 1's data acquisition channels has not been taken into account in Figures IV.1a through IV.1h.

The rms levels indicated by the first 28 records is misleading. Actually, the voltage signals are clipped all during this time as the AGC level, initially at 14 dB gain, steps down to 0 dB in 1/2-dB increments. Therefore, the gain-corrected rms levels for clipped signals are smaller when the AGC gain is high than when it is low.

The rms velocity recorded by float 1's three geophone components show high levels as RUM descended. The z axis level and the variability on the y axis both decrease once RUM reaches the bottom at record 868. In contrast, the x axis level remains high until RUM lifted off the ocean bottom at record 1428. The collection of the box core by RUM results in a jump in y and z axis levels at record 1032. RUM's return to the ocean bottom after its system inexplicably recoved (re Swallow Float Log Summary) is marked by a jump in the y axis rms levels after record 1135. The levels remain quite high almost the whole time until RUM lifted off the sediment at record 1428. The levels then decrease to very low values until the float released from the bottom after record 1800. During the period of low levels, the rms velocity on the horizontal components is about 4 times as large as on the vertical component.

Regarding float 3's rms pressure, plotted in Figures IV.2a through IV.2h, the temporary loss of hydrophone circuit sensitivity is evident in the extremely low rms pressure levels recorded between records 868 and 1032. After that, the levels remain high until the float is deployed by RUM; the deployment started around record 1310 and was completed at record 1329. The movement of RUM away from the floats after their deployment results in a small jump in rms pressure levels between records 1420 and 1425, after which the departure of RUM from the bottom at record 1428 is indicated by a small peak.

Only electronic self noise was recorded by the geophone data acquisition channels on floats 3 and 5 and the hydrophone channel on float 1. Spikes occurring once every record are clearly seen on the x and z channels of float 3, the y axis of float 5, and especially on the z axis of float 5. No such contamination is present in float 1's hydrophone channel. This geophone channel electronic self noise is the result of ground loop currents generated by the float cassette tape recorder operation. The contamination does not appear to be present in float 1's hydrophone channel because the hydrophone circuit front end provides better electronic protection against this form of self noise. Note that the fixed gain in the hydrophone and geophone circuits in this experiment differ by only 3 dB; 80 dB in the hydrophone circuit and 83 dB in the geophone circuit.

V. Particle Velocity and Pressure Time Series

Selected time series from the three orthogonal geophone components of float 1 and the hydrophone channel of float 3 are plotted in Figures V.1 through V.5. The data are sampled at a 50 Hz rate, but only every other point is plotted. Three record sequences are presented; records 1655 to 1666 (04:52 to 05:00, 4 June), records 1685 to 1696 (05:15 to 05:23, 4 June), and records 1992 to 2003 (09:05 to 09:13, 4 June). These sequences were chosen for plotting since the arrivals from the first four and the seventh seal bombs were recorded during this time; the first two occur in records 1661 and 1662, the third and fourth in records 1693 and 1694, and those from the seventh seal bomb are in record 1997. For the seventh seal bomb, only the time series from float 3 are presented since float 1 had released prematurely from the bottom and was ascending during this time.

For float 1, the arrival structure of the seal bombs is most clearly seen in the vertical geophone component time series. The reason for this is probably that the noise levels are much lower on this component than on the horizontal components. The detonations of the first two seal bombs, clearly recorded in records 1661 and 1662 of Figure V.1c, result in arrivals composed of three main phases, the direct (plus surface-reflected) path, the bottom-to-surface-to-receiver path, and the bottom-to-surface-to-bottom-to-surface-to-receiver path. Note that the direct path phase is clipped. The second two seal bomb detonation arrivals, in records 1693 and 1694 in Figure V.3c, contain mainly the direct path and the bottom-to-surface-to-receiver path.

The arrivals from the first four seal bombs don't appear to be present at all in the hydrophone data, in Figures V.2 and V.4. They are not readily visible since the AGC gain has been determined by the background sound pressure levels and the arrival of the relatively loud seal bomb phases result in clipping. In addition, the background noise recorded by the hydrophone has the same frequency character as the seal bomb arrivals. This is in contrast to float 1's horizontal geophone components where the background noise is dominated by lower frequency components than the seal bomb arrivals; re Figures V.1a, V.1b, and V.3a, V.3b. The arrivals from the seventh seal bomb are visible in float 3's time series, re Figure V.5. Three phases which have resulted in clipping are discernible.

In order to demonstrate that the first and third seal bomb detonations are recorded in float 3's hydrophone data, the arrivals in float 1's vertical geophone time series were used to construct matched filters. The results of passing float 3's time series through these matched filters are presented in Figures V.6 through V.12. The following table lists the phases used to construct the matched filter for each figure.

Figure Number	Record Number	Float 1's Vertical Axis Phases included in the Matched Filter
V.6	1661	All 3 phases
V.7	1661	Just the 1st phase
V.8	1661	Just the 2nd phase
V.9	1661	Just the 3rd phase
V.10	1993	Both phases
V.11	1993	Just the 1st phase
V.12	1993	Just the 2nd phase

The matched filter output results generally show peaks in the expected locations of phase arrivals in float 3's data, although it appears that float 1's time base is about a half-second faster than float 3's time base. For example, the peak output in Figure V.6 occurs about a half-second before the direct arrival in Figure V.1c. The alignment of the two floats' time bases is discussed in the next section.

A few other features in the time series are worthy of note. First, float 1's z axis geophone appears to detect the 8 kHz localization ping generated by float 3's ITC transducer. That is, a small spike is visible in records 1659 and 1695 about 10.4 seconds after the start of the record; re Figures V.1c and V.3c. The coupling of float 3's localization ping energy into sediment motion was probably aided by the fact that the localization transducer was resting upon the ocean bottom; the transducer cable was 1.83 meters long whereas the tether was only 0.5 meters in length. In float 3's infrasonic hydrophone data, the localization ping results in over 4 seconds of sensitivity loss due to saturation of the front end electronics.

Finally, float 1's three geophone components detect large impulsive arrivals, e.g., in records 1655, 1663, 1692, and 1695, which are not detectable in the hydrophone data. The fact that these signals are not present in the hydrophone data was verified by examining float 3's filtered output with the signals recorded by float 1 acting as the matched filter (identical to the procedure described above). These large impulsive arrivals therefore appear to be non-acoustic in nature. They may have been generated by motion of the cable connecting float 1's geophones to the electronics.

VI. Time Base Alignment

In typical deployments, the reciprocal travel time estimates from the 8 kHz localization data are used to estimate and correct for the time base misalignment between Swallow floats [4]. However, in this

experiment, float 1 was not equipped with an 8 kHz hydrophone since all its glass shell penetrators were used to connect the external geophone package to the internal electronics. Instead, the time base offset was estimated using both the seal bomb arrivals and the recording of float 3's 8 kHz localization ping by float 1. Both of these approaches assume that the two floats were co-located in space. However, they may have been separated by as much as 2 meters horizontal distance.

The seal bomb arrivals in the two floats' data were used to estimate the time base offset by first calculating the transfer function between the two time series' arrivals [5], and then calculating the corresponding impulse response by taking the inverse fft. The peak in the impulse response occurs at the time delay between the two data sets. Figures VI.1 through VI.4 show the impulse response estimates between float 3's hydrophone time series and float 1's x geophone (upper left), y geophone (lower left), and z geophone (upper right) time series for the first four seal bomb arrivals. The following table lists the data sample offset where the peak occurs and the equivalent time delay for each of the impulse responses.

Figure Number	Record Number	Geophone Component	Point Offset at Impulse Response Peak	Time Delay (sec)
VI.1	1661	x	14	-0.28
VI.1	1661	y	212	+0.88
VI.1	1661	z	21	-0.42
VI.2	1662	x	12	-0.24
VI.2	1662	y	255	+0.02
VI.2	1662	z	22	-0.44
VI.3	1693	x	24	-0.48
VI.3	1693	y	22	-0.44
VI.3	1693	z	21	-0.42
VI.4	1694	x	22	-0.44
VI.4	1694	y	253	+0.06
VI.4	1694	z	22	-0.44

These results strongly suggest that the time base offset is somewhere between 21 and 22 points, or 0.42 to 0.44 seconds. A negative time delay means that float 1's clock is faster than float 3's clock, so that float 1 has recorded a greater number of points than float 3.

The results of cross correlating the two floats' time series during the seal bomb arrivals were consistent with the impulse response results above, although they were more ambiguous; re [5].

As mentioned in the previous section, float 1's vertical geophone surprisingly recorded the 8 kHz localization pings generated by float 3. Since float 3 issued the localization pulse at almost exactly 10 seconds after the start of the record in which it pinged, according to its clock, then the difference between the time of the ping arrival in float 1's data and 10 seconds is equal to the time base offset. In order to increase the signal-to-noise ratio, float 1's time series for all records in which float 3 pinged (every 12th record) between records 1440 and 1800 were coherently averaged together. Record 1440 was written shortly after RUM lifted off the ocean bottom and record 1800 was recorded shortly before float 1 started to ascend to the ocean surface. The resulting average of the 30 records is plotted in Figure VI.5 for each of the three geophone components; the averaged x component is in the upper left, the averaged y component is in the lower left, and the averaged z component is in the upper right. The averaged z component clearly has the greatest signal-to-noise ratio. However, the two averaged horizontal components also contain a spike starting at 10.44 seconds, exactly the same time as the spike on the averaged z component. These results again suggest that the time base offset is somewhere between 21 and 22 points, or that float 1's clock is 0.42 to 0.44 seconds faster than float 3's clock.

As an aside, the peaks every 1/2-second in the averaged z axis time series are the result of electronic self noise occurring between the float's 1/2-second-duration acoustic subrecords. This contamination was discussed in Section IV. Its effect on the spectral estimates in Section VII is minimal, and can be almost completely eliminated by further data processing.

The time base offset of 0.42 to 0.44 seconds calculated from the seal bomb arrivals and from the recording of float 3's 8 kHz localization ping by float 1 is fairly consistent with GOES (geostationary operational environmental satellite) clock measurements made in the July, 1989 experiment [6]. From the

table on p. 16 of reference [6], float 1's clock, just before recall, was 0.37 seconds too fast and float 3's clock was only 0.05 seconds too fast. Therefore, from these measurements, float 1's clock should be about 0.32 seconds faster than float 3's clock. The difference between the GOES clock results and those in this experiment *may* be due to the greater deployment depths, and therefore colder temperatures, in this experiment. That is, float 1's clock crystal may display a greater temperature dependence than float 3's crystal.

VII. Acoustic Particle Velocity and Pressure Spectral Properties

Estimates of the calibrated autospectra for float 1's geophone velocity components and float 3's hydrophone pressure channel are presented first in this section. The spectral estimates are made after the two floats' time series have been aligned using the results from the previous section. Spectral estimates with two different frequency resolutions are calculated. Those with a 98 mHz resolution are made by dividing 40.96 seconds in a data record (obtained after skipping the first 2.5 seconds of data) into seven 10.24-second-long segments, with a 50 percent overlap between segments. The segments are fast Fourier transformed after using a Kaiser-Bessel window of $\alpha = 2.5$ to window the data. The resulting seven spectra within a record are incoherently averaged together. The averaged spectra for four consecutive records (equal to three minutes of data) are then incoherently averaged in order to further reduce the variance of the spectral estimates. For spectral estimates with a 24 mHz resolution, the segment length which is transformed is quadrupled to 40.96 seconds and the spectra for twenty consecutive records are incoherently averaged. For some of the plots presented later in this section (e.g., the coherence estimates), additional averaging across records was done.

The autospectra are properly calibrated to units of dB re 1 $(\text{m/sec})^2/\text{Hz}$ for the geophone components and dB re 1 $(\mu\text{Pa})^2/\text{Hz}$ for the hydrophone component. The pressure-particle velocity cross spectra are calibrated to units of dB re 1 $\mu\text{Watts/m}^2/\text{Hz}$. Refer to Appendix 1 for a description of the geophone and hydrophone data acquisition systems.

a) Auto Spectra and Intensity Magnitude Spectra

Spectra estimated from three minutes of data from both float 1 and float 3 for four different time periods are shown in Figure VII.1. The dotted line in each plot is the pressure autospectrum calculated from float 3's hydrophone data, the solid line is the equivalent pressure spectrum calculated from float 1's geophone data, i.e., $S_p^G(f) = (\rho_o c)^2 \sum_{j=1}^{3} S_{v_j}(f)$, and the dashed line is the equivalent pressure spectrum calculated from the active acoustic intensity magnitude, i.e., $(\rho_o c)\,|\underline{C}_{p\underline{v}}|(f)$, where $\underline{C}_{p\underline{v}}(f)$ is the real part of the cross spectrum between float 1 and float 3's data. The scaling factor used in the equivalent pressure spectral calculations is the characteristic impedance; it is set equal to $2.1 \times 10^6 \frac{\text{kg}}{\text{m}^2\text{sec}}$ $= (1.4 \times 10^3\ \text{kg/m}^3)(1.5\ \text{km/sec})$ rather than the value of $1.5 \times 10^6 \frac{\text{kg}}{\text{m}^2\text{sec}}$ used in previous experiments since float 1's geophones are resting on the more-dense sediment. Note that the calculation of the equivalent pressure spectrum, $(\rho_o c)\,|\underline{C}_{p\underline{v}}|(f)$, assumes that float 1's geophones and float 3's hydrophone are co-located in space. In particular, the pressure measured by float 3 is assumed to be the same as the pressure at the ocean-sediment interface. For each of the plots in the figure, the following table lists the data records and the corresponding time interval used in the spectral estimates.

The 4-Rec Sequence and 3-Min Time Period for Plots in Figure VII.1

Spectral Plot	Record Interval	Local Time Interval (on 4 June)	Comments
Upper right	1512 - 1515	03:05 - 03:08	Before RUM was recovered.
Lower right	1624 - 1627	04:29 - 04:32	After RUM was recovered and before steaming away.
Upper left	1700 - 1703	05:26 - 05:29	Steaming away from site.
Lower left	1748 - 1751	06:02 - 06:05	Continuing to stea away from site.

The first notable feature in these plots is that the geophone-derived spectra are much higher than the hydrophone pressure spectra. As illustrated and discussed further in the next part of this section, the reason is probably due to the decoupling of horizontal sediment motion from motion in the water column. The overall spectral level of $S_p^G(f)$ from float 1's data is similar to that of midwater Swallow float spectra in "noisy" float deployments, e.g., the July, 1989 experiment [6]. On the other hand, the spectral levels recorded by float 3's hydrophone are typical of "very quiet" deployments, e.g., the May, 1987 experiment [7].

Another notable feature of the geophone-data-derived spectra is its "raggedness", i.e., its large variability with frequency below 5 Hz. In contrast, midwater-column Swallow float geophone spectra from other experiments show a relatively smooth rise towards the microseismic peak at 0.15 Hz. This raggedness is more readily apparent in the time-averaged, log-log spectral plot shown in Figure VII.2. The spectra in Figure VII.2 were obtained by averaging over four hours of data. The raggedness below 5 Hz occurs only on the horizontal geophone components; the vertical component spectrum is relatively smooth. The reason for this difference between the sediment-mounted geophone data and the water-column data is due to the non-acoustic impulsive arrivals in the geophone data mentioned at the end of Section V. These arrivals may be due to geophone cable effects. Previously recorded bottom-tethered Swallow float geophone spectra also show this "raggedness" which is caused by tether contamination.

The log-log spectral plots in Figure VII.2 indicate that both the geophones and the hydrophone appear to detect the microseismic peak at 0.2 Hz. In contrast to the water-column geophone data collected in other Swallow float deployments, these geophone data are not contaminated by float rocking since the motion of the glass sphere was decoupled from the geophones.

By plotting the spectra on a log frequency scale as in Figure VII.2, the power law dependence of the spectra can be determined. However, both the geophone and hydrophone spectra show a decreasing spectral slope with decreasing frequency between 5 Hz and 0.4 Hz. A straight-line fit to the spectra between these two frequencies shows an approximate 18 dB/octave increase to the microseismic peak in the geophone data and about an 8 dB/octave increase in the hydrophone data. The hydrophone spectral results may be affected by calibration error; a comparison of float 3's hydrophone and geophone spectra in both the July, 1989 and August, 1990 deployments [6, 8] indicate that this hydrophone suffers from an inexplicable decrease in sensitivity with decreasing frequency [9]. Float 3's hydrophone electronic system response has been checked in the laboratory and the results indicate that the loss in sensitivity must be caused by the hydrophone itself. Another float's hydrophone, the one on float 5, also showed this loss in low-frequency sensitivity in the July, 1989 and August, 1990 experiments [9]. The reason why both the Swallow float hydrophones that were used in this RUM experiment now suffer this loss in sensitivity is as yet unknown.

The noise generated by the New Horizon as it steamed away from the deployment site appears to result in a hump of spectral energy between 7 and 12 Hz, re Figure VII.1. Upon this hump exist three or four spikes. Additional spikes occur between 15 and 20 Hz. Evidence to be presented below in Section VII.c suggests that these spectral lines were generated by more than one source (ship). The following table lists the frequencies of these spectral spikes and the type of sensor, geophone or hydrophone, which detected them.

Frequency of Spectral Spikes (Hz)	Sensor which Contains Spike
5.0	hydro
7.5	geo, hydro
8.3	geo, hydro
8.9	geo, hydro
10.0	geo, hydro
15.0	geo, hydro
16.5	geo, hydro
17.8	geo, hydro

The spike at 5.0 Hz, which is recorded only by float 3's hydrophone, appears to be intermittent; it occurs predominantly in the hydrophone spectra for records 1512 - 1515 (upper left) and records 1748 - 1751 (lower right), whereas it is not readily visible in other two hydrophone spectra in Figure VII.1. The source of this spike is unknown.

The intensity magnitude spectrum scaled to pressure spectral units, $(\rho_o c)\,|\underline{C}_{pv}|(f)$, is plotted as a dashed curve in Figures VII.1 and VII.2. It is calculated from the real parts of the three cross spectra between float 3's hydrophone time series and each of the three geophone time series recorded by float 1. The scaled acoustic intensity magnitude spectrum generally agrees well with the pressure spectrum above 3 or 4 Hz; at the lower frequencies, it is larger than the pressure spectrum. However, the properties of this spectrum are difficult to interpret, in contrast to the intensity magnitude spectrum calculated from the simultaneous measurement of acoustic pressure and particle velocity by a single Swallow float in the water column (re [9, 10]). One reason for the difficulty in interpretation is that the effects of the spatial separation between floats 1 and 3 may be significant; e.g., sediment interface waves may significantly contribute to the time series recorded by float 1, but not be present in float 3's data either because of a lack of coupling of horizontal motion at the ocean-sediment interface or because of the potentially high attenuation of interface wave effects away from the ocean bottom. In addition, the two floats' time bases can only be aligned to within a 1/2-second or so using the infrasonic acoustic data. Therefore, the intensity magnitude spectrum in this experiment is probably distorted by the additional misalignment remaining after approximate alignment of the two floats' time bases.

In order to get a qualitative picture of the ocean-borne and sediment wave fields during the course of the whole deployment, gray level plots of the normalized spectral amplitudes as a function of time (in units of Swallow float record number) are shown in the lower panels of Figures VII.3 and VII.4. An analytical spectrum was used to normalize the spectra before creating the gray level plots; it is shown in the upper panel of each figure. This normalization was done in order to decrease the dynamic range of the infrasonic spectra. The functional form of the normalizing spectra in both figures is given by $S_p(f) = Af^{-5}$ from 0 to 3 Hz, $S_p(f) = Bf^{+0.75}$ from 8 to 25 Hz, and $S_p(f)$ is a linear combination of these two functional forms between 3 and 8 Hz. The values of A and B are determined by specifying the desired spectral level at 5 Hz; for the normalizing hydrophone spectrum in Figure VII.3, the spectral level at 5 Hz is set at 65 dB re 1 $\mu Pa^2/Hz$ and for the normalizing geophone-data-derived spectrum in Figure VII.4, it is 80 dB. These plots are especially useful in showing the time-dependent amplitude of spectral lines. For example, the 5 Hz line in the hydrophone data does not appear until after about record 1510, and then intermittently becomes quite predominant. The dark patches at 21 Hz and 23 Hz and centered about record 1460 in both figures are probably generated by RUM since they no longer exist after RUM was recovered, i.e., after record 1600 or so. A number of other spectral lines between 5 and 20 Hz are also visible, and are present in both the hydrophone and geophone spectra; re the previous table. The difference between the hydrophone and geophone spectra in the frequency dependence of the rise towards the microseismic peak is evidenced by the increasing lightness of the gray level plot with decreasing frequency in Figure VII.3 versus the increasing darkness with decreasing frequency in Figure VII.4. The dashes which are spaced every 12 records in the hydrophone gray level plot near 0 Hz are caused by float 3's 8 kHz localization pings. It is also apparent that the background hydrophone spectra have a different frequency dependence than the geophone spectra above 10 Hz. Another interesting feature is that the spectral level around 2.5 Hz in both types of spectra decreases after record 1650.

b) Spectral Ratios

An effective way of comparing two spectra is by plotting their ratio. For example, the solid curves in the four plots in Figure VII.5 show the ratios of the geophone-data-derived pressure spectra to the hydrophone pressure spectra corresponding to the four time periods in Figure VII.1. (The dashed curves are the ratios of the scaled intensity magnitude spectra and the hydrophone pressure spectra). The spectral ratio is frequency dependent, becoming increasingly more positive as the frequency decreases. The ratio has been clipped at + 20 dB at the lowest frequencies in order to fit on the plots. This frequency dependence may be partially due to a increasing loss in sensitivity with decreasing frequency for float 3's hydrophone, as discussed previously. It may also be the result of the difference in the frequency dependence of attenuation in sediments compared to sound attenuation in the ocean.

The positive spectral ratios are mainly due to the large levels on float 1's horizontal geophone components. That is, since horizontal sediment motion is not coupled into motion in the water column, then larger horizontal geophone spectral levels measured by float 1 need not be related to larger hydrophone levels measured by float 3. Horizontal sediment movement has a much smaller effective acoustic impedance than vertical motion since the overlying water provides no resistance to motion. If instead of using all three geophone components, only the vertical geophone component spectrum is used to derive the equivalent pressure spectrum, i.e., $S_p^G(f) = 3(\rho_o c)^2 S_{v_z}(f)$, then the agreement with the hydrophone pressure spectrum is much better. This is illustrated in Figure VII.6, where the solid curves in the four plots are the ratios of the *vertical*-geophone-data-derived pressure spectra to the hydrophone pressure spectra corresponding to the four time periods in Figure VII.1. The ratio is generally between ± 5 dB for frequencies from 5 to 20 Hz. Below 5 Hz, the ratio becomes increasingly positive probably because of the aforementioned loss in sensitivity of float 3's hydrophone. (The dashed curves in Figure VII.6 are the ratios of the scaled *vertical* intensity spectra and the hydrophone pressure spectra).

A comparison of the sediment motion measured by float 1's geophone and that measured by an ocean bottom seismometer (OBS) is presented in Figure VII.7. The uppermost panel shows the ratio of the OBS vertical geophone autospectrum to float 1's vertical geophone autospectrum and the lower two plots show the corresponding spectral ratios for the two horizontal geophone components. The OBS data were recorded in May, 1987 during a concurrent Swallow float deployment [7]. The May, 1987 experiment was conducted at nearly the same site as this experiment with RUM. The OBS horizontal geophone component data in the May, 1987 experiment are known to be of low quality [11]. One problem is that they suffered from poor OBS-to-sediment coupling due to the drag and inertia of the OBS package through the water [Prof. L. Dorman, private communication]. In contrast, the spectra recorded by the two instruments' vertical geophone components agree remarkably well. Reasons for this agreement are that the two experiments were conducted at nearly the same location, and the wind speeds of 6 - 10 knots and sea surface conditions in the two experiments were very similar.

c) Signal-to-Noise Ratio and "Directionality" of Spectral Lines

Further analysis of many of the spectral lines discussed in Section VII.a is presented in Figures VII.8 through VII.11. The following list specifies which plots pertaining to each frequency spike.

Frequency of Spectral Spike (Hz)	Location of Plots	Figure Number
5.0	upper two plots	VII.8
7.5	lower two plots	VII.8
8.3	upper two plots	VII.9
8.9	lower two plots	VII.9
10.0	upper two plots	VII.10
15.0	lower two plots	VII.10
17.8	upper two plots	VII.11

The leftmost two plots in each figure show the signal-to-noise (SNR) ratios of the spectral spike as a function of time (in units of Swallow float record number) in three types of spectra; the solid curves are the

signal-to-noise ratios in the equivalent geophone-data-derived pressure spectra calculated from float 1's data, $S_p^G(f) = (\rho_o c)^2 \sum_{j=1}^{3} S_{v_j}(f)$, the dotted lines are the SNRs in float 3's hydrophone pressure spectra, and the dashed curves pertain to the SNRs in the scaled intensity magnitude spectra, $(\rho_o c) \mid \underline{C}_{p\underline{v}} \mid (f)$. The signal-to-noise ratios are calculated by dividing the spectral level in the frequency bin of interest by the average of the levels in the fourth and fifth bins on either side of the bin of interest. The horizontal dashed line in each of these plots indicates a SNR of 0 dB. The time period shown in the plots is from records 1660 to 1800 (04:56 to 06:41, local time on 4 June). This period starts after the New Horizon had departed to the east, southeast from the deployment site and extends to the time when float 1 prematurely released from the ocean bottom. These plots indicate that none of the three types of spectra show a clear signal-to-noise ratio advantage over the other two types of spectra (except for the spike at 5 Hz which doesn't appear in the geophone spectra). Similar plots were created using just the vertical geophone component in the equivalent geophone pressure spectrum calculation. At many times and at certain frequencies, the hydrophone spectra SNR was greater than in the vertical-geophone-data-derived spectra. However, in some cases, the reverse was true. Therefore, the best type of near-ocean-bottom measurement to make for detecting near-surface-generated tones appears to vary with frequency (in the infrasonic band) and with propagation geometry.

The rightmost two plots in each of these figures show the sum of the horizontal projection of the active intensity vectors, in the frequency bin of interest, as a function of time over the time period in the lefthand plots. The active intensity vectors are calculated from the real parts of the cross spectrum between float 3's hydrophone data and float 1's horizontal geophone components [9, 10]. Since the New Horizon traveled to the east, southeast away from the site, it would have produced energy flux to the northwest. Therefore, the spectral lines at 8.3 Hz and possibly at 10.0 Hz may have been generated by this ship. The spectral lines at 7.5 Hz, 8.9 Hz, 15.0 Hz, and 17.8 Hz, however, appear to have been generated by a different, single source. Note that these directional results may be misleading since the two floats' time bases can only be aligned to within 20 msec (one data sample) using the infrasonic acoustic data. In order to examine the sensitivity of these results to time base misalignment, the calculations were redone for relative time base shifts of both + 12 msec and - 12 msec from the alignment used for Figures VII.8 through VII.11. Although a reshifting caused a change in the vector sum magnitude and its behavior; e.g., the vector sum for a given frequency could become "meandering" in nature; it never caused a reversal in the overall directionality. Therefore, even though these plots are not explicitly correct, they may provide a general indication of the directionality of the spectral lines.

d) Coherence Functions

Finally, the uppermost two plots in Figure VII.12 show the coherence between the acoustic pressure measured by float 3's hydrophone and the vertical sediment motion measured by float 1's vertical geophone component. The upper plot of this pair of plots shows the coherence squared, on a scale from 0 to 1.0, and the lower plot shows the complex coherence phase. Both plots are for a frequency range from 0 to 5 Hz. Again, the coherence phase above a few hertz is probably corrupted by time base misalignment. For comparison, the corresponding plots of the coherence between the acoustic pressure and vertical particle velocity measured by two bottom-tethered Swallow floats, float 9 (middle two plots) and float 10 (bottom two plots) in the July, 1989 experiment [6] are also presented. Since the vertical particle velocity must be continuous at the ocean-sediment interface, the comparison of the data from these two experiments is valid. Below about 1.25 Hz, the coherence squared plots for all three sets of data are nearly identical, including the notch in the coherence squared function centered at 0.5 Hz. However, the July, 1989 data indicate that an approximate 90° coherence phase shift occurs at the 0.5 Hz notch in the coherence squared function, but the data from this RUM experiment show no such phase shift. Above 1.5 Hz, the coherence squared values in this experiment are much higher than those in July, 1989. The reason for this difference is unknown. Note that the 4 Hz peak in the uppermost coherence squared plot is the result of electronic self noise; this type of self noise can be easily removed by additional processing.

Acknowledgements

We would like to thank Marvin Darling, the other member of the Swallow float team, for his many contributions to the project. Also, the members of the RUM team, Dr. Vic Anderson, Ron Horn, Gerry Denny, and Fred Uhlman, deserve special thanks.

This work was supported by the Office of Naval Research under contract # N00014-88-K-2040.

Appendix - Swallow Float Infrasonic Data Acquisition System

A block diagram of the Swallow float infrasonic system appears in Figure A.1. Float 1 was equipped with three orthogonally-oriented Geo Space geophones, whereas float 3 was equipped with the Ocean and Atmospheric Science (OAS) model E-4SD hydrophone. (The hydrophone channel on float 1 and the three geophone channels on float 3 were shorted out so that only electronic self noise were recorded by these components). The geophone channels will be described first, followed by a description of the hydrophone channel.

The sediment motion is first coupled into motion at float 1's geophones. The three orthogonal components of particle velocity at the geophone are then converted into voltages. The geophones are electromagnetic transducers in which a voltage is produced across a moving, conducting coil by its motion through the magnetic field lines produced by a permanent magnet [12]. The resulting voltage is proportional to the velocity of the coil with respect to the magnet. Constraining the coil to move in only one direction are elastic springs connecting the coil to the instrument casing. (Laboratory tests have determined that the geophones can withstand a maximum tilt from vertical of about 15°). The geophone package for Swallow float 1 is composed of three such transducers oriented to measure in three orthogonal directions.

The geophone amplitude and phase response was calculated using the theoretical equation of motion for this system [12]. (The amplitude response curve is nearly identical to the manufacturer's calibration curve provided with the geophones). Near-critical damping of the coil is achieved using a 60 kΩ shunt resistor. Note that the f^2 roll-off of the geophone amplitude response below the natural frequency of 8 Hz effectively pre-whitens the ocean ambient noise so that no additional pre-whitening needs to be implemented.

The three signals next undergo a fixed gain of 83 dB before being input to the automatic gain control (AGC). (Recall that this fixed gain is reduced by 12 dB from the 95 dB gain typically used in the Swallow float geophone data acquisition system). Included in the geophone channel circuitry are nine RC circuits. Five of these RC circuits act as high pass filters, with poles located at 0.000034, 0.034, 0.07, 0.26, and 0.47 Hz, in order to eliminate DC bias and decrease ultra-low frequency self noise. The other four RC circuits act as low pass filters, with poles at 34, 34, 72, and 337 Hz, in order to eliminate AC coupling noise (i.e. "cross-talk"). These RC circuits are lumped together with the geophone channel "fixed gain" in Figure A.1.

The water-borne pressure fluctuations (acoustic and non-acoustic) are converted into voltage fluctuations by the sensing material in the infrasonic hydrophone installed on float 3. The sensing material is electrostrictive; that is, it develops a voltage in response to an implied stress [13]. (From laboratory tests, it has been determined that the sensing material is also pyroelectric, i.e. it generates a voltage in response to a change in temperature). The electrostrictive material in the OAS hydrophones is pre-polarized lead zirconate-titanate, a polycrystalline ceramic. The hydrophone has a sensitivity of -182 dB re 1 V/μPa and a frequency response which is flat (within ±1 dB) from 0 to 5 kHz. Because the ocean ambient noise spectrum increases as f^{-4} to f^{-6} below about 5 Hz, the pressure-induced voltage output by the hydrophone is then passed through a pre-whitening filter. This high-pass filter is comprised of two RC circuits in cascade, both with corner frequencies of about 8 Hz, the same as the natural frequency of the geophone components.

The "fixed gain" triangle for the infrasonic hydrophone channel in Figure A.1 represents somewhat different circuitry than in the geophone channels. The fixed gain is set to 80 dB (rather than 83 dB), since the hydrophone is more sensitive than the geophones; -182 dB re 1 V/μPa for the hydrophone versus about -201 dB re 1 V/μPa above 8 Hz for the geophones. Also, since the hydrophone pre-whitening filter already includes two high pass RC circuits, only two additional high-pass circuits, with poles located at 0.034 and 0.47 Hz, were added. An additional equivalent high-pass RC circuit with resonant pole at 0.2 Hz is formed by the capacitance of the hydrophone itself (0.004 μf) and the resistance (200 MΩ) of a temperature-stable, metal film resistor. These three high-pass RC circuits are included in the "fixed gain" triangle along with four low-pass circuits, with poles at 34, 34, 72, and 339 Hz.

The hydrophone component voltage and all three geophone component voltages are then sent to a automatic gain control (AGC) amplifier. The AGC is a variable gain amplifier with a range of 0 to 36 dB gain which allows the full dynamic range of the eight-bit A/D converter to be used. The AGC gain always

changes between records by approximately 0.5 dB steps; if more than 0.5 percent of all data samples from the last 40 seconds of each record are clipped, then the AGC decreases by 0.5 dB. Otherwise, it increases. Plots of the AGC level for each float during every record are given in Section III.

Before digitizing, the signals are passed through a five-pole, four-zero, elliptic, anti-aliasing filter. Elliptic filters theoretically have the sharpest transition region for a given number of poles and circuit complexity. The filter frequency response and the pole, zero locations in the *s* plane are shown in Figure A.2 [14,15]. Incoming signals are amplified by a maximum of 4.6 dB in the passband, which has a 0.28 dB equal ripple. The cut-off frequency (the highest frequency at which the amplitude gain is equal to the minimum passband gain) is 20 Hz, and the attenuation is 19.5 dB at the Nyquist frequency of 25 Hz. The maximum equal ripple level in the stop band is 50.1 dB below the level in the pass band and is first reached at 31 Hz. Before installation in the floats, all filters were adjusted so that broadband noise input to the filters yielded the same amplitude response and same null location at the filters' output.

The geophone channel response, including all components in the system except the AGC gain (which varies over the time of the experiment) and excluding the 12 dB decrease in the standard fixed gain, is plotted in Figure A.3. The hydrophone channel response, including all components in the channel except the AGC gain, is plotted in Figure A.4. In deriving the phase response in Figure A.4, it was assumed that no phase shift was introduced by the hydrophone's electrostrictive material in the conversion of pressure to voltage.

The channel voltage signals are then digitized at a 50 Hz sampling rate and put into a temporary buffer. After 44 seconds of data (equal to one data record) have accumulated in the buffer, a one second period of writing the data to cassette tape takes place. During this time, no data is sampled. The 45 second cycle then repeats until the cassette tape is full. The cassette tape can store up to 17 Mbytes of unformatted data, which is sufficient space for up to 1600 four-component data records.

Both the RMS plots discussed in Section IV and the time series plots of Section V have been corrected for the variable AGC level. No other adjustments have been made in these plots. The spectral plots of Section VII, however, have been corrected for all electronic system gains including the geophone/hydrophone sensitivities and the anti-aliasing filter response and therefore report estimates calibrated to the input at the sensors.

Excellent agreement between the laboratory-measured and theoretically-predicted amplitude and phase responses of both the geophone and hydrophone channel circuitry, and the sensors themselves, has been obtained [16].

References

[1] J. Churgin and S. J. Halminski, Temperature, Salinity, Oxygen, and Phosphate in Waters off the United States, Eastern North Pacific, National Oceanographic Data Center, 3, (1974).

[2] K. V. MacKenzie, "Nine-term equation for sound speed in the oceans" J. Acoust. Soc. Am., 70 (3), (1981).

[3] G. L. D'Spain, R. L. Culver, W. S. Hodgkiss, and G. L. Edmonds, "Freely drifting Swallow float array: August 1988 trip report" MPL Tech. Mem. 407, Marine Physical Laboratory, Scripps Institution of Oceanography, San Diego, CA (1989).

[4] R. L. Culver, G. L. D'Spain, W. S. Hodgkiss, and G. L. Edmonds, "Estimating 8 kHz Pulse Travel Times and Travel Time Errors from Swallow Float Localization System Measurements" Marine Physical Laboratory, Scripps Institution of Oceanography, San Diego, CA (in press).

[5] P. R. Roth, "Effective measurements using digital signal analysis" IEEE Spectrum, (April, 1971).

[6] G. C. Chen, G. L. D'Spain, W. S. Hodgkiss, and G. L. Edmonds, "Freely drifting Swallow float array: July 1989 trip report" MPL Tech. Mem. 420, Marine Physical Laboratory, Scripps Institution of Oceanography, San Diego, CA (1990).

[7] G. L. D'Spain, R. L. Culver, W. S. Hodgkiss, and G. L. Edmonds, "Freely drifting Swallow float array: May, 1987 trip report" MPL Tech. Mem. 402, Marine Physical Laboratory, Scripps Institution of Oceanography, San Diego, CA (1988).

[8] G. L. D'Spain, G. L. Edmonds, W. S. Hodgkiss, and M. Darling, "Freely drifting Swallow float array: trip report for first deployment in the August, 1990 NATIVE 1 experiment" Marine Physical Laboratory, Scripps Institution of Oceanography, San Diego, CA, (in preparation).

[9] G. L. D'Spain, "The energetics of the ocean's infrasonic sound field" Ph.D. thesis, University of California, San Diego, CA (1990).

[10] G. L. D'Spain, W. S. Hodgkiss, and G. L. Edmonds, "The energetics of the deep ocean's infrasonic sound field" accepted for publication in J. Acoust. Soc. Am. (in press).

[11] G. L. D'Spain and W. S. Hodgkiss, "Comparison of Swallow float, ocean bottom seismometer, and sonobuoy data in the VLF band" MPL Tech. Mem. 404, Marine Physical Laboratory, Scripps Institution of Oceanography, San Diego, CA (1988).

[12] M. Pieuchot, Seismic Instrumentation, vol. 2, from Handbook of Geophysical Exploration, Section I - Seismic Exploration, ed. K. Helbig and S. Treitel, Geophysical Press (1982).

[13] R. Urick, Principles of Underwater Sound, 3rd ed., McGraw-Hill, (1983).

[14] A. B. Williams, Electronic Filter Design Handbook, McGraw-Hill (1981).

[15] A. Antoniou, Digital Filters: Analysis and Design, McGraw-Hill (1979).

[16] G. L. D'Spain, W. S. Hodgkiss, and G. L. Edmonds, "The simultaneous measurement of infrasonic acoustic particle velocity and acoustic pressure in the ocean by freely drifting Swallow floats," accepted for publication in J. Oceanic Engin. (1990).

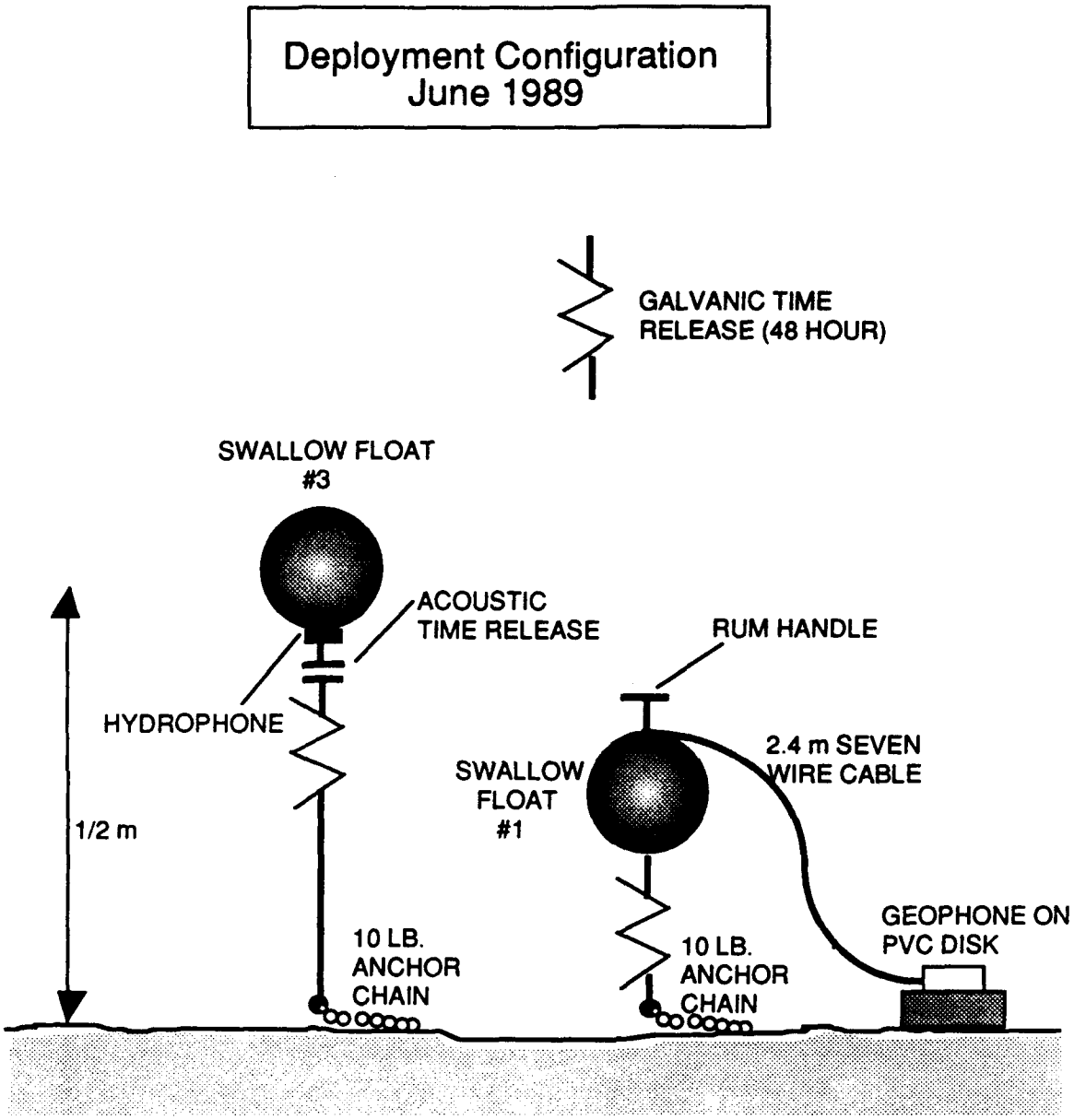
Deployment Configuration
June 1989
GALVANIC TIME
RELEASE (48 HOUR)
SWALLOW FLOAT
#3
ACOUSTIC
TIME RELEASE
RUM HANDLE
HYDROPHONE
2.4 m SEVEN
WIRE CABLE
SWALLOW
FLOAT
#1
1/2 m
GEOPHONE ON
PVC DISK
10 LB.
ANCHOR
CHAIN
10 LB.
ANCHOR
CHAIN

Figure 1

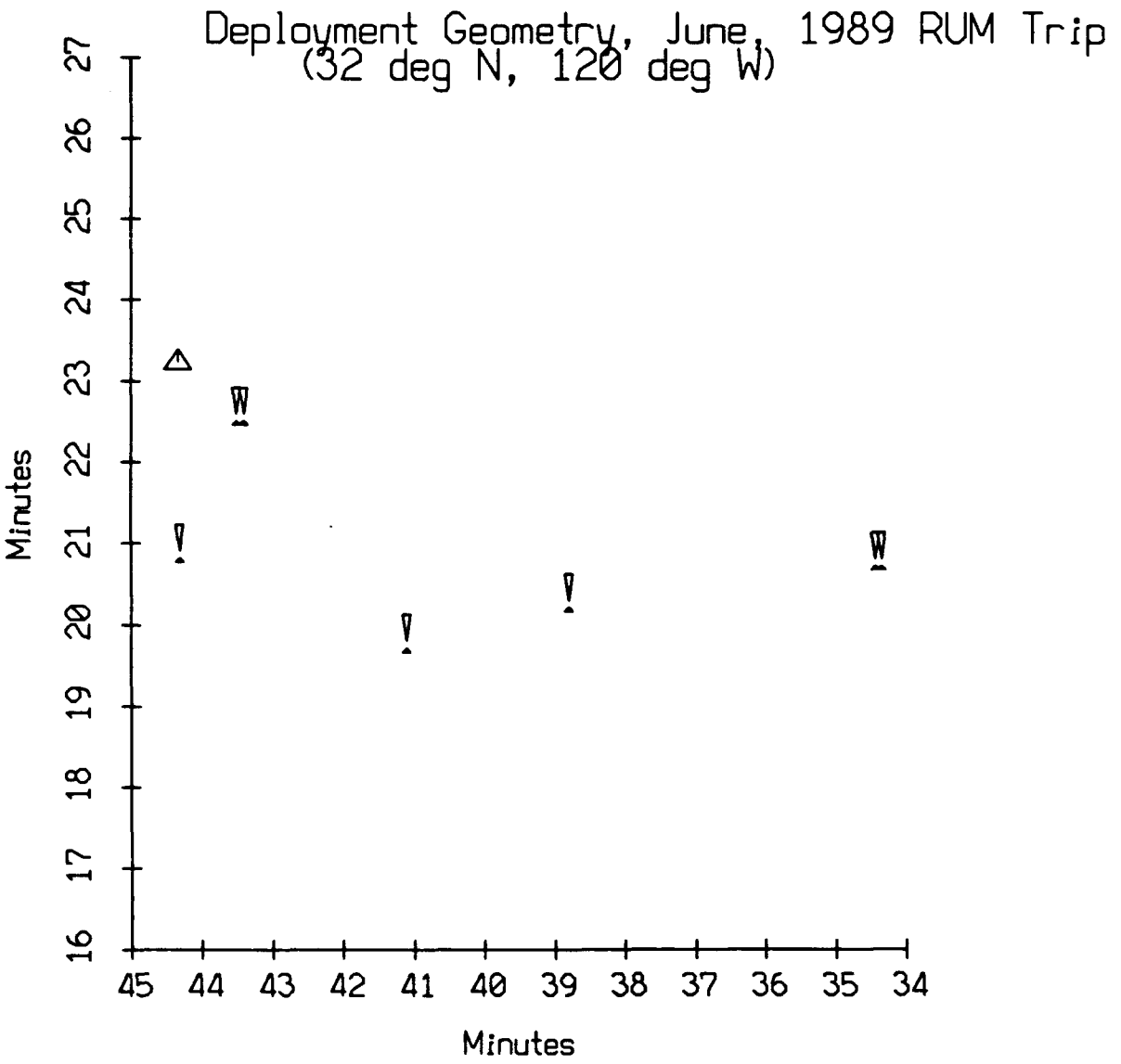
Deployment Geometry, June, 1989 RUM Trip
(32 deg N, 120 deg W)
Minutes
27
26
25
24
23
22
21
20
19
18
17
16
45
44
43
42
41
40
39
38
37
36
35
34
Minutes

Figure 2

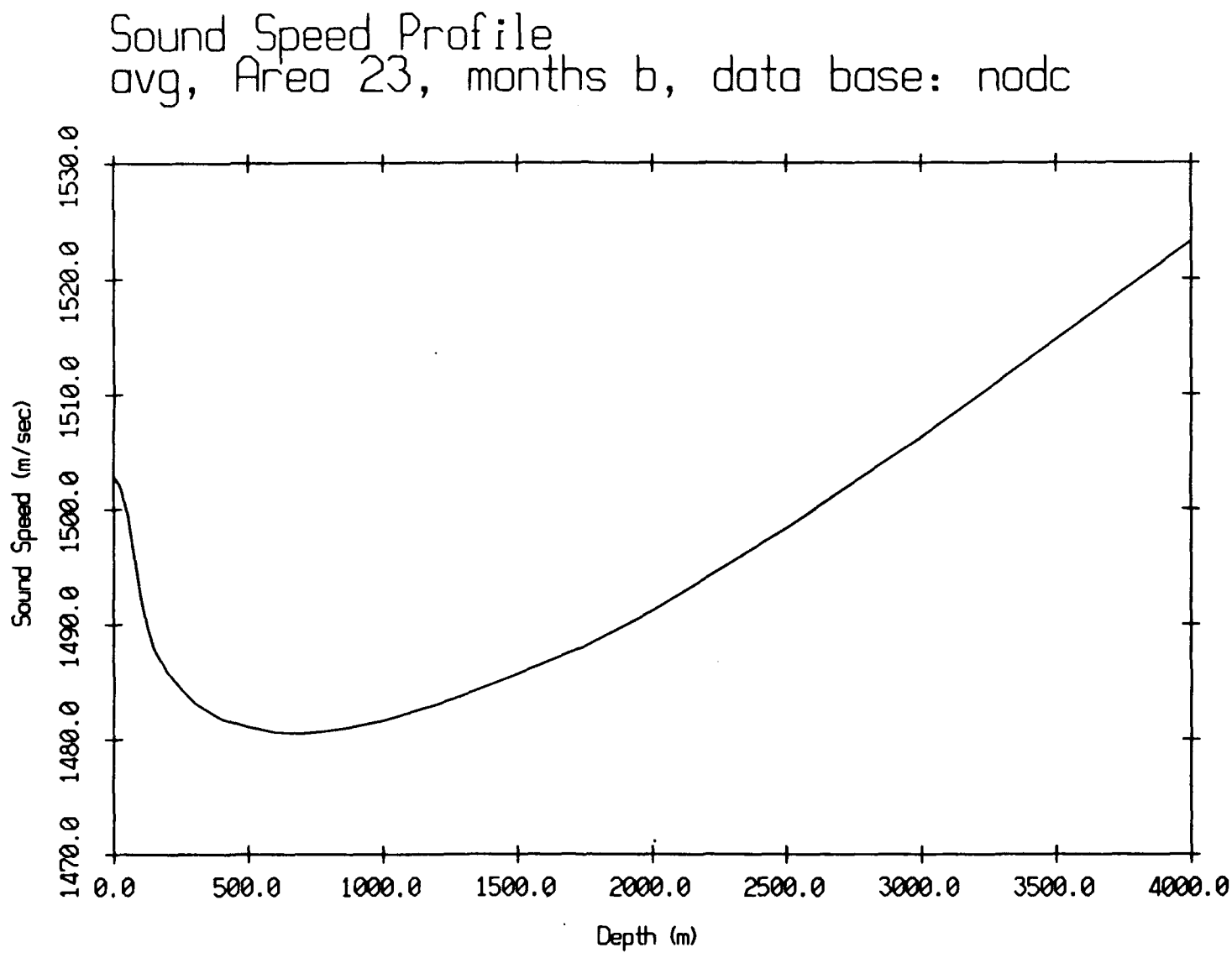
Sound Speed Profile
avg, Area 23, months b, data base: nodc
Sound Speed (m/sec)
1470.0
1480.0
1490.0
1500.0
1510.0
1520.0
1530.0
0.0
500.0
1000.0
1500.0
2000.0
2500.0
3000.0
3500.0
4000.0
Depth (m)

Figure 3

June 1989 RUM Trip Data Screening Results

record number	internal record number	# of bytes written	first missing resync	pass header checksum?	pass range checksum?	# of failed acoustic checksums?
			Float 1			
654	1293	4052	0	yes	yes	1
655	255	5004	1	no	no	43
1413	2050	0	0	yes	yes	0
			Float 3			
372	1011	6020	0	yes	yes	1
373	-489	3030	1	no	no	25
1387	2024	0	0	yes	yes	0
			Float 5			
168	807	9766	0	yes	yes	1

Figure I.1

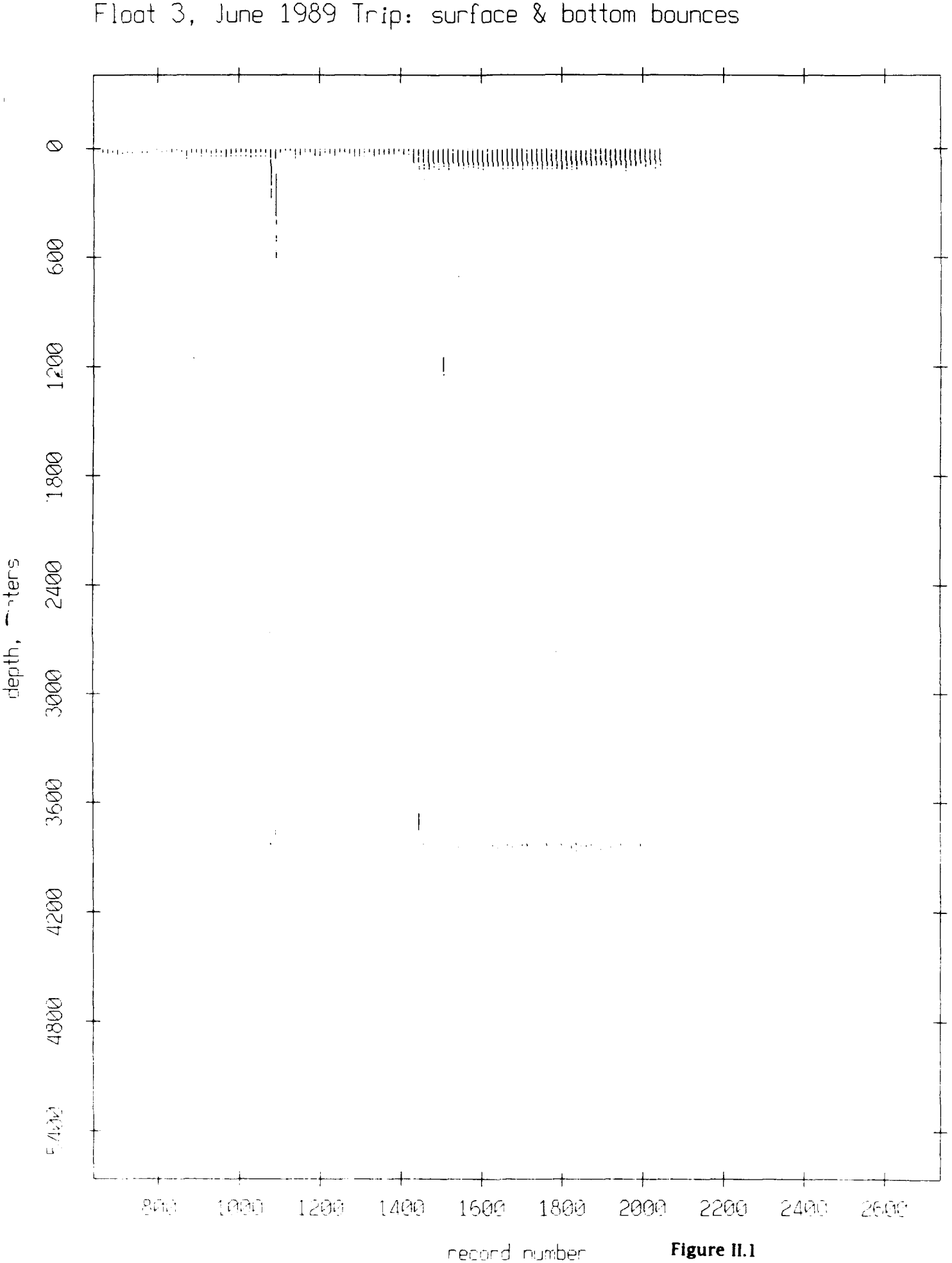
Float 3, June 1989 Trip: surface & bottom bounces
depth, meters
0
600
1200
1800
2400
3000
3600
4200
4800
record number

Figure II.1

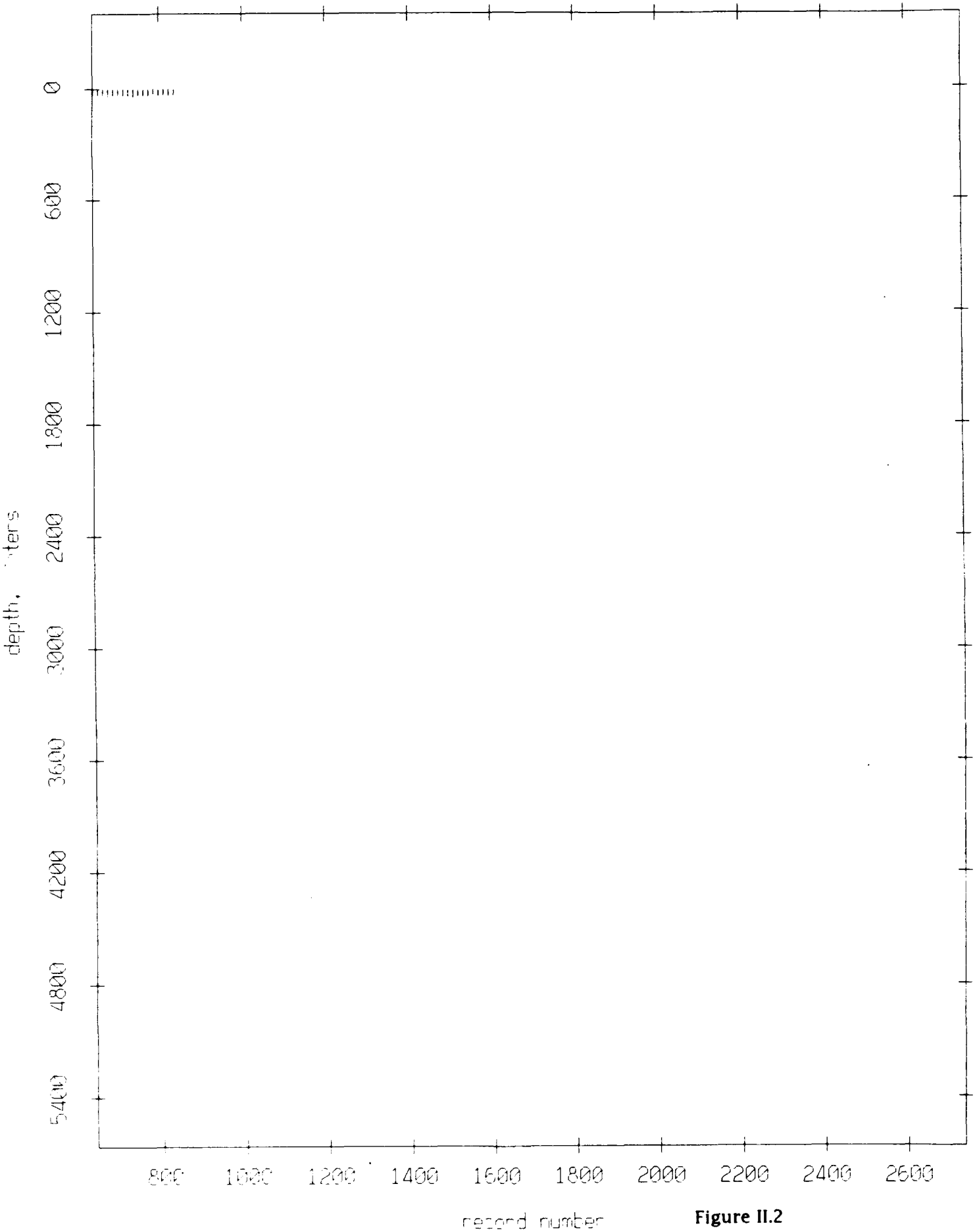
Float 5, June 1989 Trip: surface & bottom bounces
depth, meters
0
600
1200
1800
2400
3000
3600
4200
4800
5400
800
1000
1200
1400
1600
1800
2000
2200
2400
2600
record number

Figure II.2

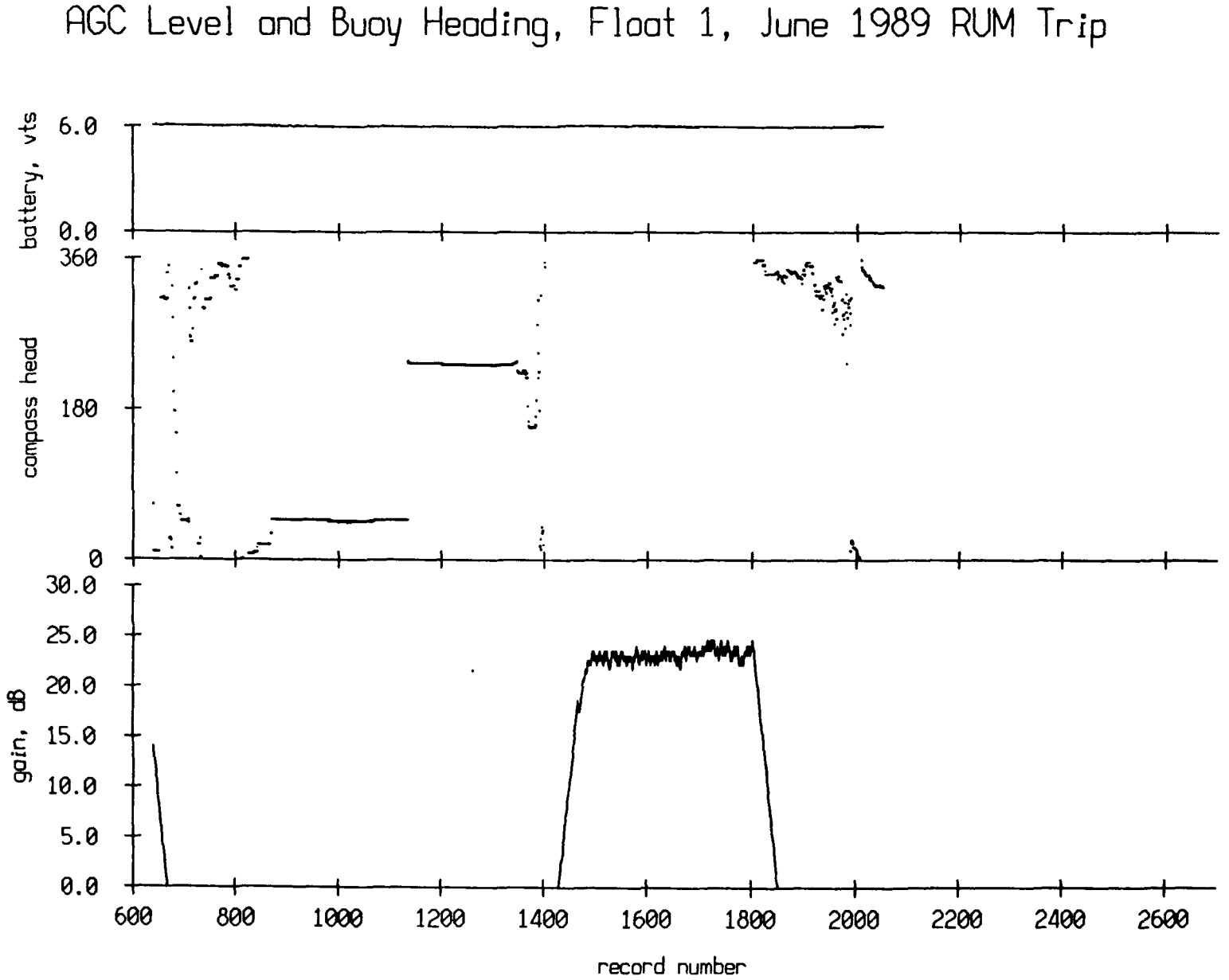
AGC Level and Buoy Heading, Float 1, June 1989 RUM Trip
battery, vts
6.0
0.0
compass head
360
180
0
gain, dB
30.0
25.0
20.0
15.0
10.0
5.0
0.0
600
800
1000
1200
1400
1600
1800
2000
2200
2400
2600
record number

Figure III.1

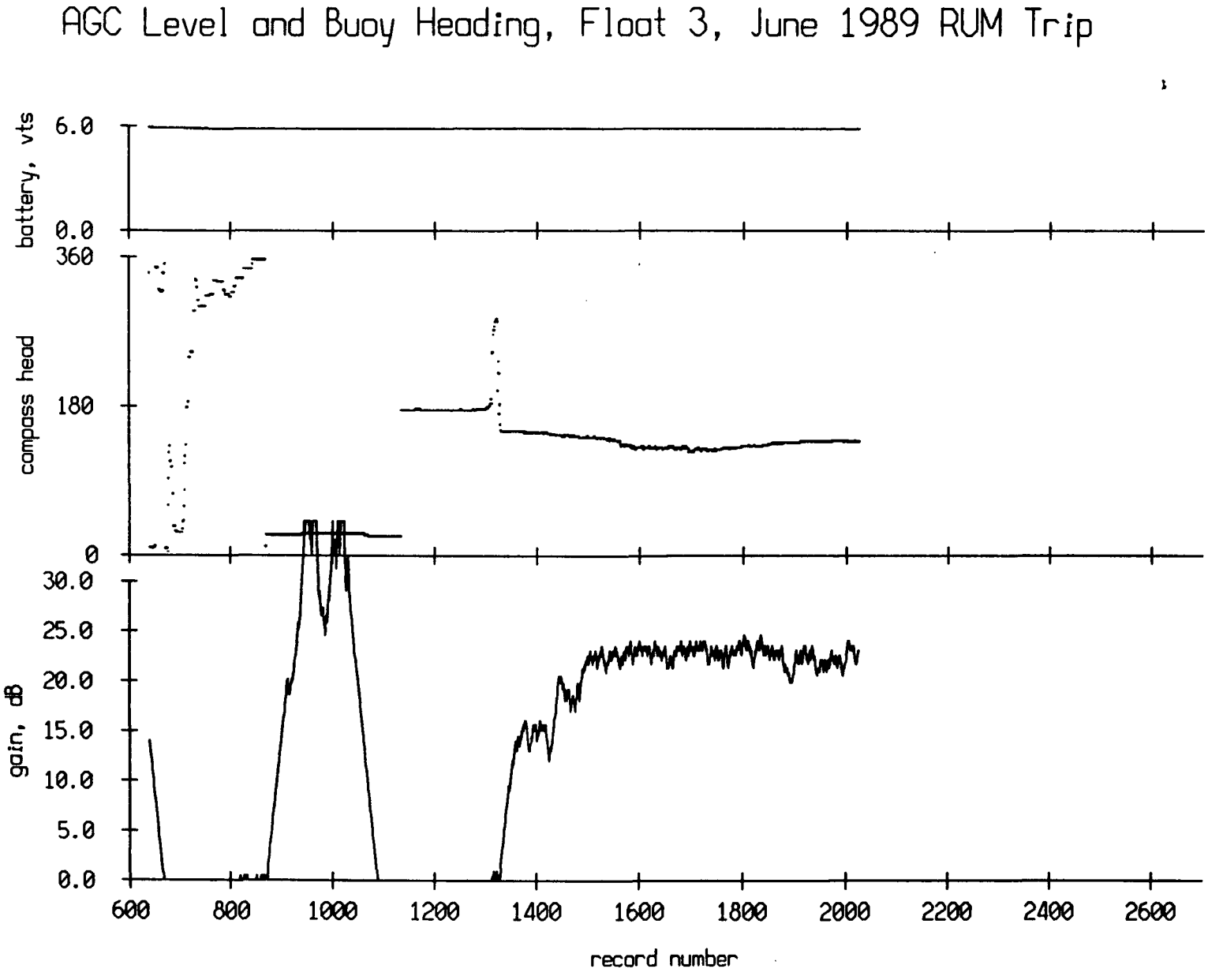
AGC Level and Buoy Heading, Float 3, June 1989 RUM Trip
battery, vts
6.0
0.0
compass head
360
180
0
gain, dB
30.0
25.0
20.0
15.0
10.0
5.0
0.0
600
800
1000
1200
1400
1600
1800
2000
2200
2400
2600
record number

Figure III.2

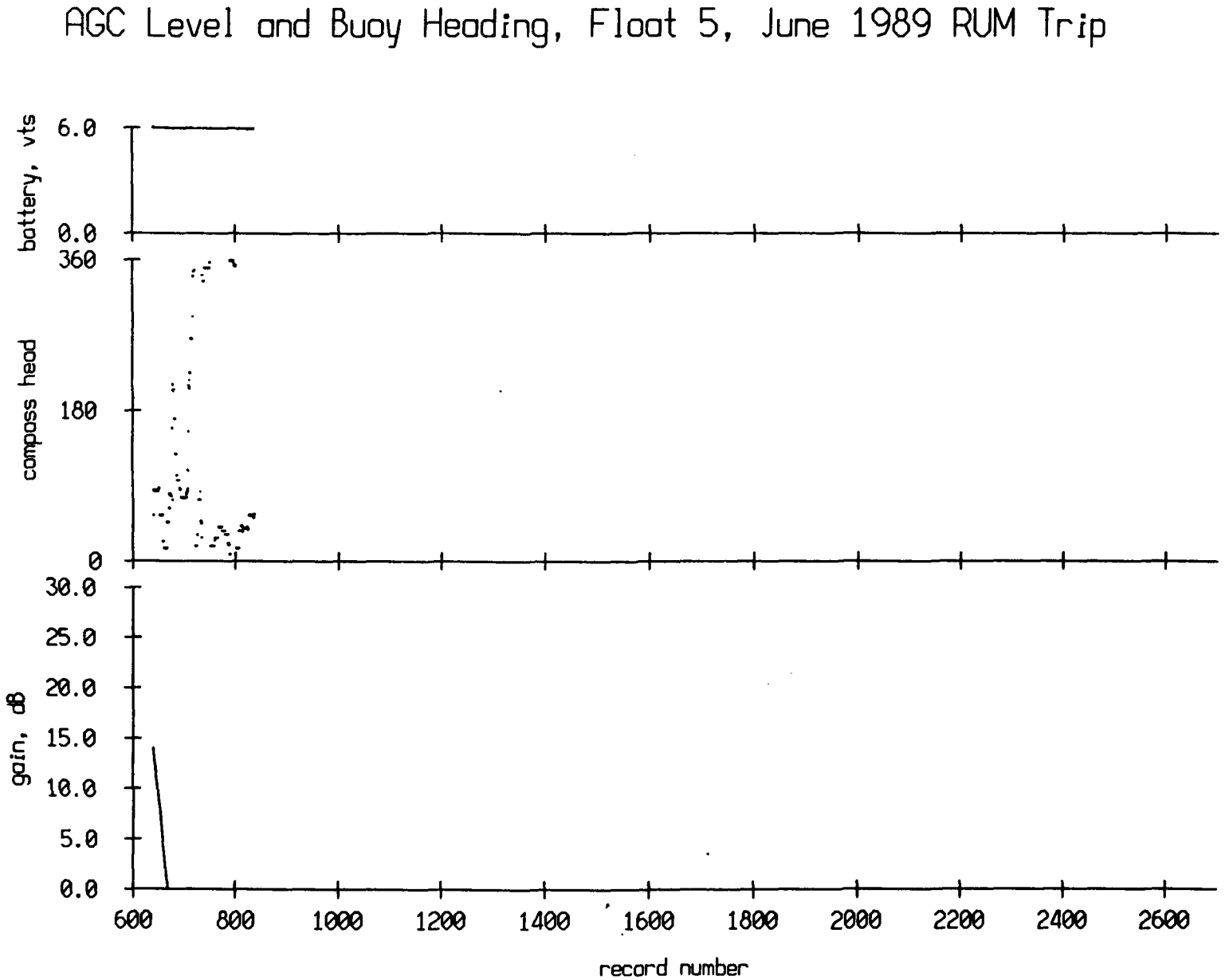
AGC Level and Buoy Heading, Float 5, June 1989 RUM Trip
battery, vts
6.0
0.0
compass head
360
180
0
gain, dB
30.0
25.0
20.0
15.0
10.0
5.0
0.0
600
800
1000
1200
1400
1600
1800
2000
2200
2400
2600
record number

Figure III.3

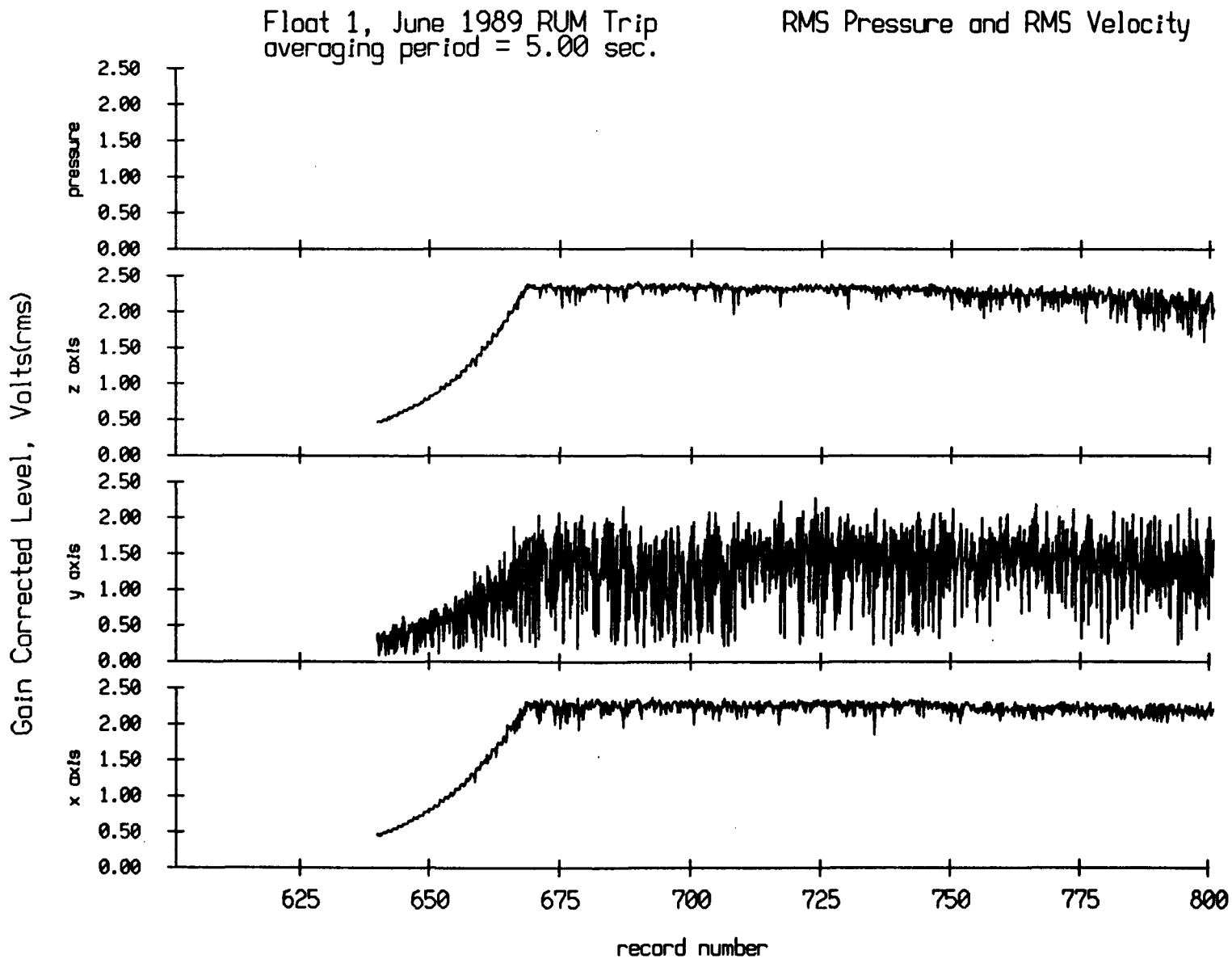
Float 1, June 1989 RUM Trip
averaging period = 5.00 sec.
RMS Pressure and RMS Velocity
Gain Corrected Level, Volts(rms)
pressure
z axis
y axis
x axis
2.50
2.00
1.50
1.00
0.50
0.00
625
650
675
700
725
750
775
800
record number

Figure IV.1a

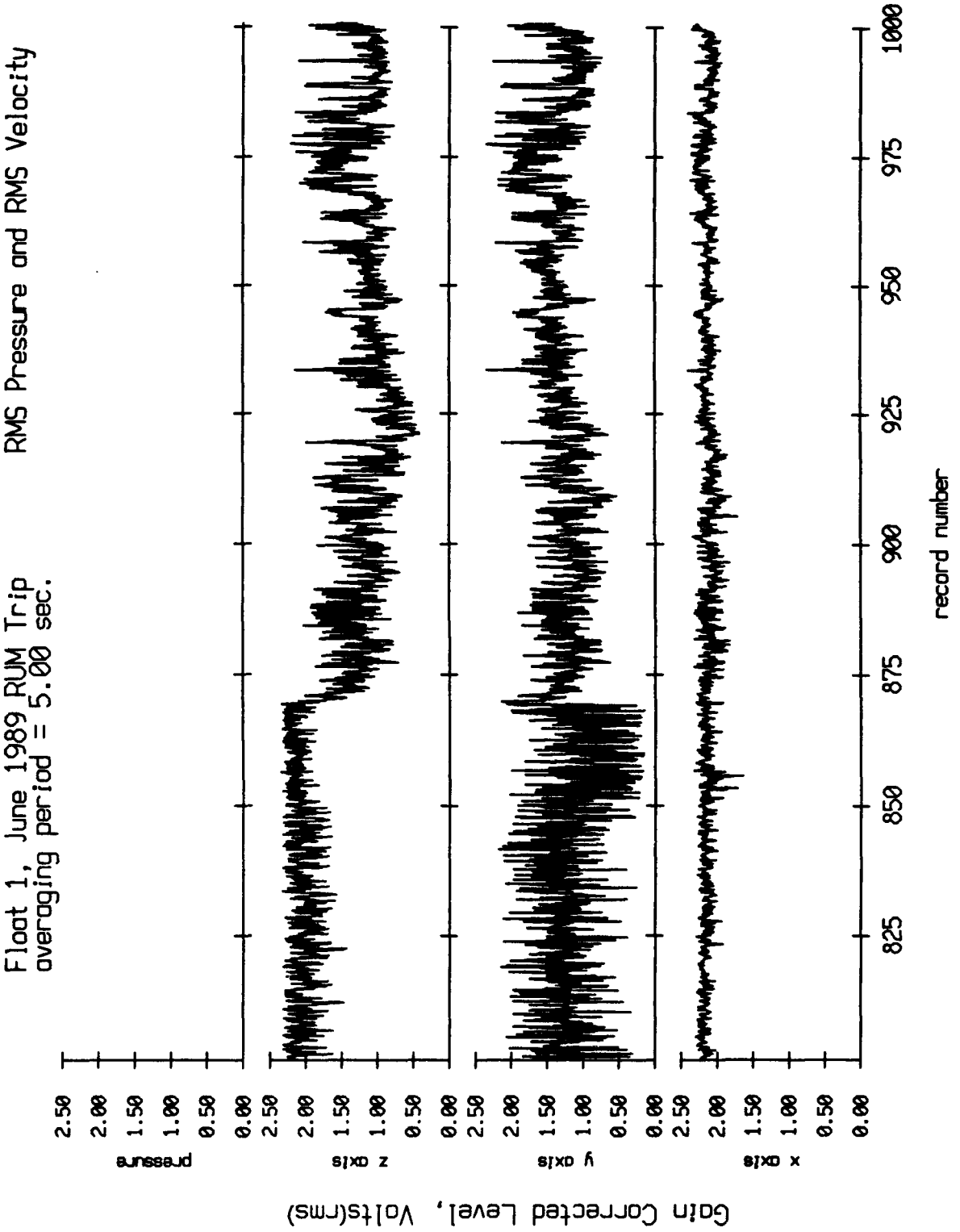
RMS Pressure and RMS Velocity
Float 1, June 1989 RUM Trip
averaging period = 5.00 sec.
Gain Corrected Level, Volts(rms)
pressure
z axis
y axis
x axis
2.50
2.00
1.50
1.00
0.50
0.00
825
850
875
900
925
950
975
1000
record number

Figure IV.1b

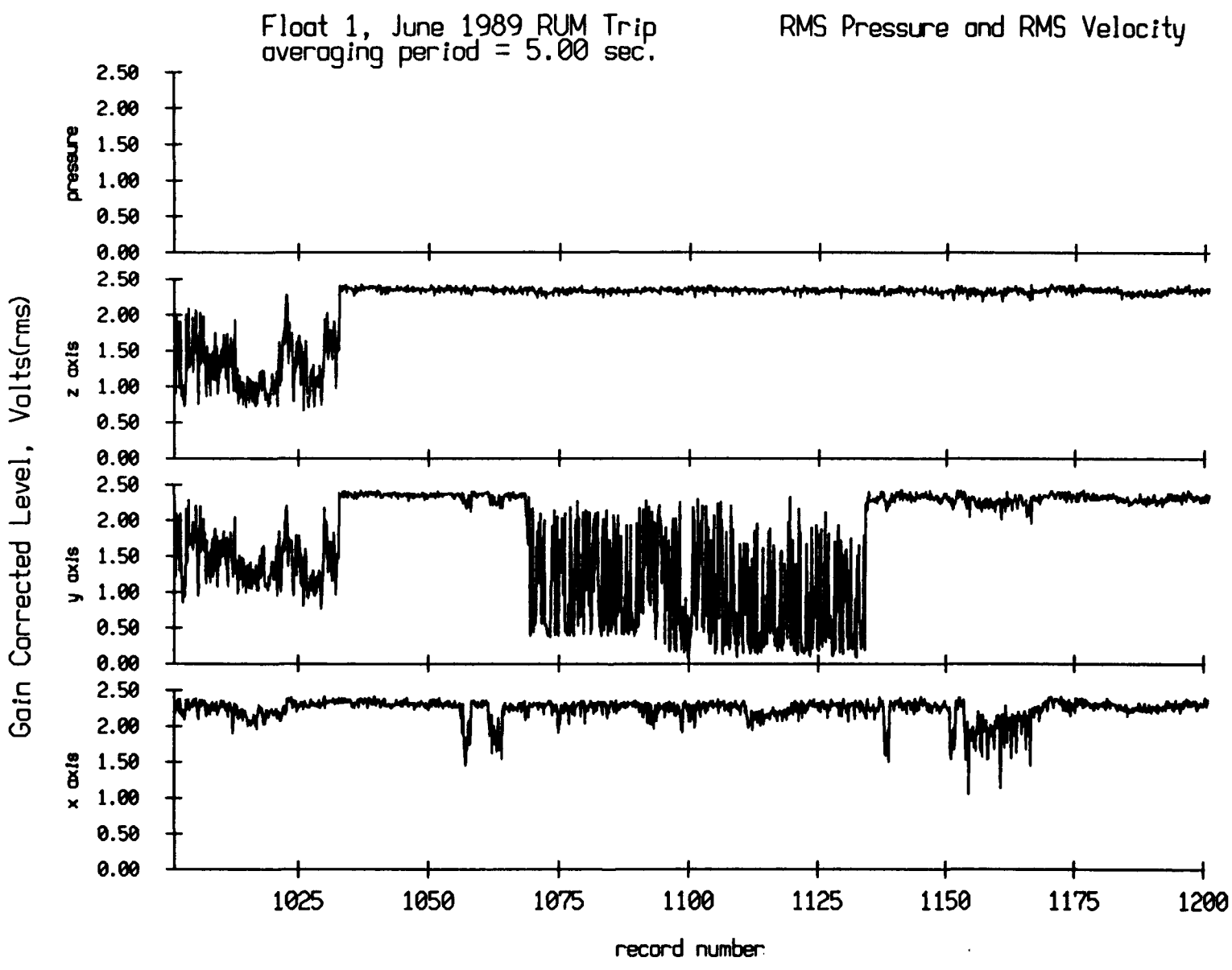
Float 1, June 1989 RUM Trip
averaging period = 5.00 sec.
RMS Pressure and RMS Velocity
Gain Corrected Level, Volts(rms)
pressure
z axis
y axis
x axis
2.50
2.00
1.50
1.00
0.50
0.00
1025
1050
1075
1100
1125
1150
1175
1200
record number

Figure IV.1c

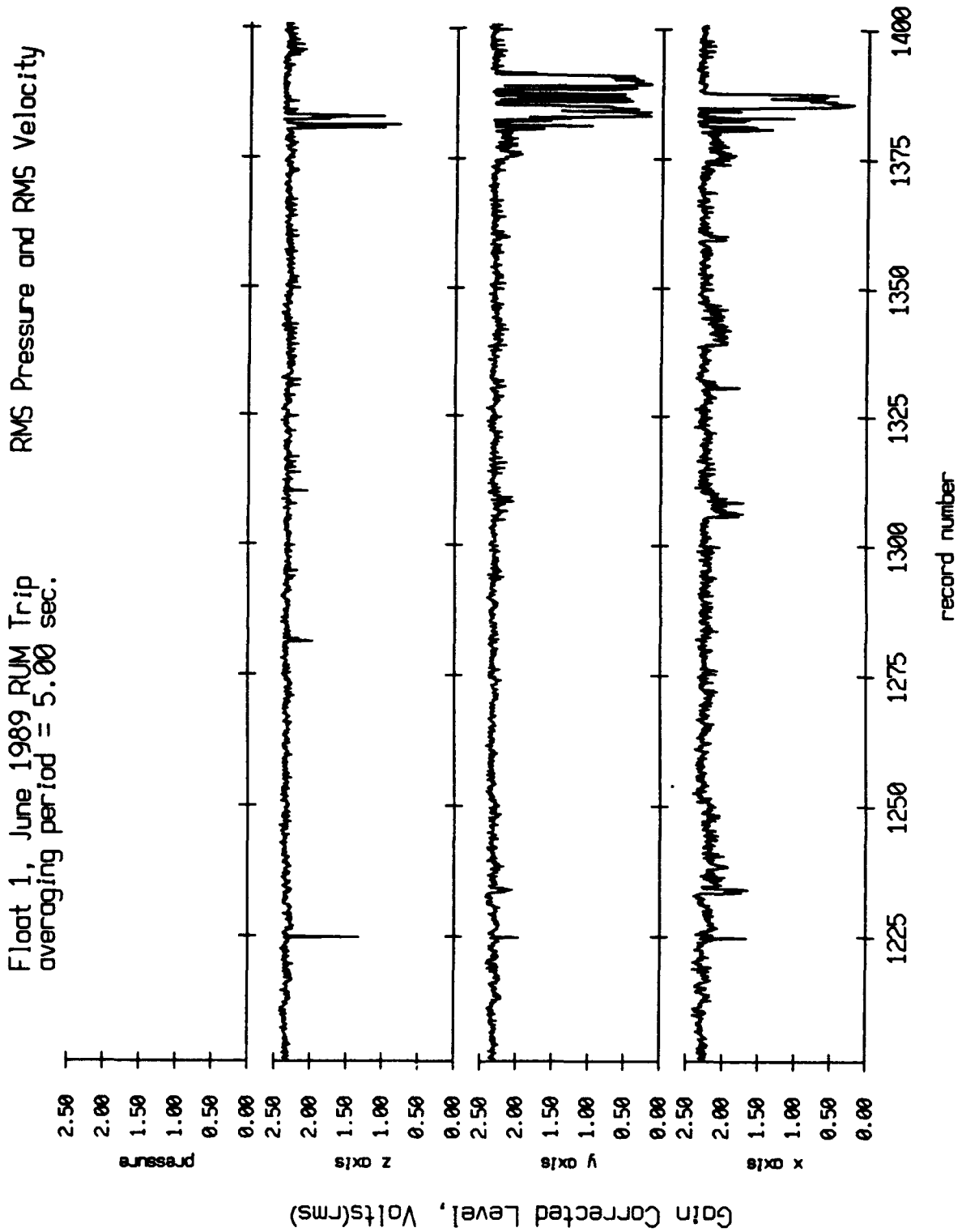
Float 1, June 1989 RUM Trip
averaging period = 5.00 sec.
RMS Pressure and RMS Velocity
Gain Corrected Level, Volts(rms)
pressure
z axis
y axis
x axis
2.50
2.00
1.50
1.00
0.50
0.00
1225
1250
1275
1300
1325
1350
1375
1400
record number

Figure IV.1d

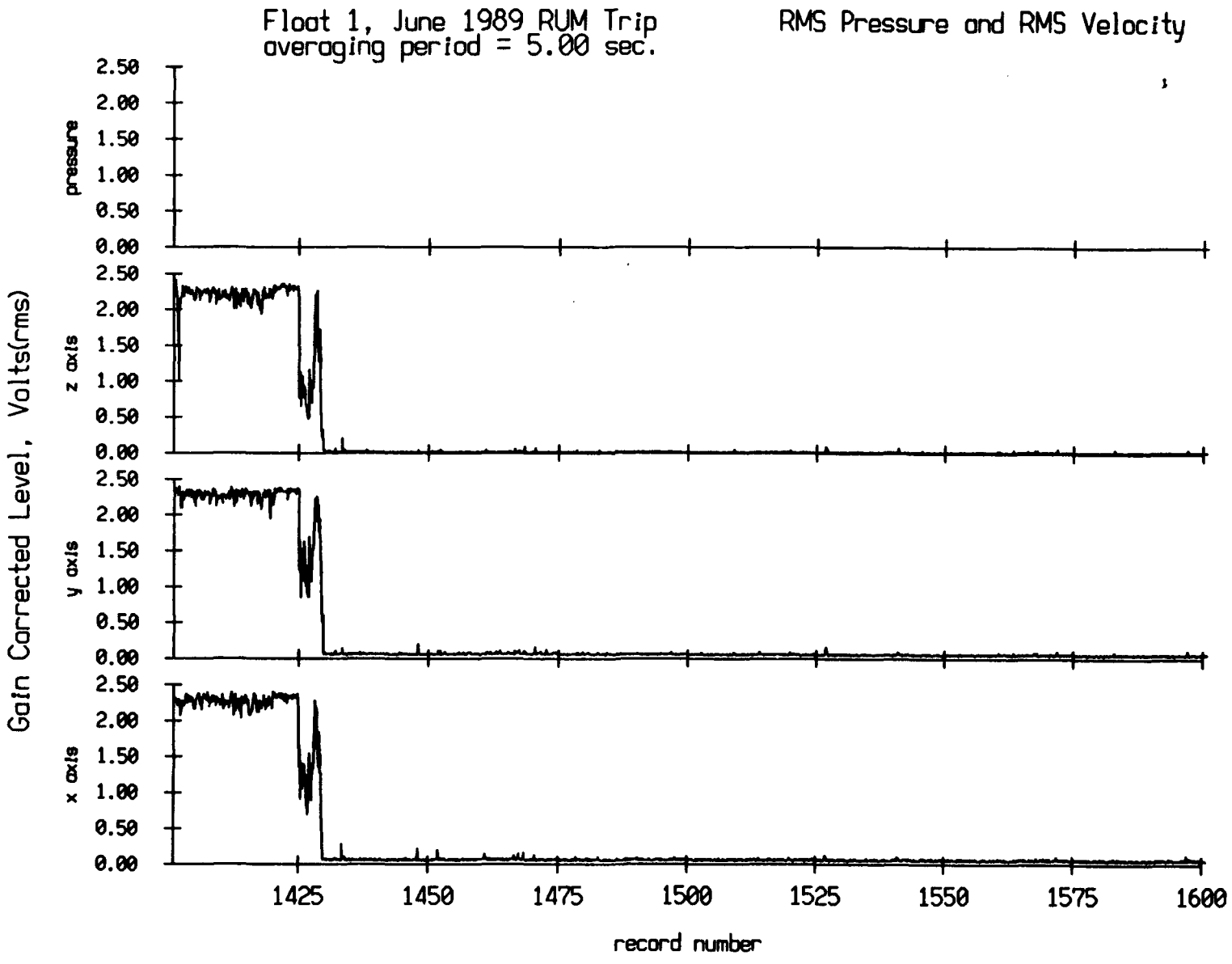
Float 1, June 1989 RUM Trip
averaging period = 5.00 sec.
RMS Pressure and RMS Velocity
Gain Corrected Level, Volts(rms)
pressure
z axis
y axis
x axis
2.50
2.00
1.50
1.00
0.50
0.00
1425
1450
1475
1500
1525
1550
1575
1600
record number

Figure IV.1e

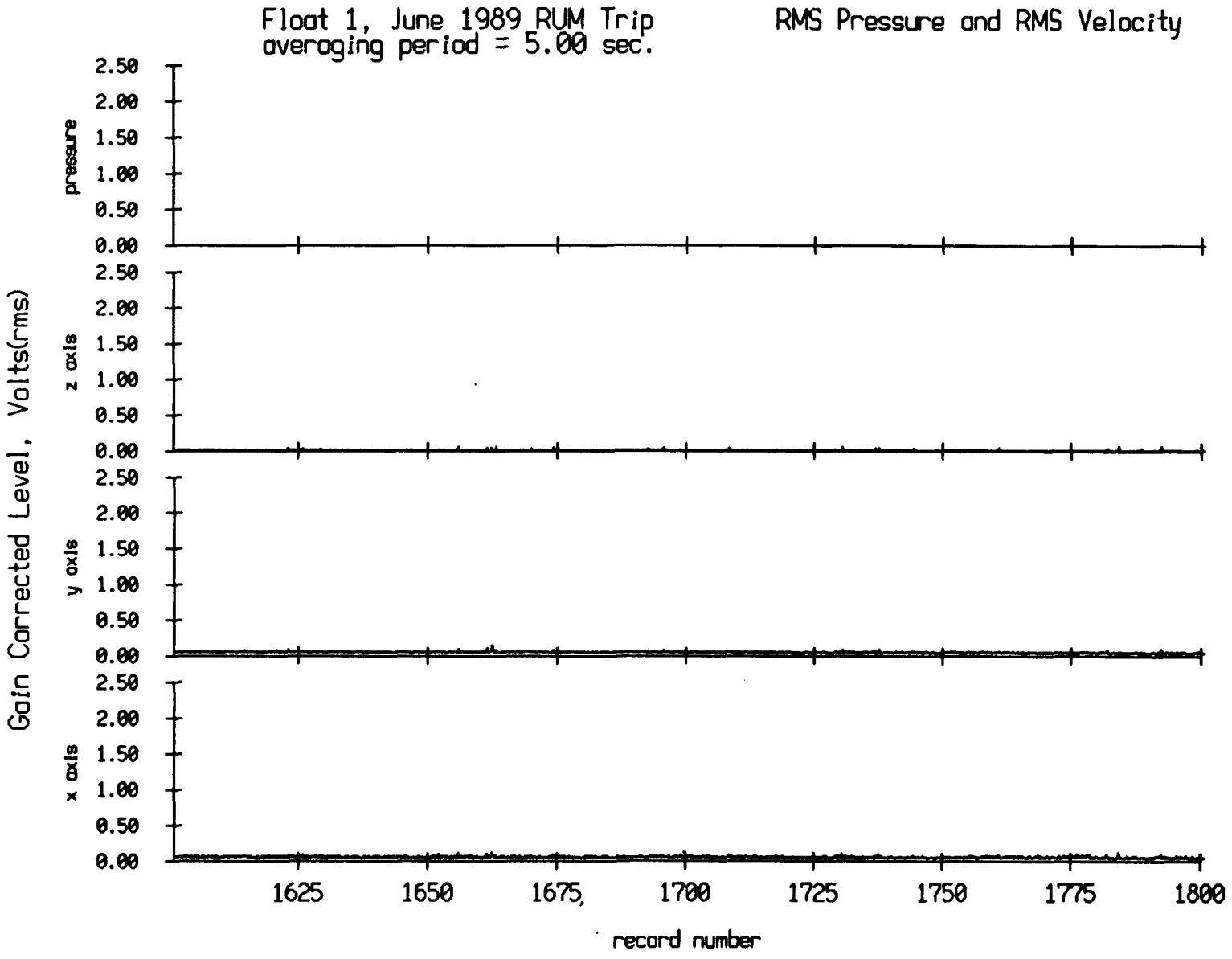
Float 1, June 1989 RUM Trip
averaging period = 5.00 sec.
RMS Pressure and RMS Velocity
Gain Corrected Level, Volts(rms)
pressure
z axis
y axis
x axis
2.50
2.00
1.50
1.00
0.50
0.00
1625
1650
1675
1700
1725
1750
1775
1800
record number

Figure IV.1f

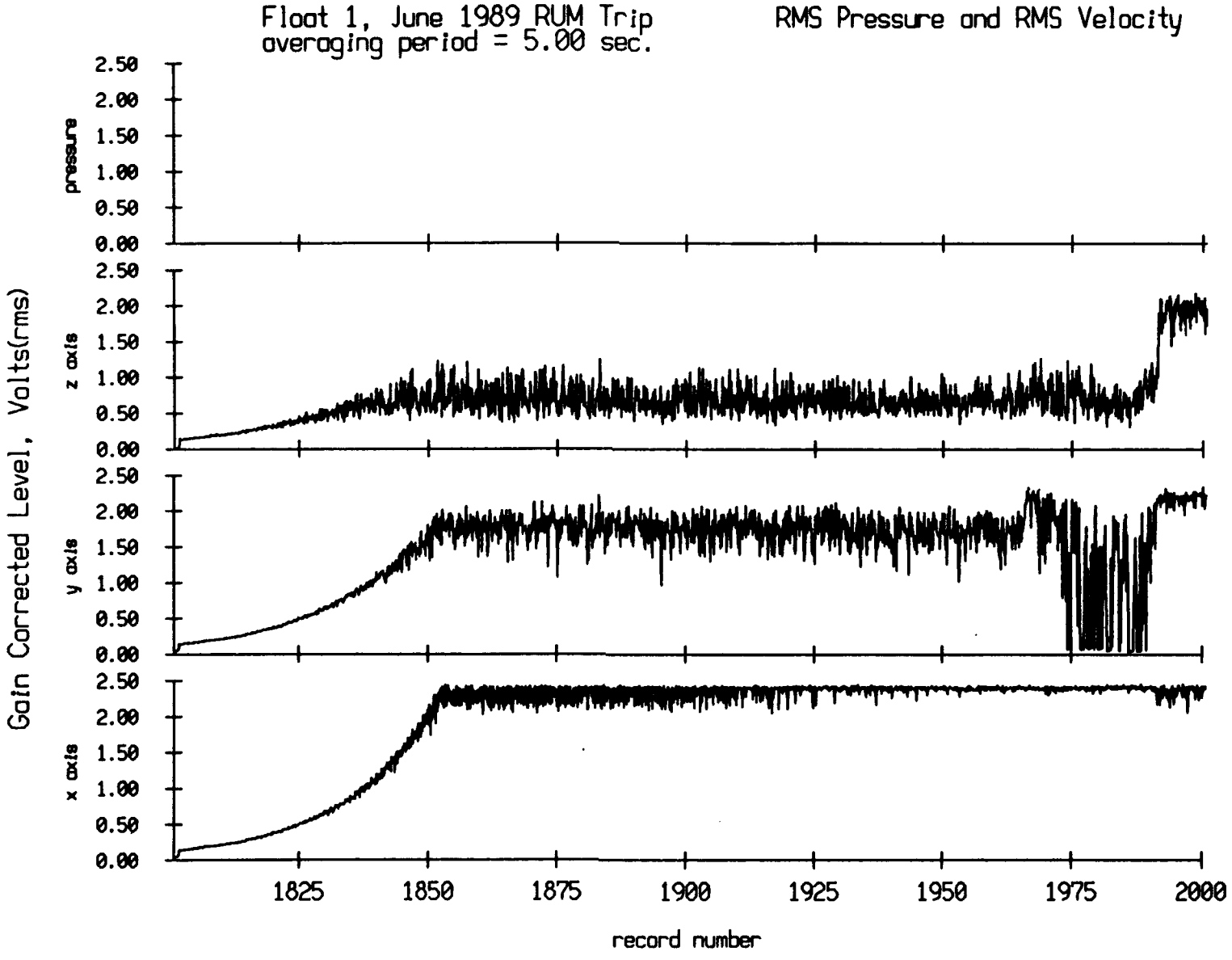
Float 1, June 1989 RUM Trip
averaging period = 5.00 sec.
RMS Pressure and RMS Velocity
Gain Corrected Level, Volts(rms)
pressure
z axis
y axis
x axis
2.50
2.00
1.50
1.00
0.50
0.00
1825
1850
1875
1900
1925
1950
1975
2000
record number

Figure IV.1g

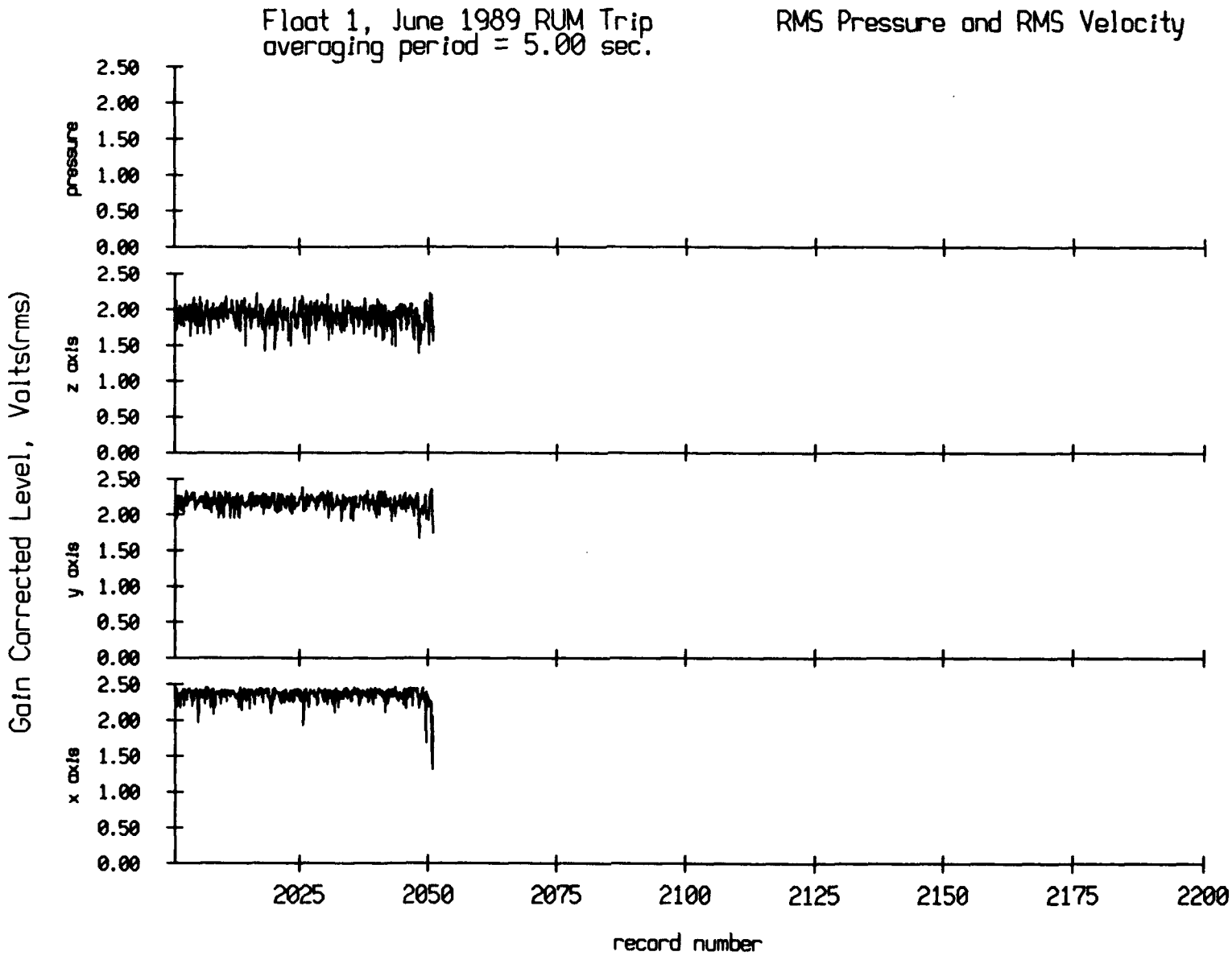
Float 1, June 1989 RUM Trip
averaging period = 5.00 sec.
RMS Pressure and RMS Velocity
Gain Corrected Level, Volts(rms)
pressure
z axis
y axis
x axis
2.50
2.00
1.50
1.00
0.50
0.00
2025
2050
2075
2100
2125
2150
2175
2200
record number

Figure IV.1h

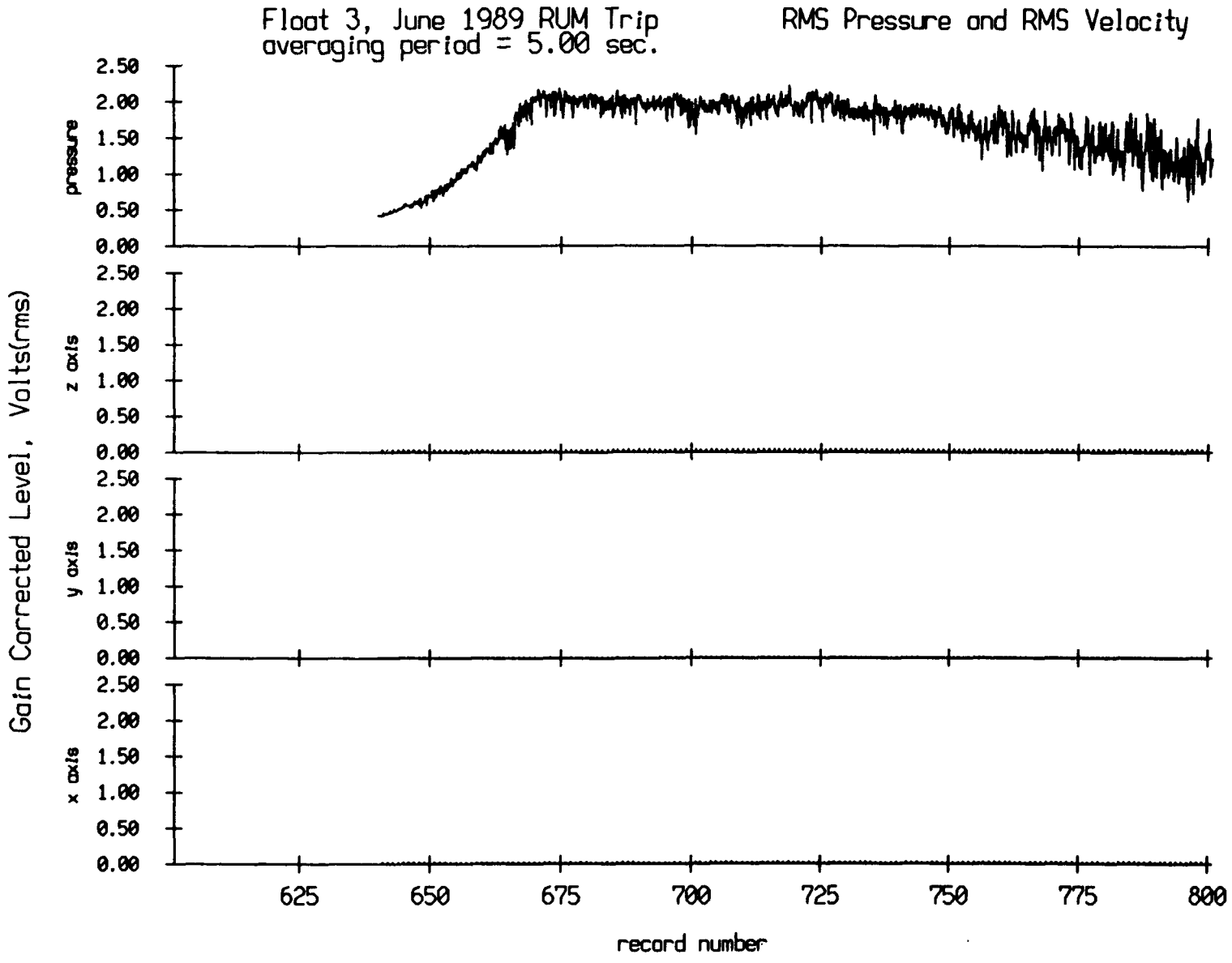
Float 3, June 1989 RUM Trip
averaging period = 5.00 sec.
RMS Pressure and RMS Velocity
Gain Corrected Level, Volts(rms)
pressure
z axis
y axis
x axis
2.50
2.00
1.50
1.00
0.50
0.00
625
650
675
700
725
750
775
800
record number

Figure IV.2a

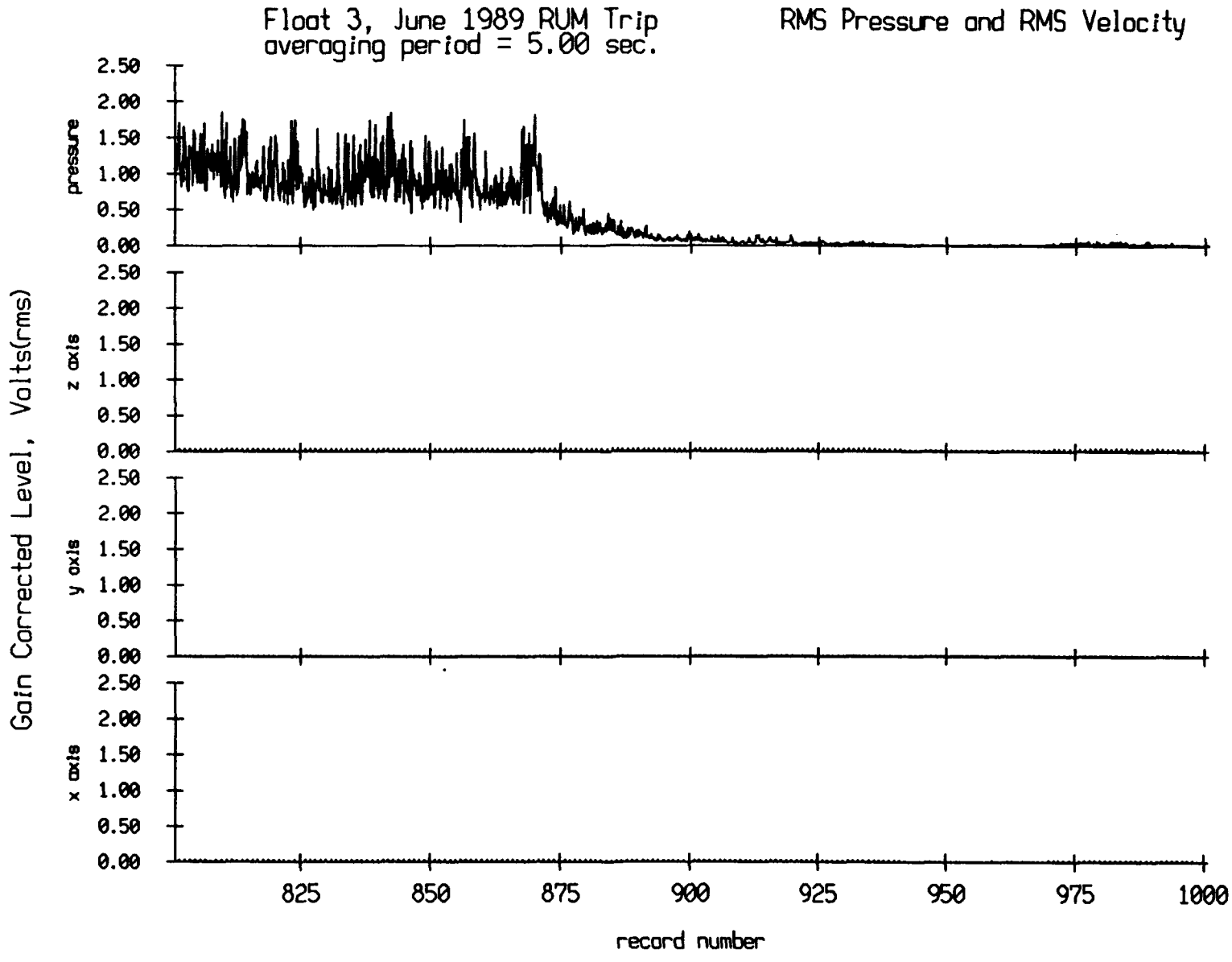
Float 3, June 1989 RUM Trip
averaging period = 5.00 sec.
RMS Pressure and RMS Velocity
Gain Corrected Level, Volts(rms)
pressure
z axis
y axis
x axis
2.50
2.00
1.50
1.00
0.50
0.00
825
850
875
900
925
950
975
1000
record number

Figure IV.2b

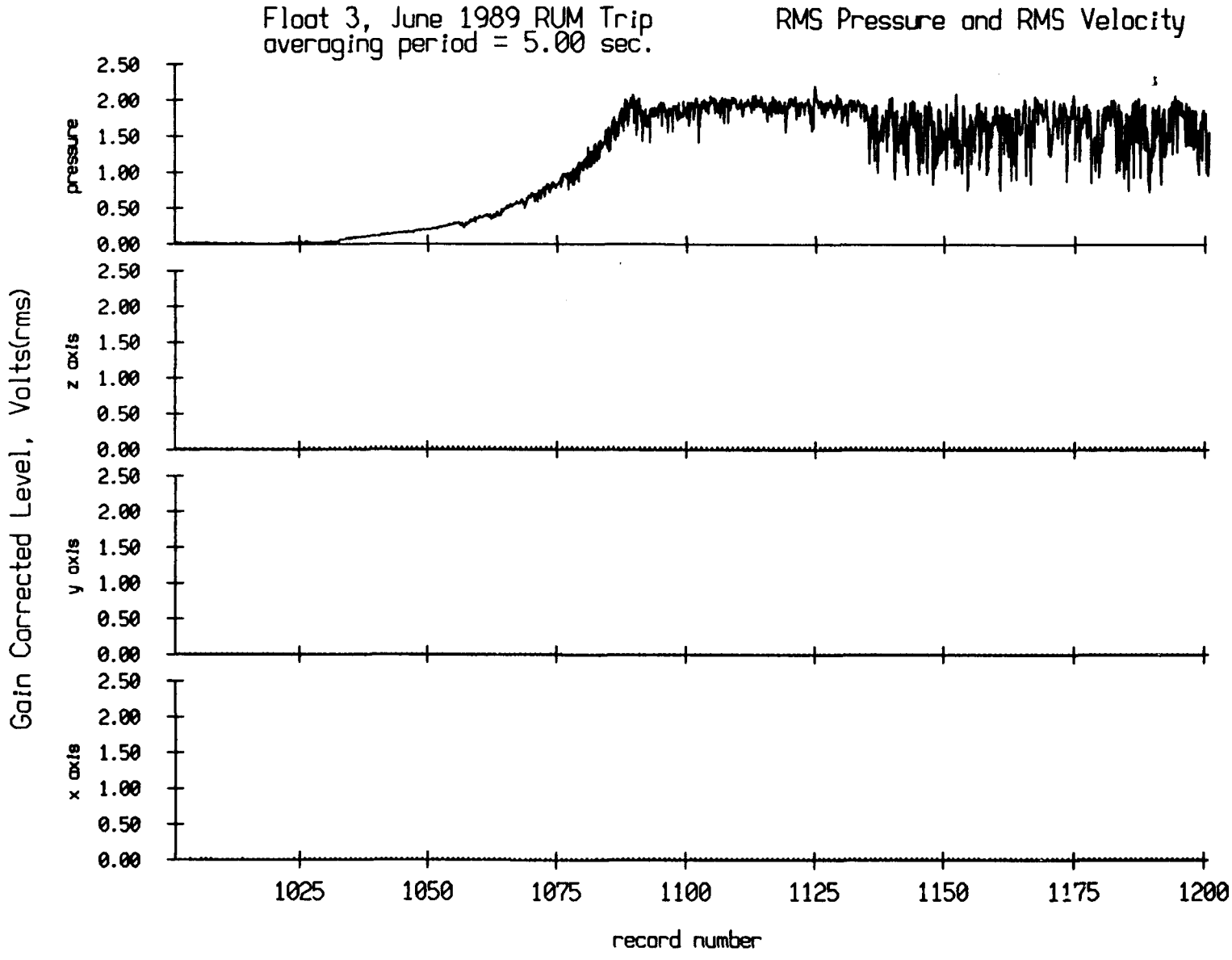
Float 3, June 1989 RUM Trip
averaging period = 5.00 sec.
RMS Pressure and RMS Velocity
Gain Corrected Level, Volts(rms)
pressure
z axis
y axis
x axis
2.50
2.00
1.50
1.00
0.50
0.00
1025
1050
1075
1100
1125
1150
1175
1200
record number

Figure IV.2c

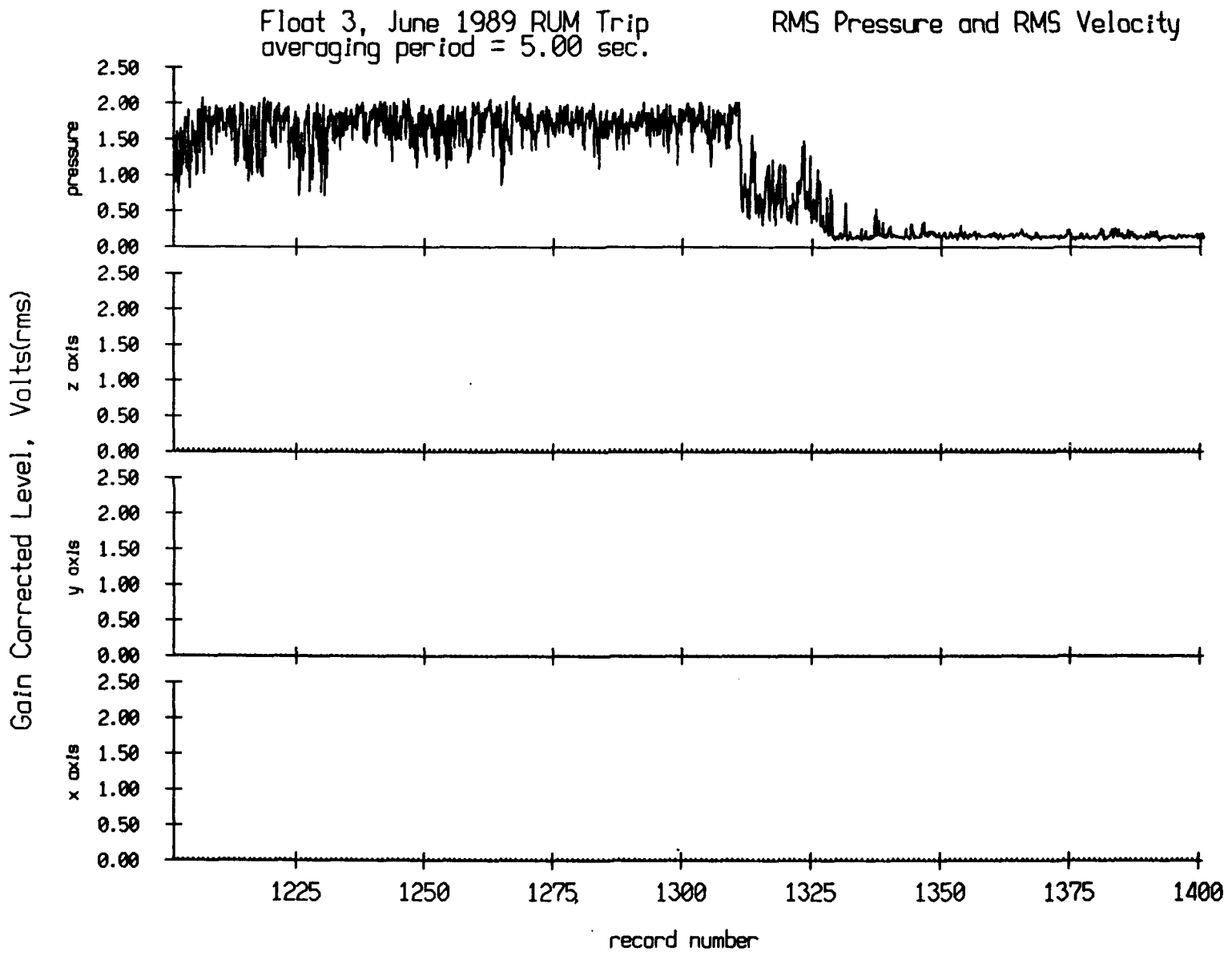
Float 3, June 1989 RUM Trip
averaging period = 5.00 sec.
RMS Pressure and RMS Velocity
Gain Corrected Level, Volts(rms)
pressure
z axis
y axis
x axis
2.50
2.00
1.50
1.00
0.50
0.00
1225
1250
1275
1300
1325
1350
1375
1400
record number

Figure IV.2d

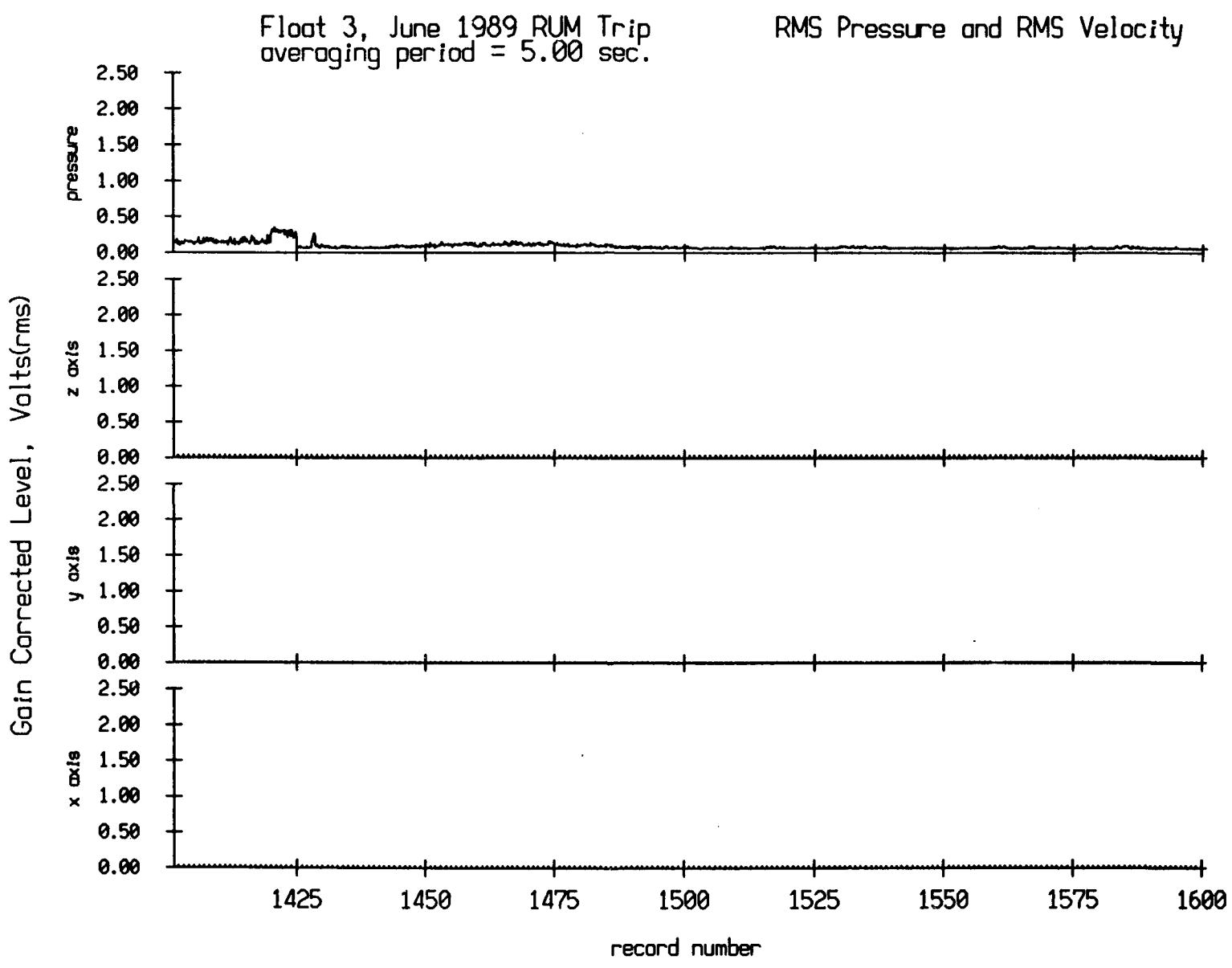
Float 3, June 1989 RUM Trip
averaging period = 5.00 sec.
RMS Pressure and RMS Velocity
Gain Corrected Level, Volts(rms)
pressure
z axis
y axis
x axis
2.50
2.00
1.50
1.00
0.50
0.00
1425
1450
1475
1500
1525
1550
1575
1600
record number

Figure IV.2e

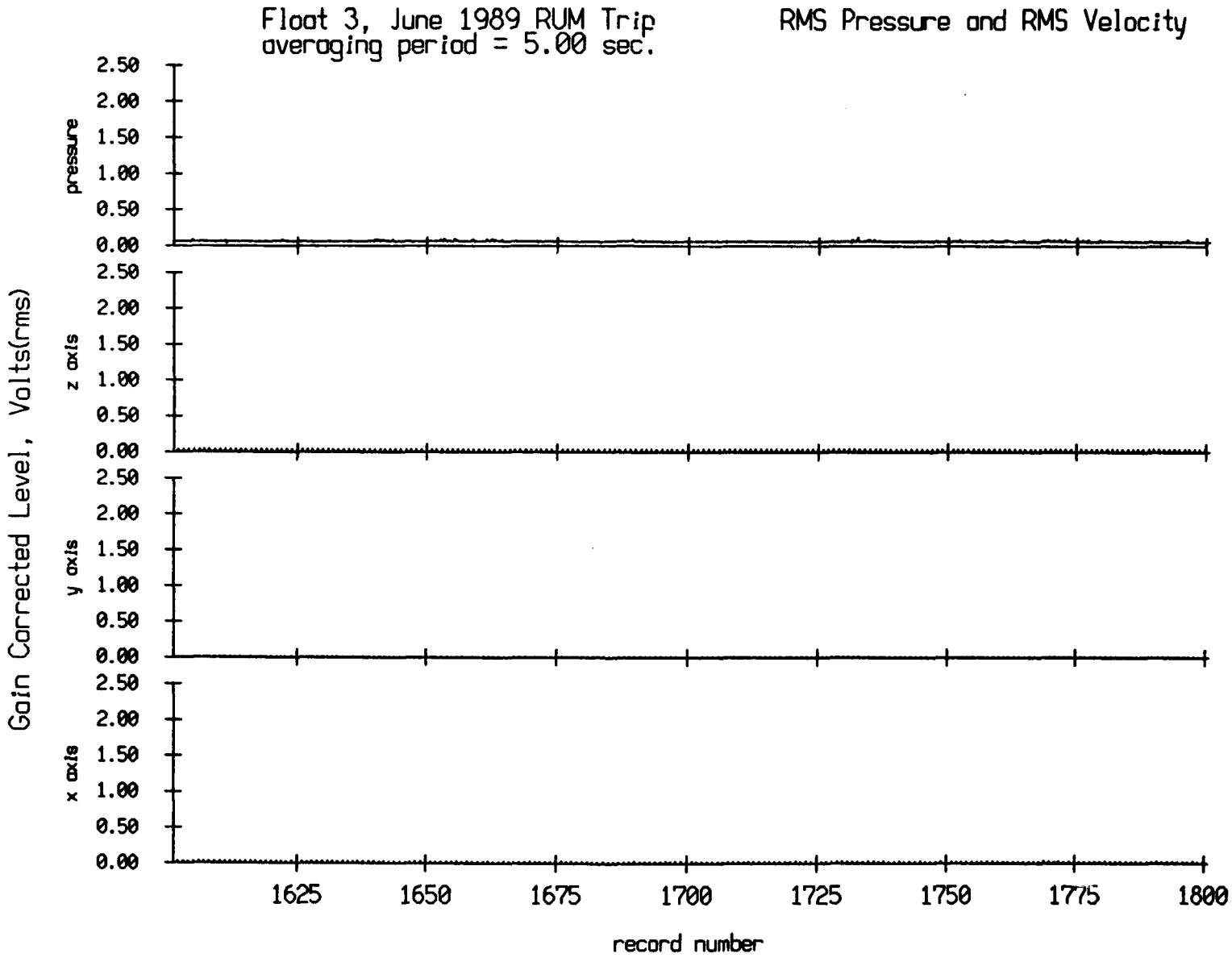
Float 3, June 1989 RUM Trip
averaging period = 5.00 sec.
RMS Pressure and RMS Velocity
Gain Corrected Level, Volts(rms)
pressure
z axis
y axis
x axis
2.50
2.00
1.50
1.00
0.50
0.00
1625
1650
1675
1700
1725
1750
1775
1800
record number

Figure IV.2f

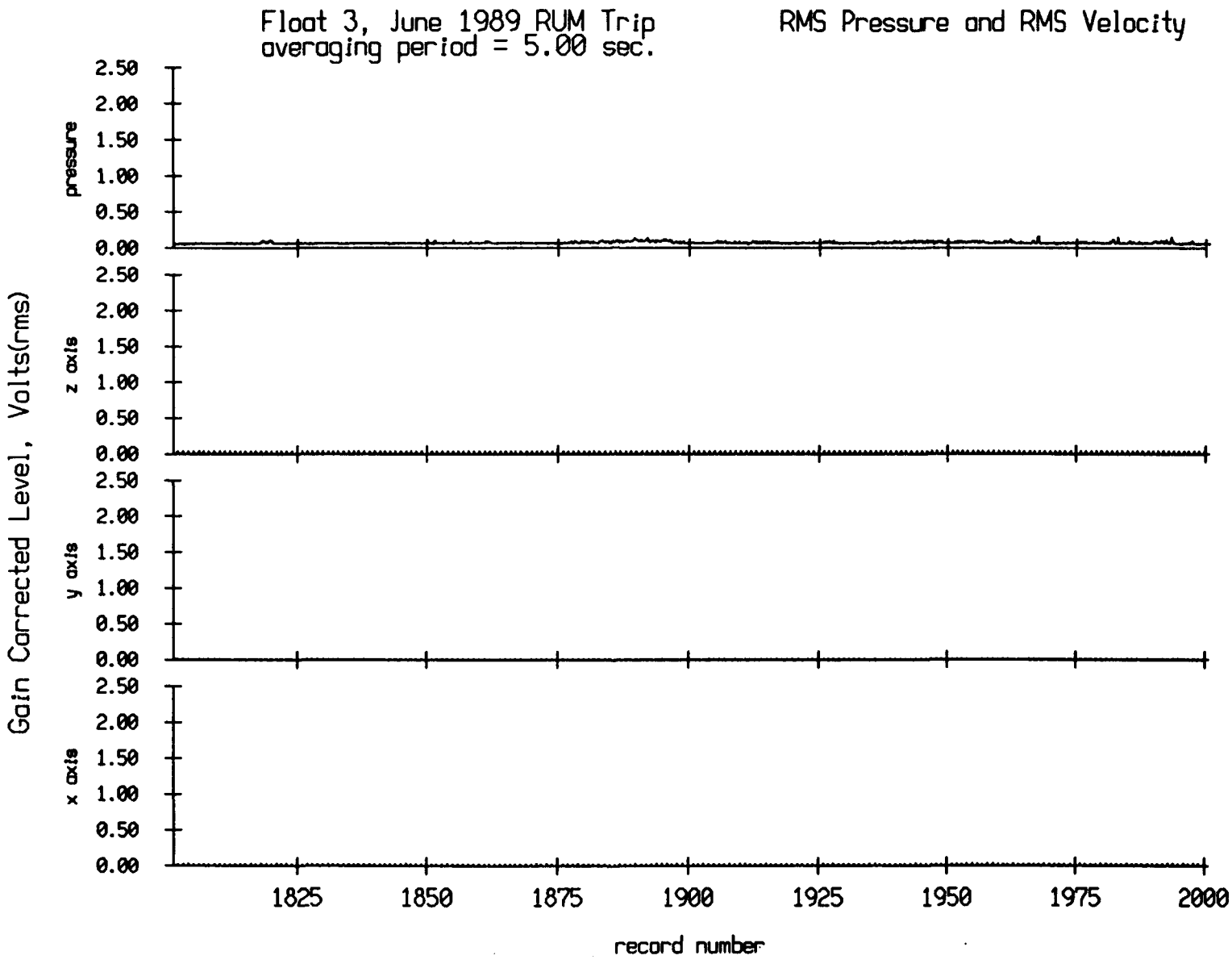
Float 3, June 1989 RUM Trip
averaging period = 5.00 sec.
RMS Pressure and RMS Velocity
Gain Corrected Level, Volts(rms)
pressure
z axis
y axis
x axis
2.50
2.00
1.50
1.00
0.50
0.00
1825
1850
1875
1900
1925
1950
1975
2000
record number

Figure IV.28

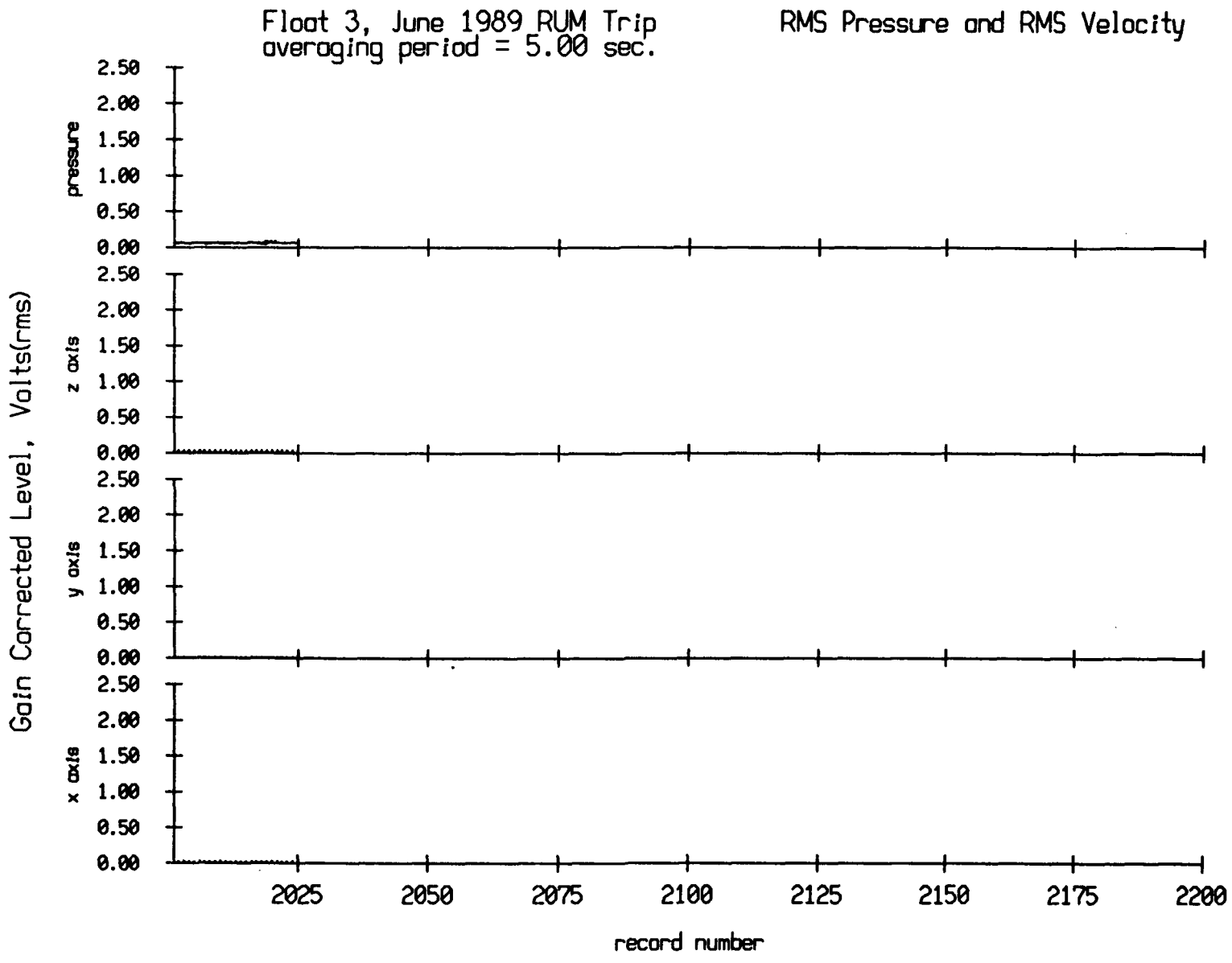
Float 3, June 1989 RUM Trip
averaging period = 5.00 sec.
RMS Pressure and RMS Velocity
Gain Corrected Level, Volts(rms)
pressure
z axis
y axis
x axis
2.50
2.00
1.50
1.00
0.50
0.00
2025
2050
2075
2100
2125
2150
2175
2200
record number

Figure IV.2h

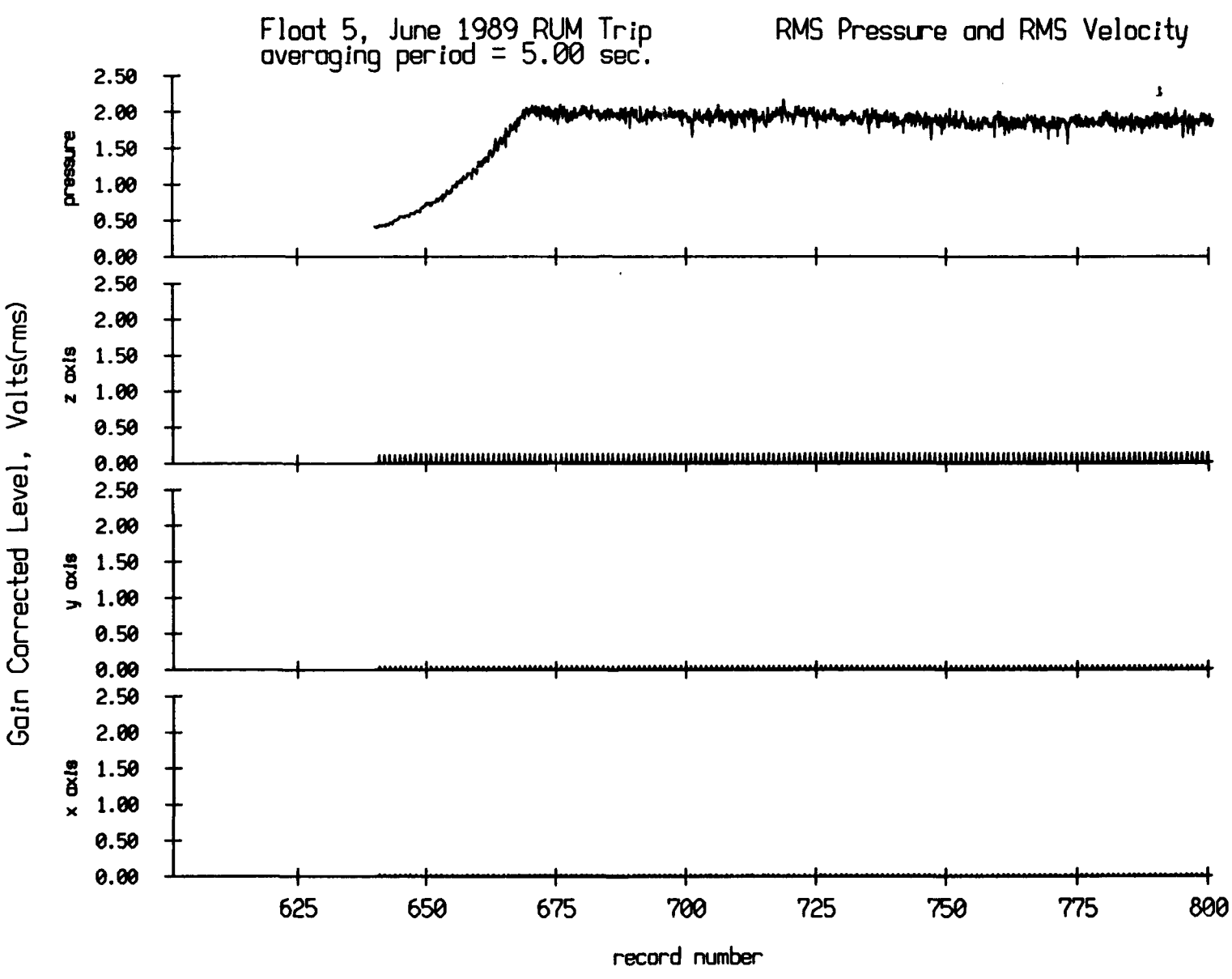
Float 5, June 1989 RUM Trip
averaging period = 5.00 sec.
RMS Pressure and RMS Velocity
Gain Corrected Level, Volts(rms)
pressure
z axis
y axis
x axis
2.50
2.00
1.50
1.00
0.50
0.00
625
650
675
700
725
750
775
800
record number

Figure IV.3a

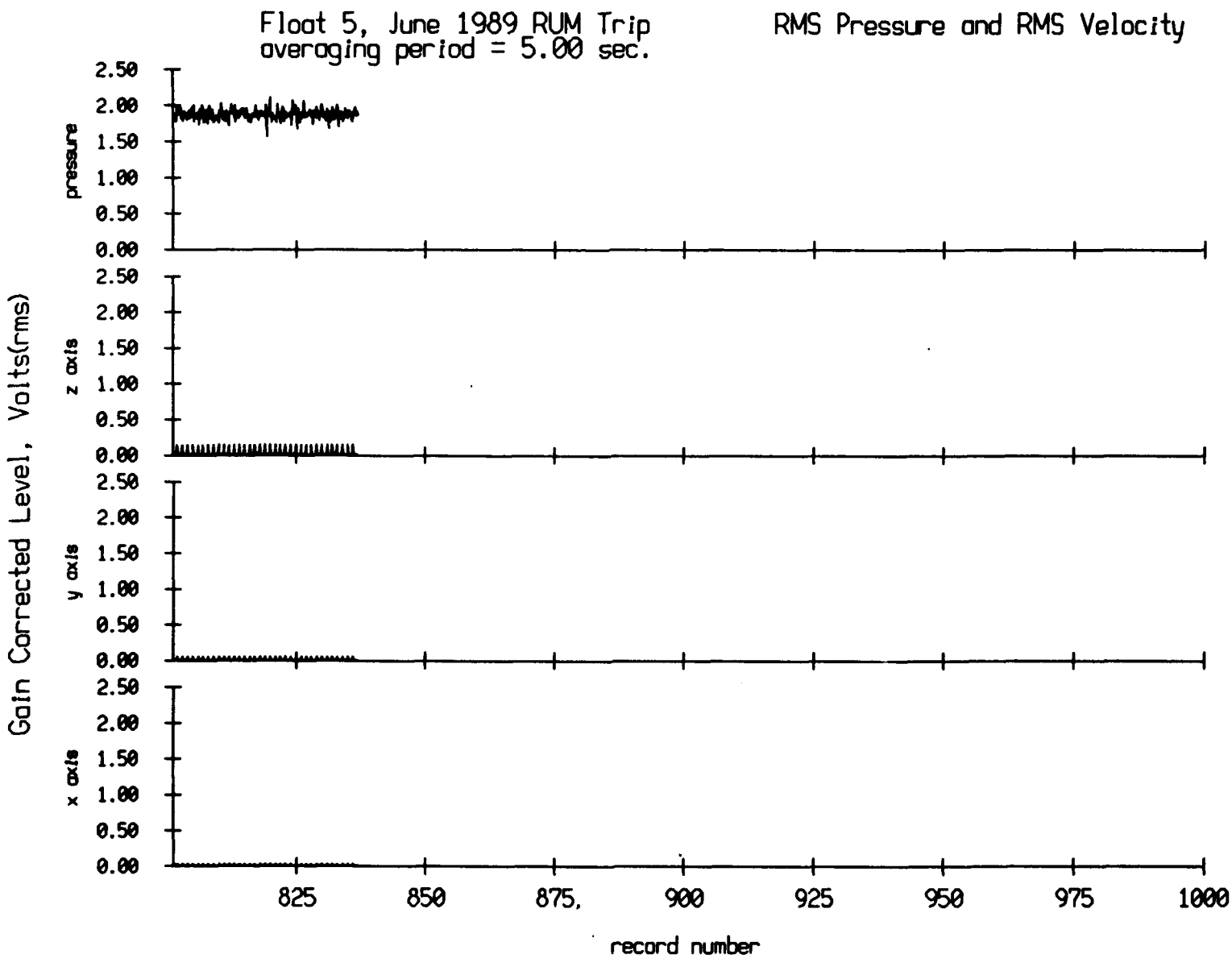
Float 5, June 1989 RUM Trip
overaging period = 5.00 sec.
RMS Pressure and RMS Velocity
Gain Corrected Level, Volts(rms)
pressure
z axis
y axis
x axis
2.50
2.00
1.50
1.00
0.50
0.00
825
850
875
900
925
950
975
1000
record number

Figure IV.3b

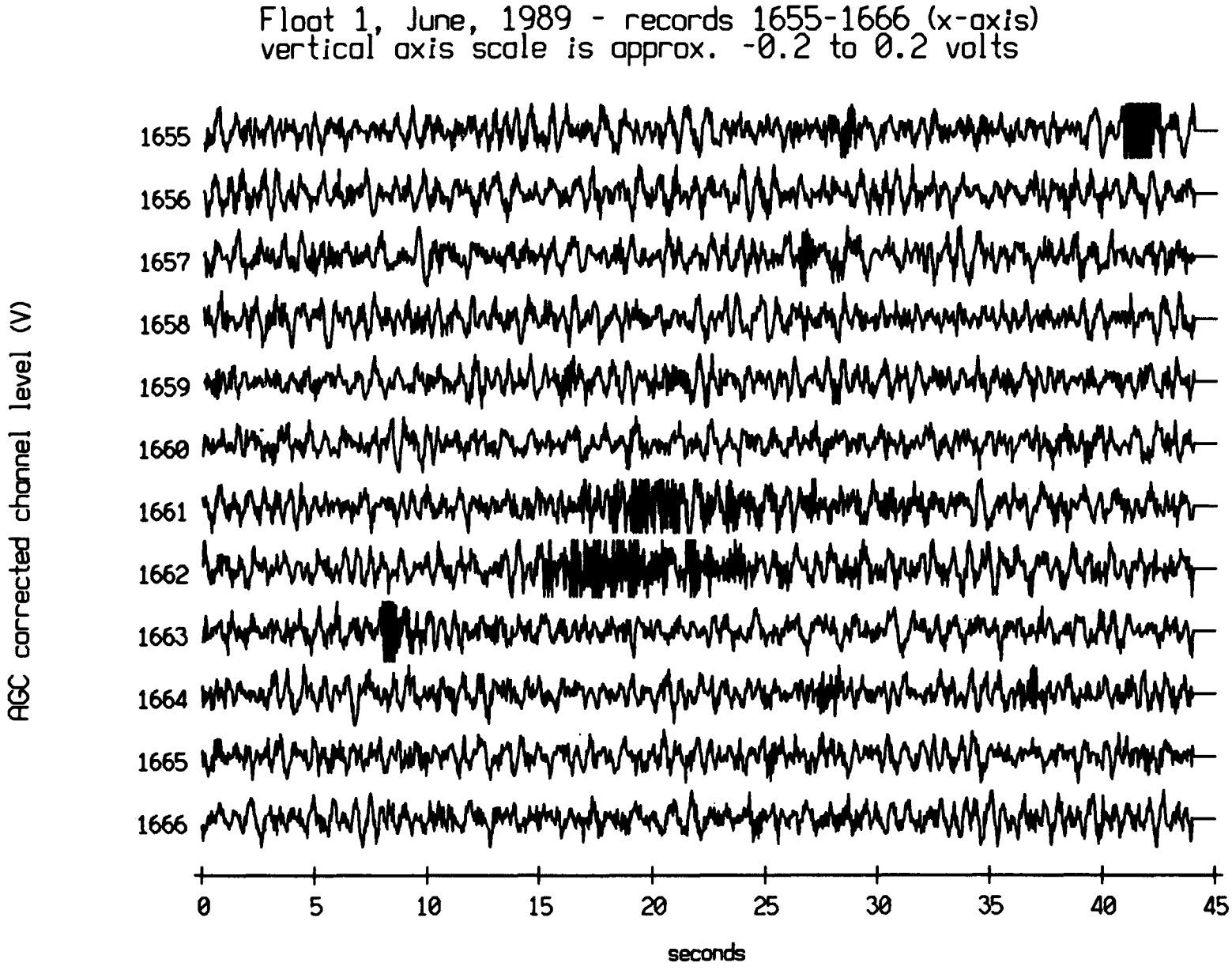
Float 1, June, 1989 - records 1655-1666 (x-axis)
vertical axis scale is approx. -0.2 to 0.2 volts
1655
1656
1657
1658
1659
1660
1661
1662
1663
1664
1665
1666
AGC corrected channel level (V)
0
5
10
15
20
25
30
35
40
45
seconds

Figure V.1a

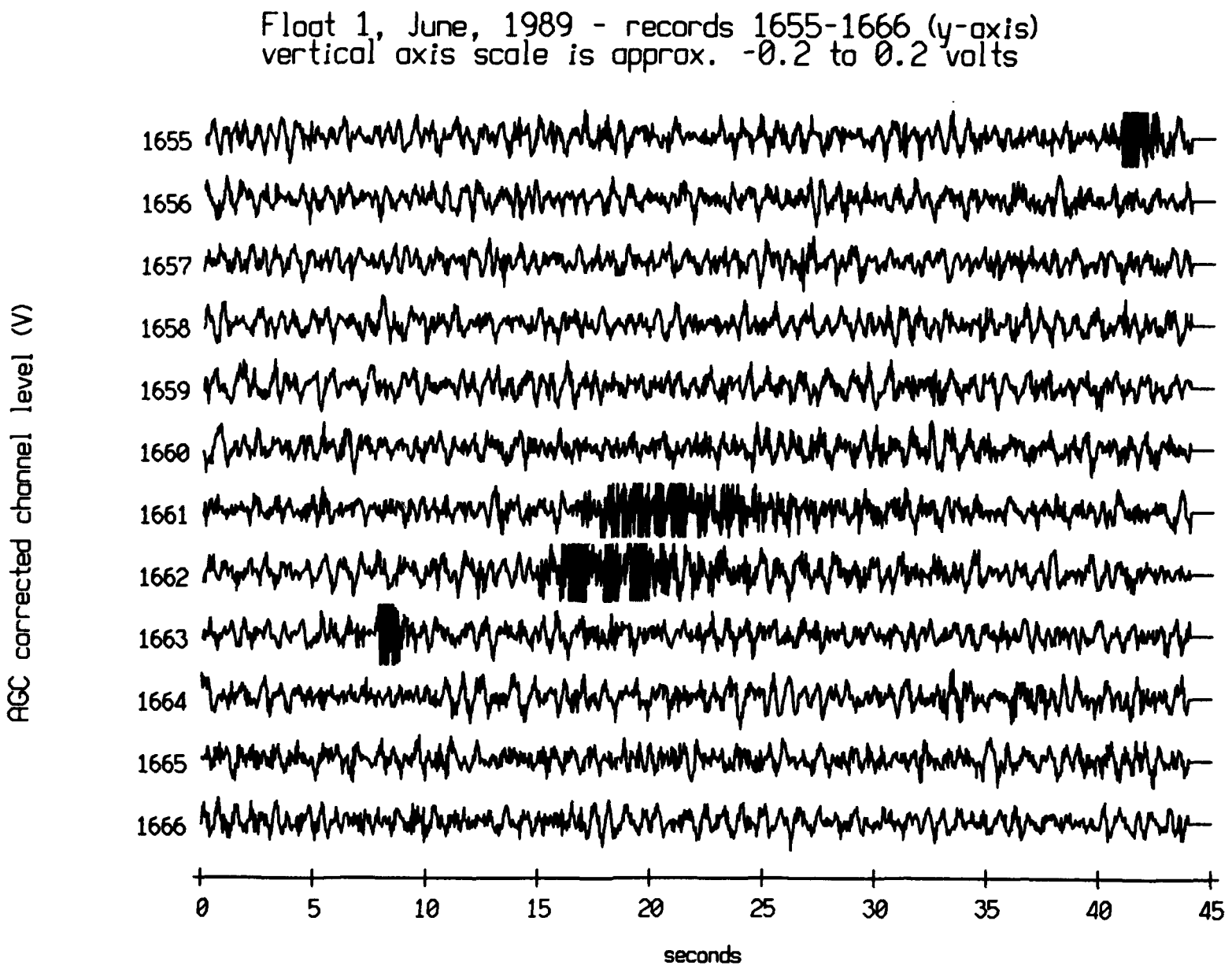
Float 1, June, 1989 - records 1655-1666 (y-axis)
vertical axis scale is approx. -0.2 to 0.2 volts
AGC corrected channel level (V)
1655
1656
1657
1658
1659
1660
1661
1662
1663
1664
1665
1666
0
5
10
15
20
25
30
35
40
45
seconds

Figure V.1b

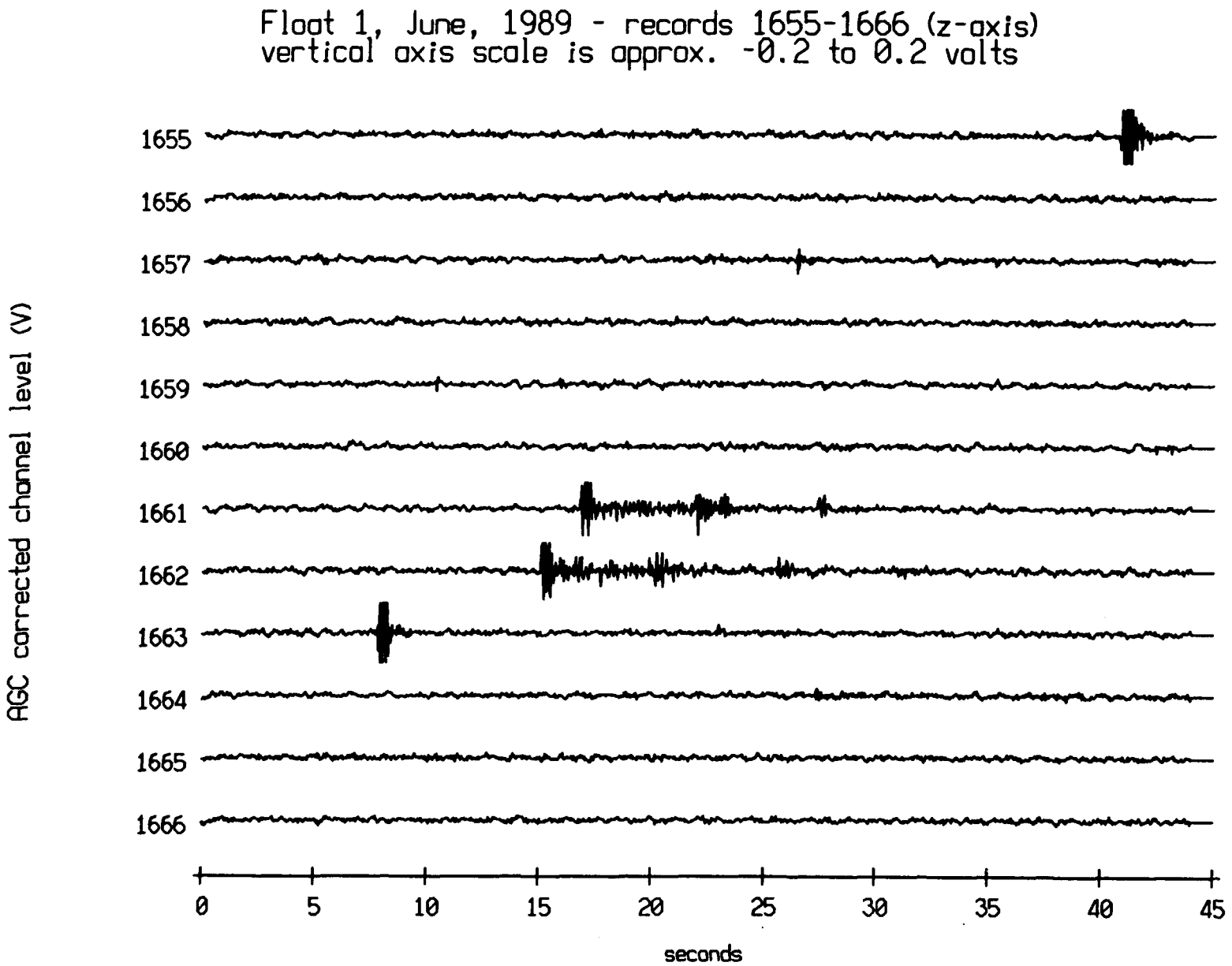
Float 1, June, 1989 - records 1655-1666 (z-axis)
vertical axis scale is approx. -0.2 to 0.2 volts
1655
1656
1657
1658
1659
1660
1661
1662
1663
1664
1665
1666
AGC corrected channel level (V)
0
5
10
15
20
25
30
35
40
45
seconds

Figure V.1c

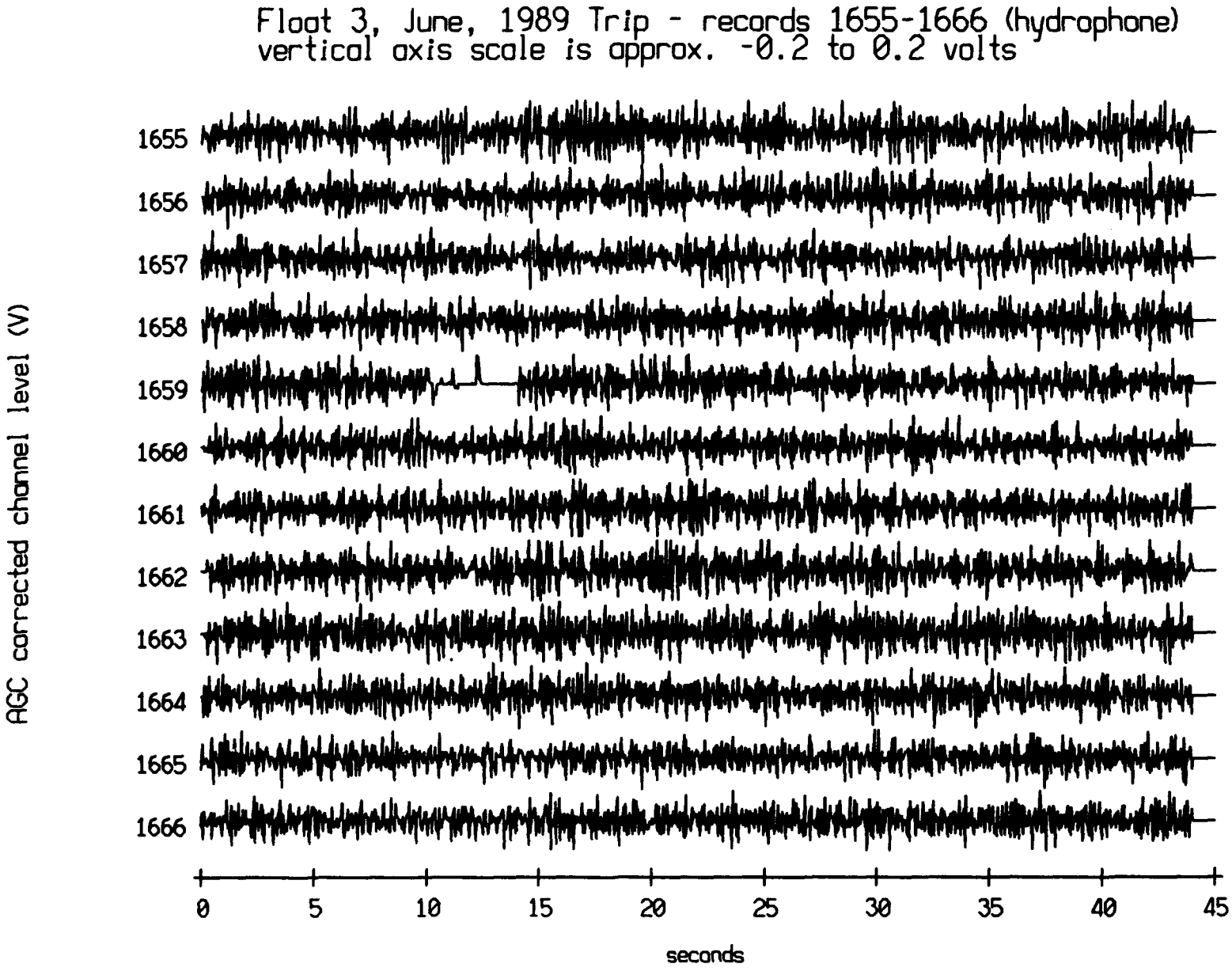
Float 3, June, 1989 Trip - records 1655-1666 (hydrophone)
vertical axis scale is approx. -0.2 to 0.2 volts
1655
1656
1657
1658
1659
1660
1661
1662
1663
1664
1665
1666
0
5
10
15
20
25
30
35
40
45
seconds
AGC corrected channel level (V)

Figure V.2

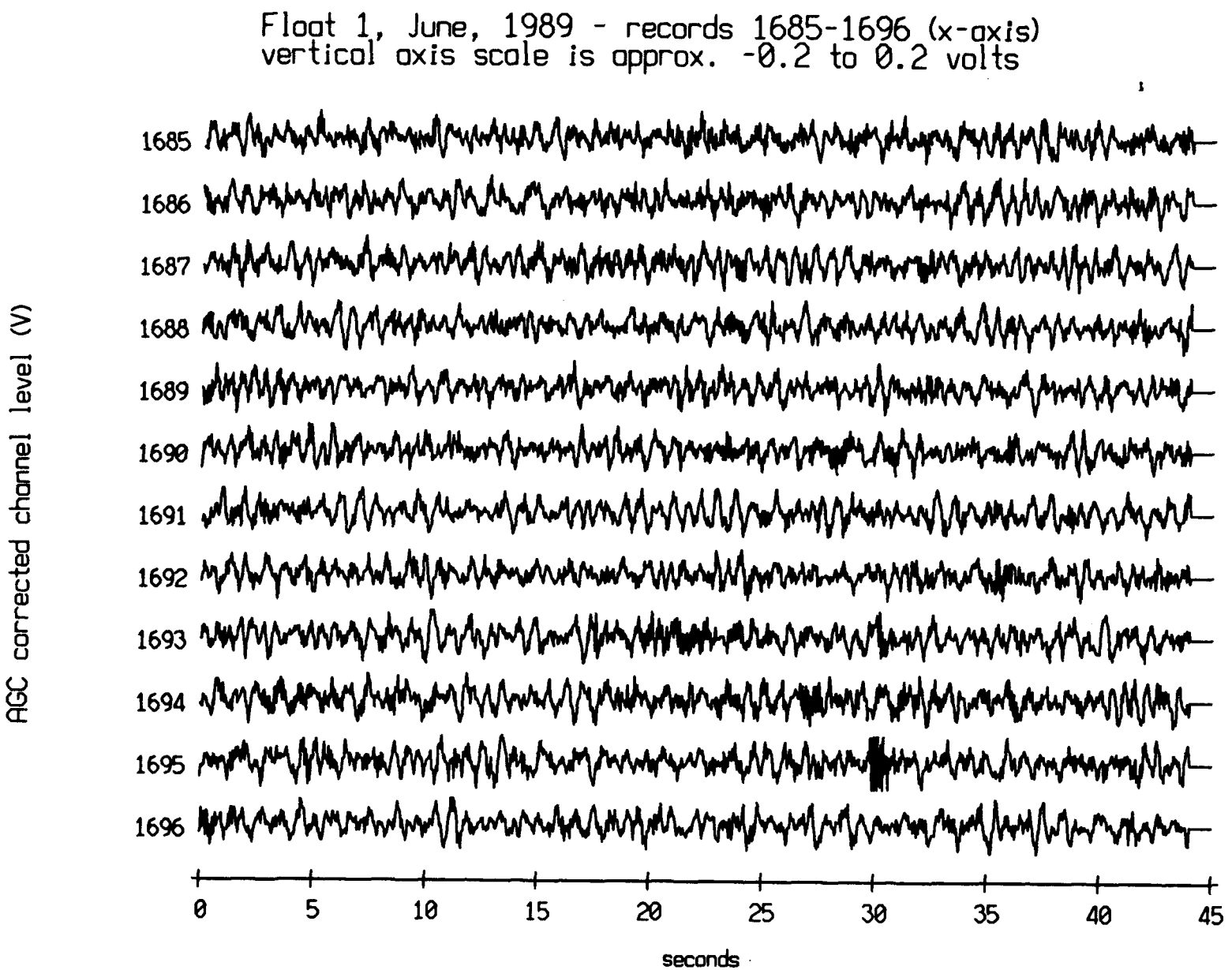
Float 1, June, 1989 - records 1685-1696 (x-axis)
vertical axis scale is approx. -0.2 to 0.2 volts
1685
1686
1687
1688
1689
1690
1691
1692
1693
1694
1695
1696
AGC corrected channel level (V)
0
5
10
15
20
25
30
35
40
45
seconds

Figure V.3a

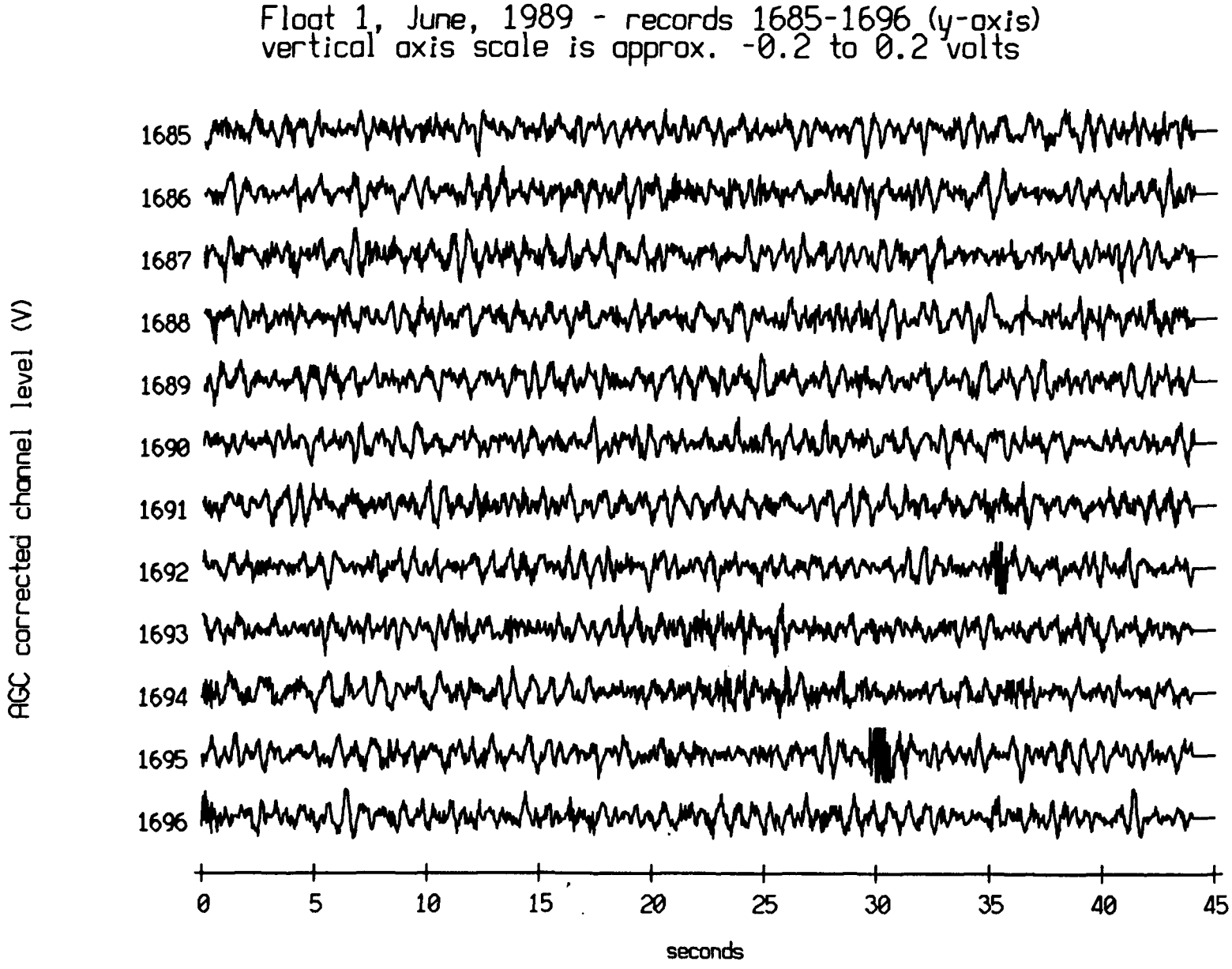
Float 1, June, 1989 - records 1685-1696 (y-axis)
vertical axis scale is approx. -0.2 to 0.2 volts
AGC corrected channel level (V)
1685
1686
1687
1688
1689
1690
1691
1692
1693
1694
1695
1696
0
5
10
15
20
25
30
35
40
45
seconds

Figure V.3b

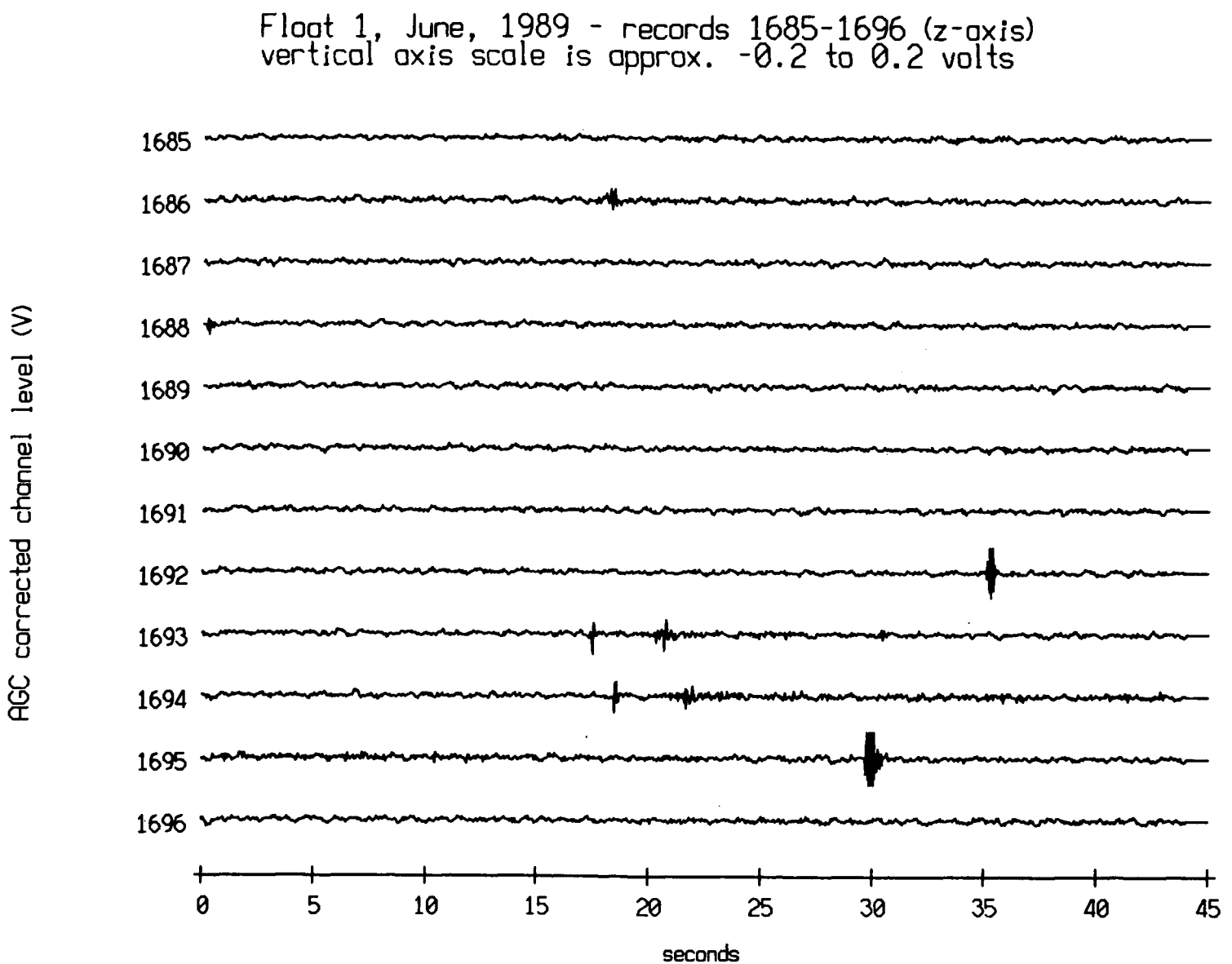
Float 1, June, 1989 - records 1685-1696 (z-axis)
vertical axis scale is approx. -0.2 to 0.2 volts
AGC corrected channel level (V)
1685
1686
1687
1688
1689
1690
1691
1692
1693
1694
1695
1696
0
5
10
15
20
25
30
35
40
45
seconds

Figure V.3c

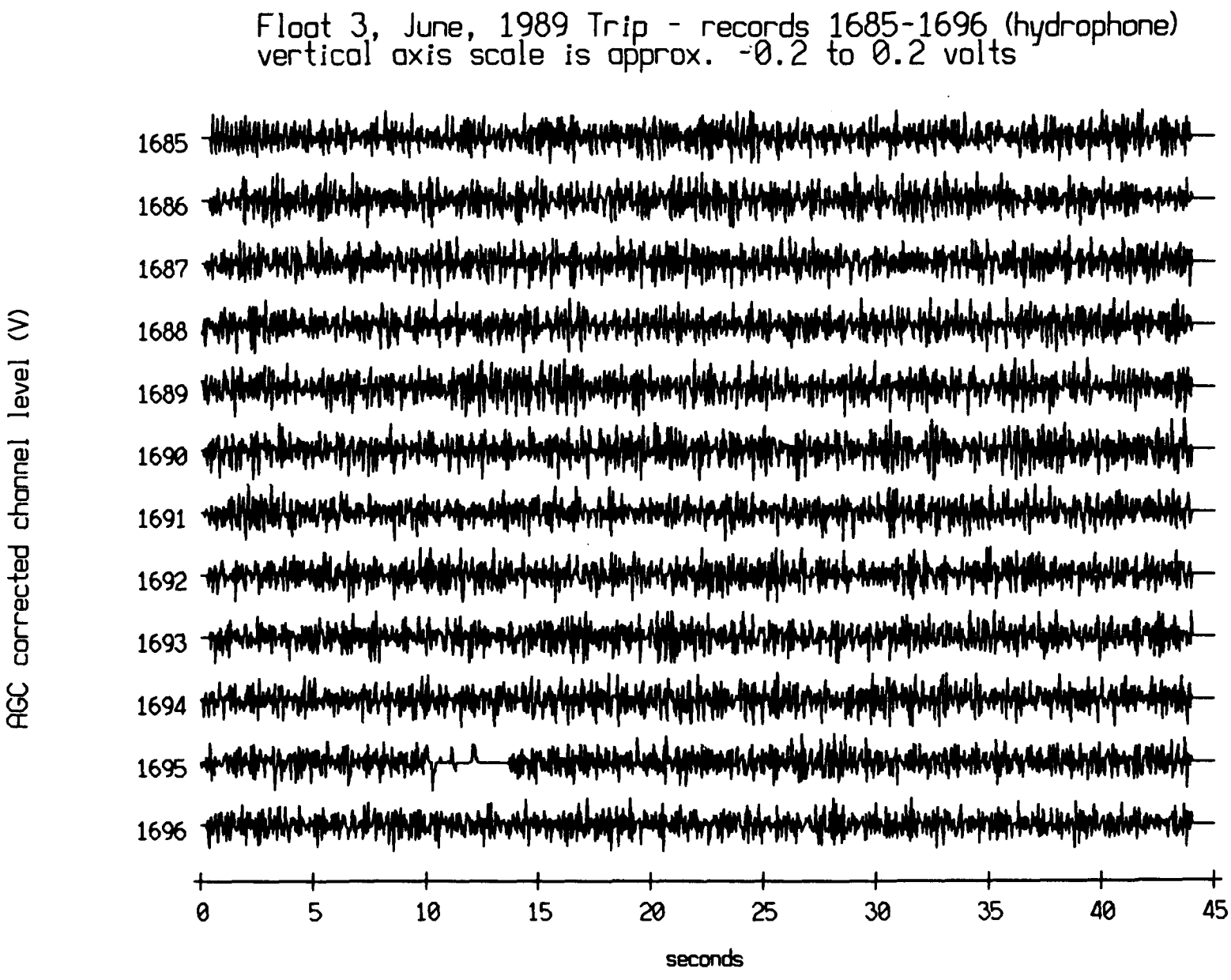
Float 3, June, 1989 Trip - records 1685-1696 (hydrophone)
vertical axis scale is approx. -0.2 to 0.2 volts
AGC corrected channel level (V)
1685
1686
1687
1688
1689
1690
1691
1692
1693
1694
1695
1696
0
5
10
15
20
25
30
35
40
45
seconds

Figure V.4

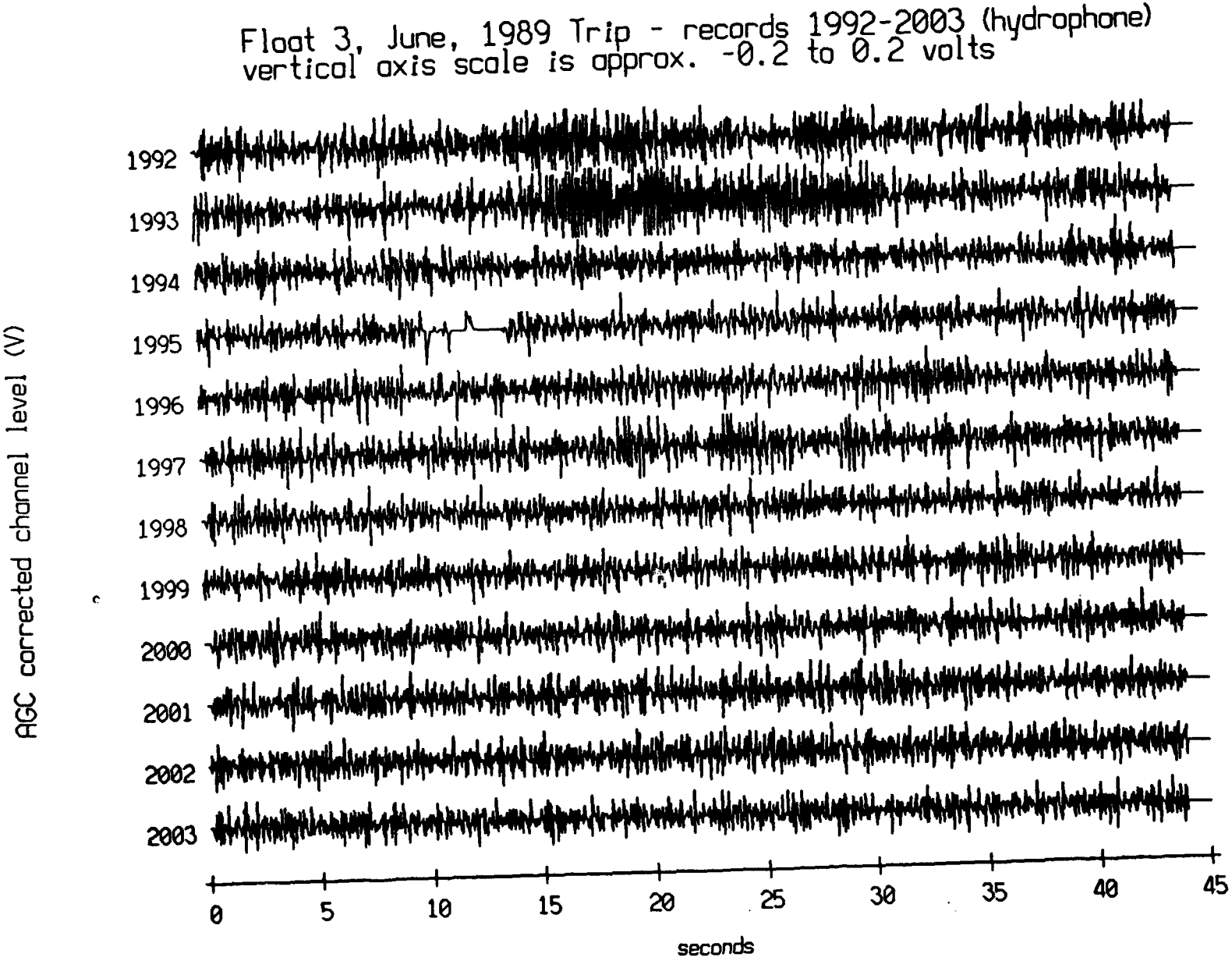
Float 3, June, 1989 Trip - records 1992-2003 (hydrophone)
vertical axis scale is approx. -0.2 to 0.2 volts
AGC corrected channel level (V)
1992
1993
1994
1995
1996
1997
1998
1999
2000
2001
2002
2003
0
5
10
15
20
25
30
35
40
45
seconds

Figure V.5

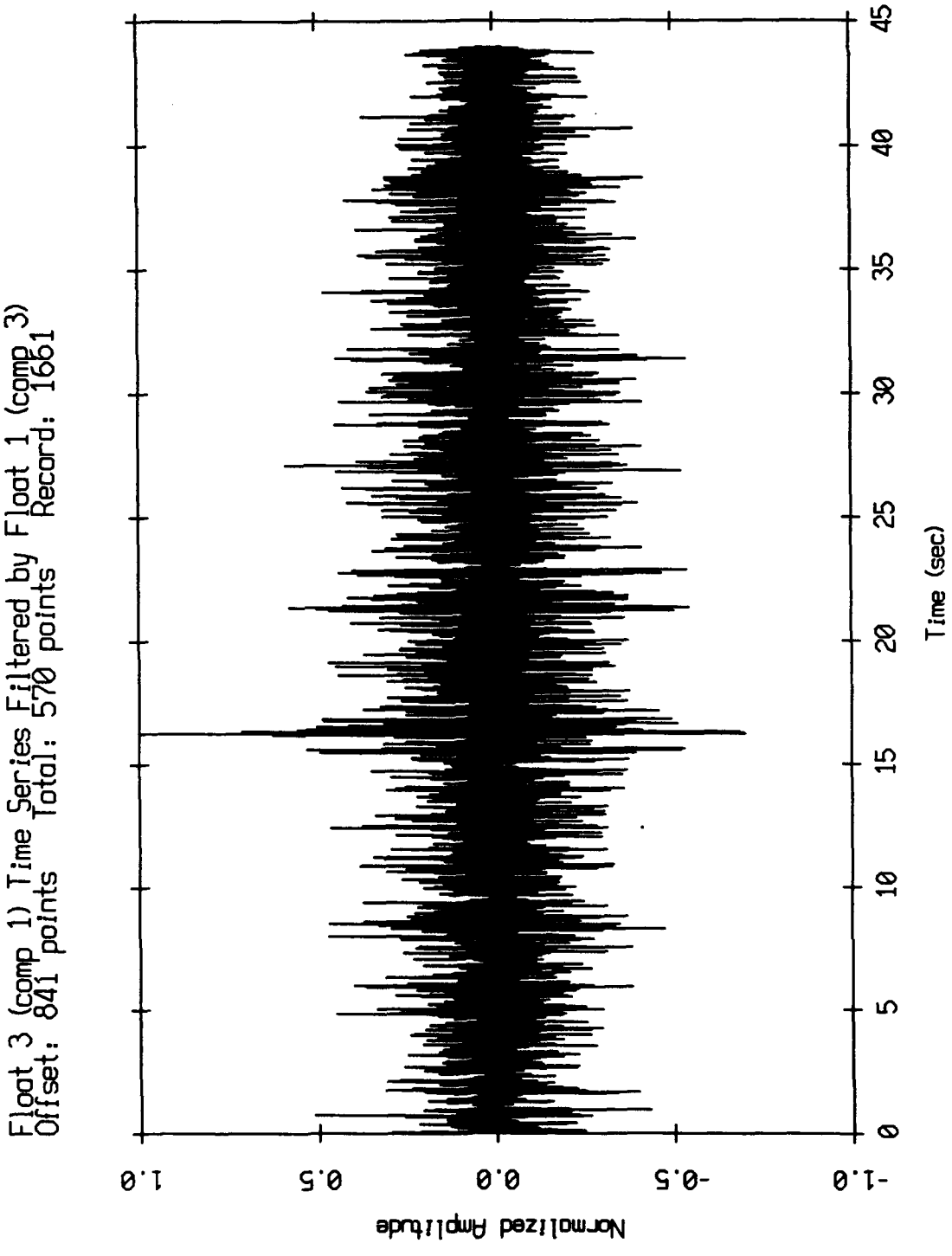
Float 3 (comp 1) Time Series Filtered by Float 1 (comp 3)
Offset: 841 points Total: 570 points Record: 1661
Normalized Amplitude
1.0
0.5
0.0
-0.5
-1.0
0
5
10
15
20
25
30
35
40
45
Time (sec)

Figure V.6

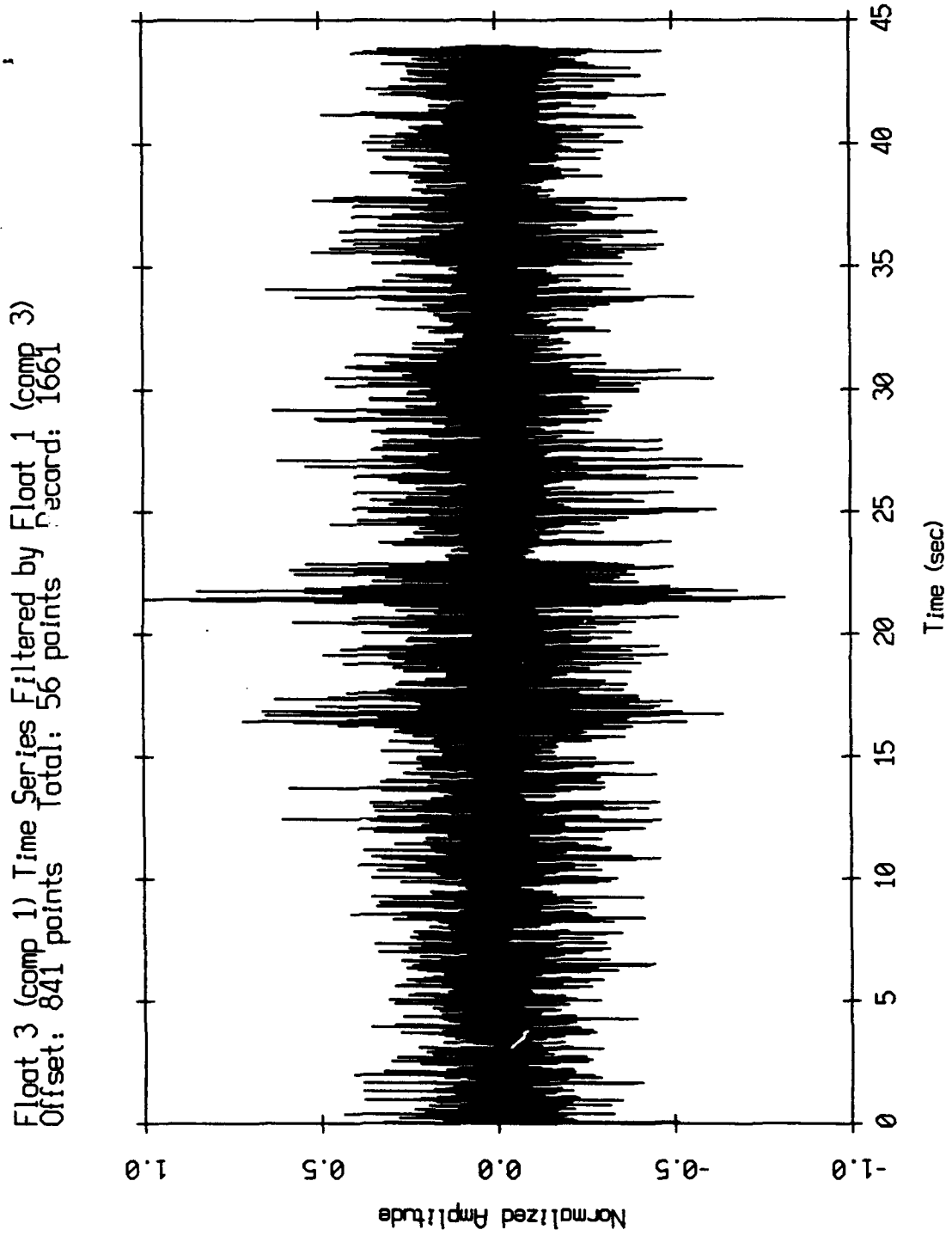
Float 3 (comp 1) Time Series Filtered by Float 1 (comp 3)
Offset: 841 points Total: 56 points Record: 1661
Normalized Amplitude
1.0
0.5
0.0
-0.5
-1.0
0
5
10
15
20
25
30
35
40
45
Time (sec)

Figure V.7

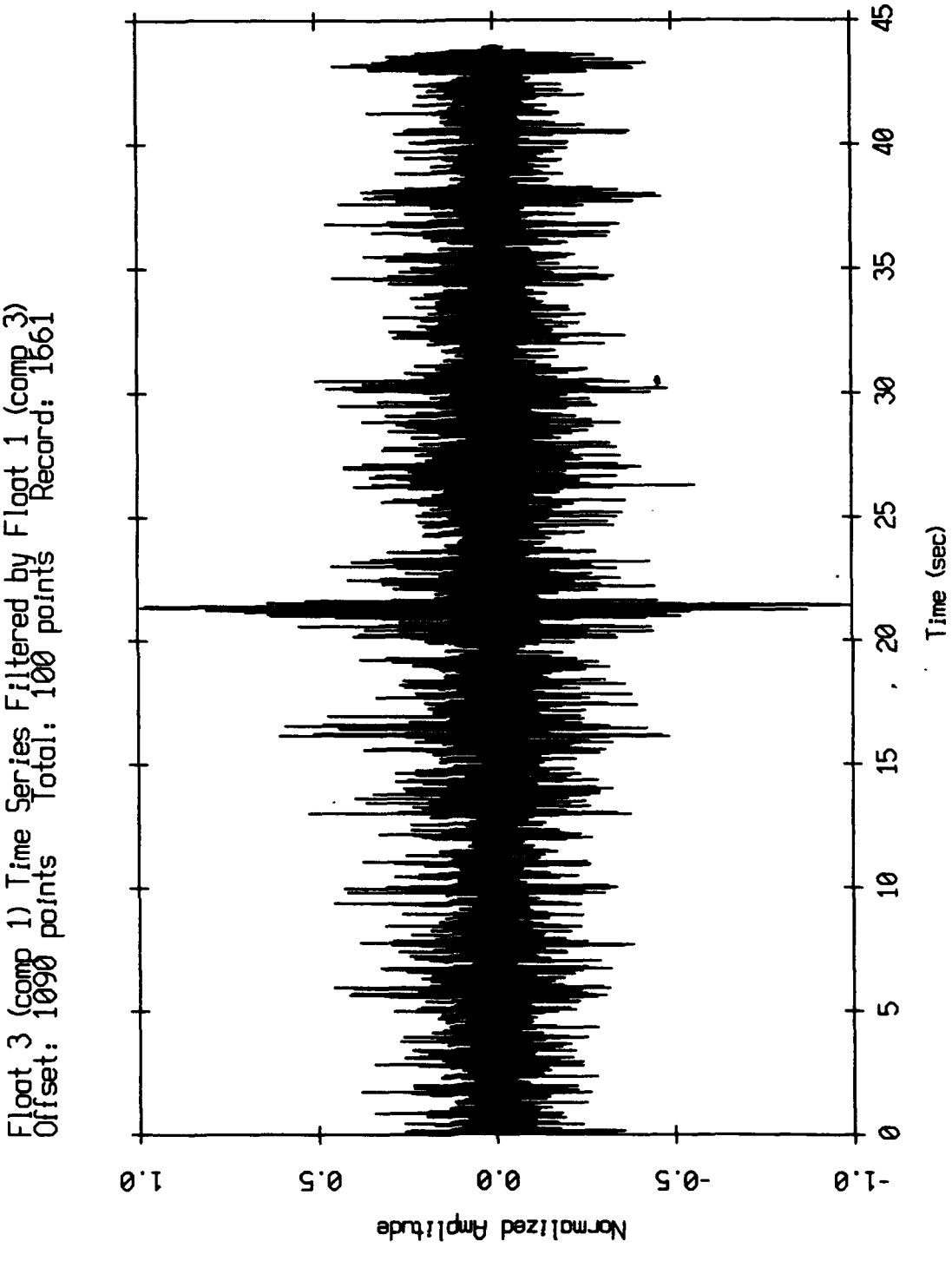
Float 3 (comp 1) Time Series Filtered by Float 1 (comp 3)
Offset: 1090 points Total: 100 points Record: 1661
Normalized Amplitude
1.0
0.5
0.0
-0.5
-1.0
0
5
10
15
20
25
30
35
40
45
Time (sec)

Figure V.8

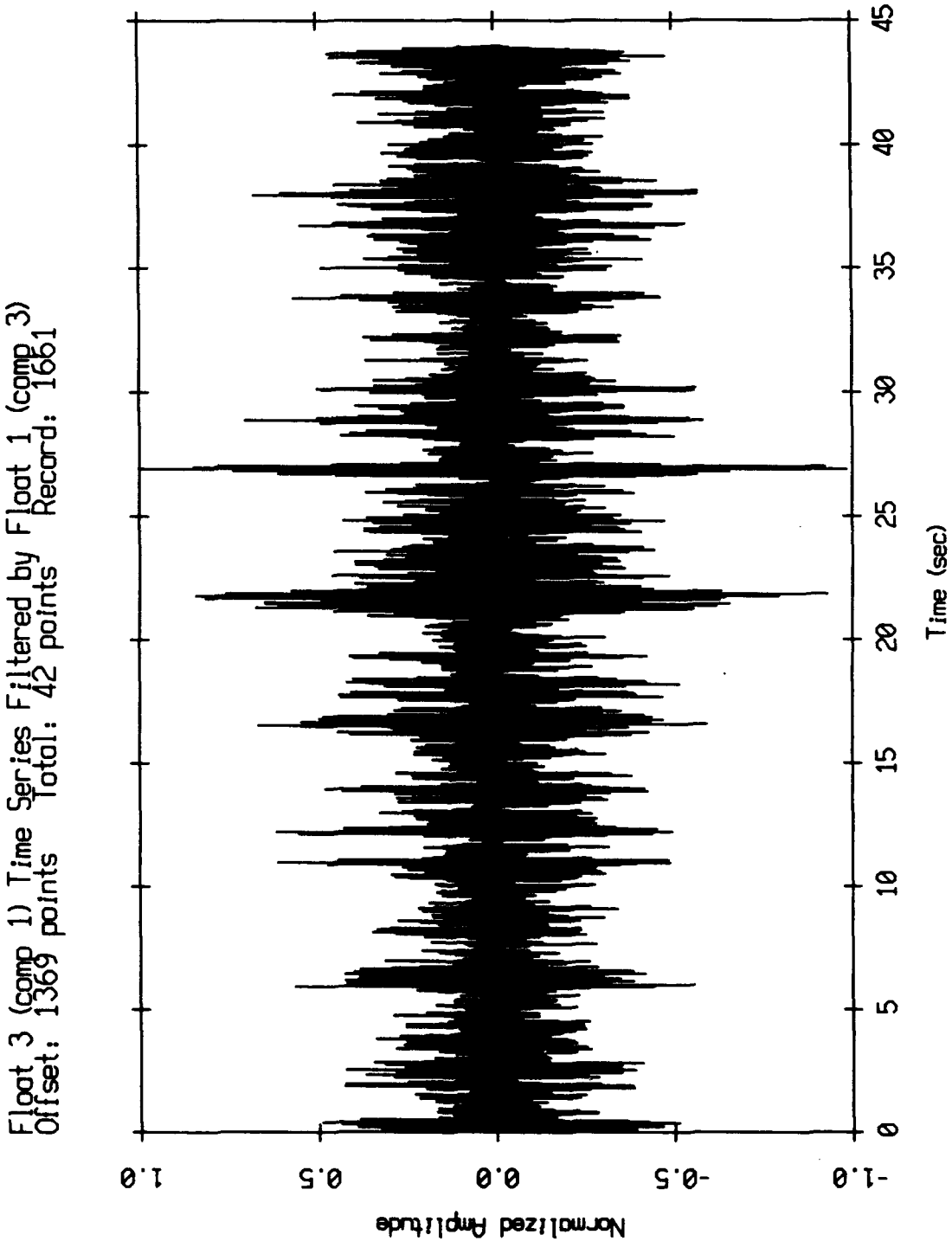
Float 3 (comp 1) Time Series Filtered by Float 1 (comp 3)
Offset: 1369 points Total: 42 points Record: 1661
Normalized Amplitude
1.0
0.5
0.0
-0.5
-1.0
0
5
10
15
20
25
30
35
40
45
Time (sec)

Figure V.9

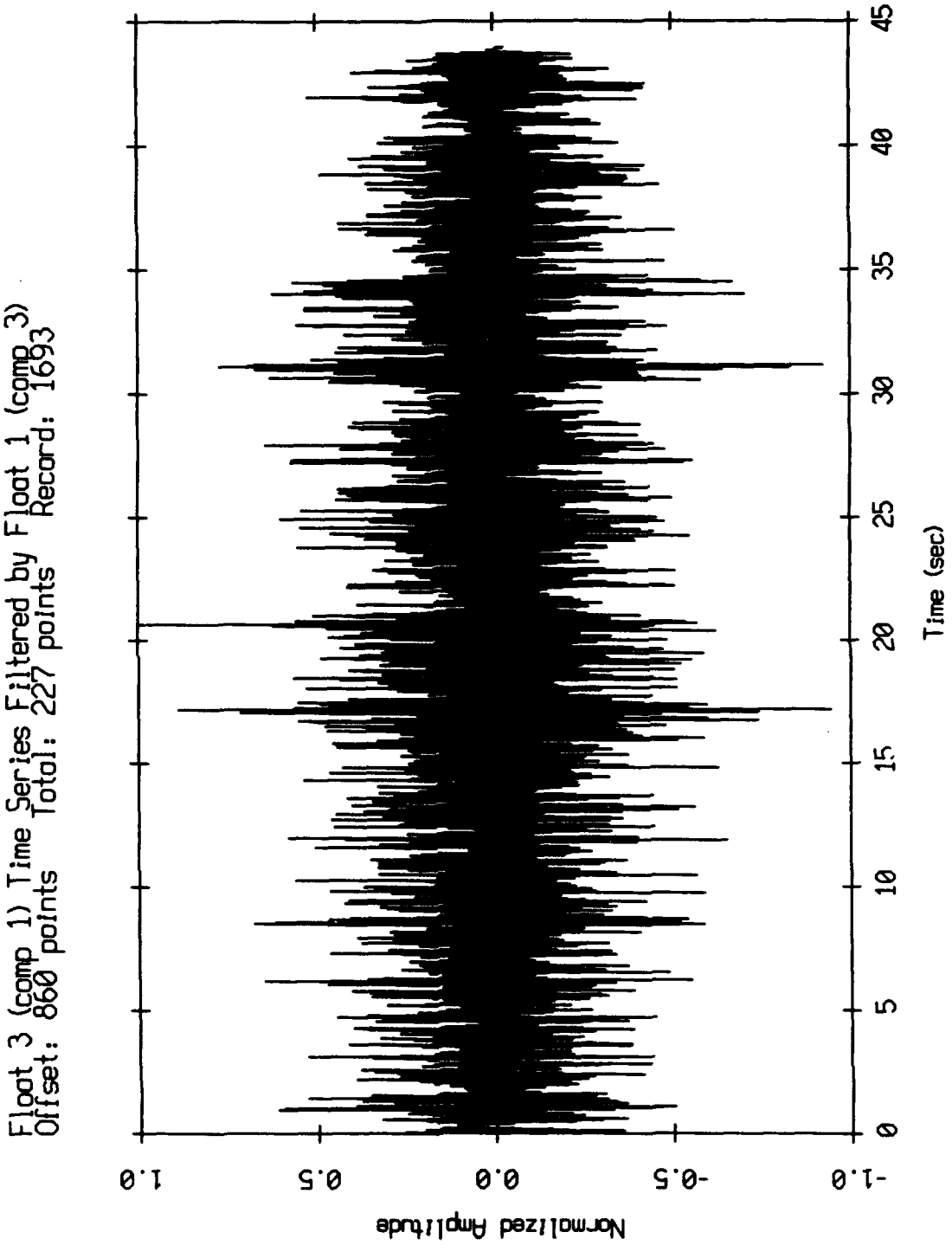
Float 3 (comp 1) Time Series Filtered by Float 1 (comp 3)
Offset: 860 points Total: 227 points Record: 1693
Normalized Amplitude
1.0
0.5
0.0
-0.5
-1.0
0
5
10
15
20
25
30
35
40
45
Time (sec)

Figure V.10

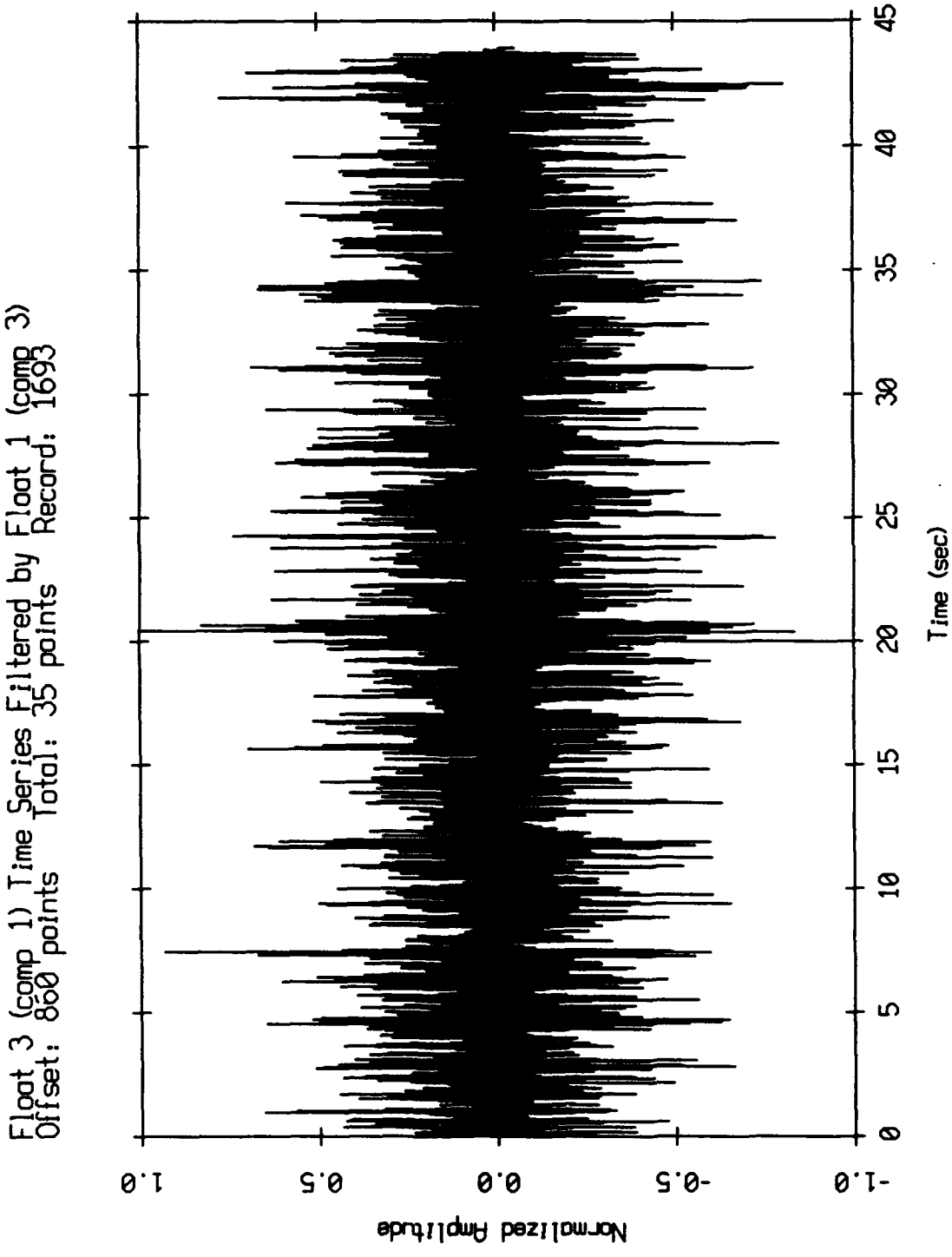
Float 3 (comp 1) Time Series Filtered by Float 1 (comp 3)
Offset: 860 points Total: 35 points Record: 1693
Normalized Amplitude
1.0
0.5
0.0
-0.5
-1.0
0
5
10
15
20
25
30
35
40
45
Time (sec)

Figure V.11

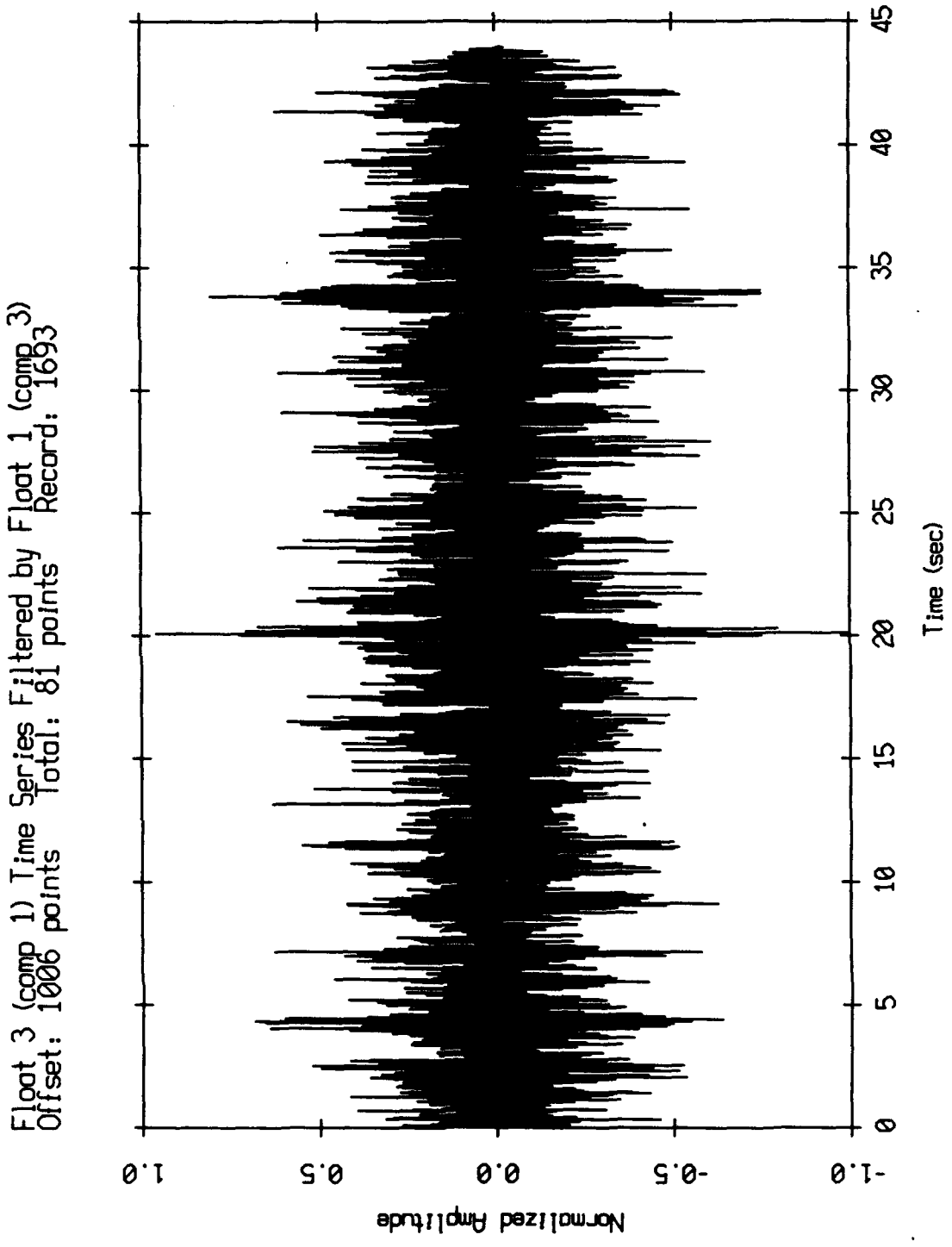
Float 3 (comp 1) Time Series Filtered by Float 1 (comp 3)
Offset: 1006 points Total: 81 points Record: 1693
Normalized Amplitude
1.0
0.5
0.0
-0.5
-1.0
Time (sec)
0
5
10
15
20
25
30
35
40
45

Figure V.12

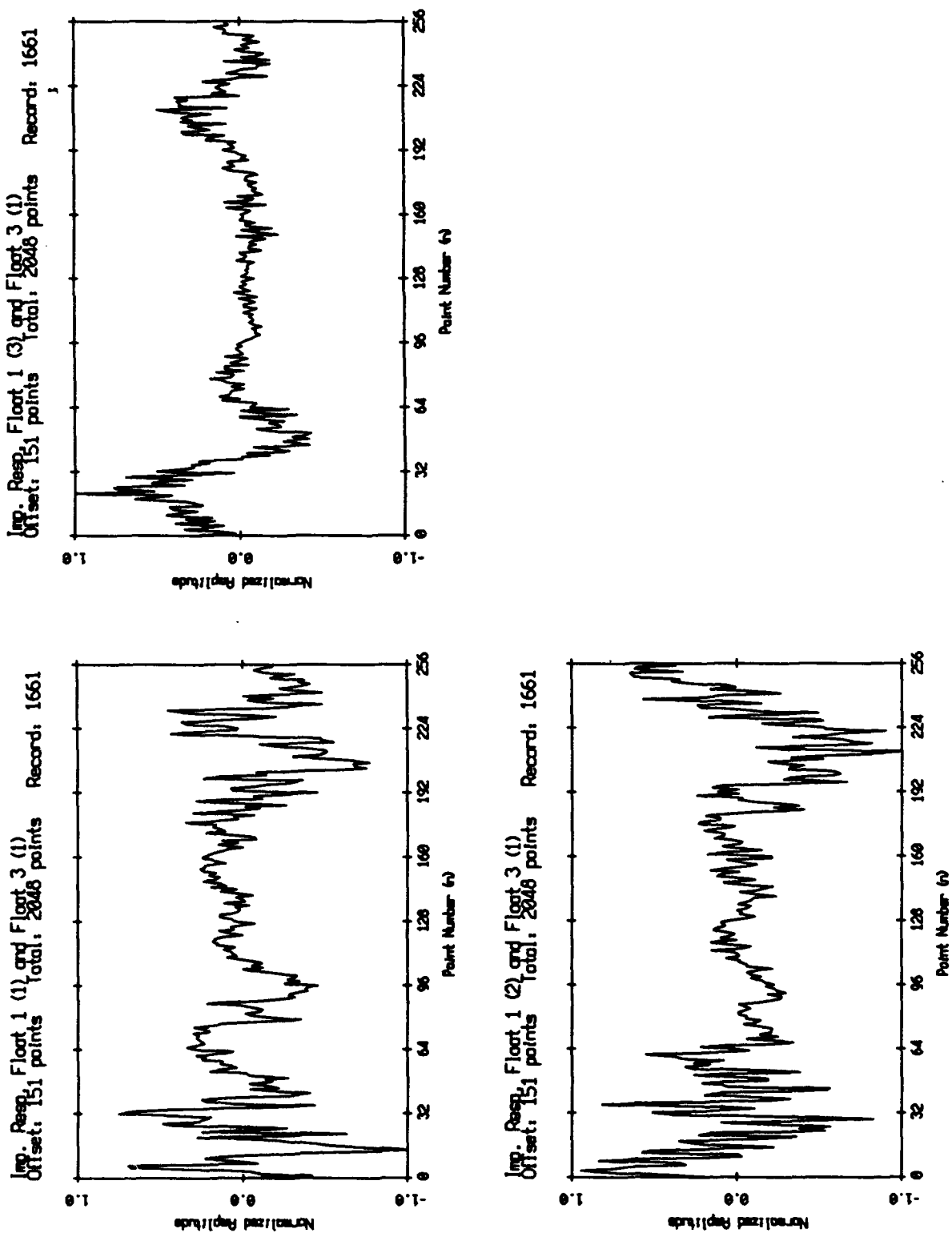
Imp. Resp. Float 1 (3) and Float 3 (1)
Offset: 151 points Total: 2048 points Record: 1661
Normalized Amplitude
Point Number (n)
Imp. Resp. Float 1 (1) and Float 3 (1)
Offset: 151 points Total: 2048 points Record: 1661
Normalized Amplitude
Point Number (n)
Imp. Resp. Float 1 (2) and Float 3 (1)
Offset: 151 points Total: 2048 points Record: 1661
Normalized Amplitude
Point Number (n)

Figure VI.1

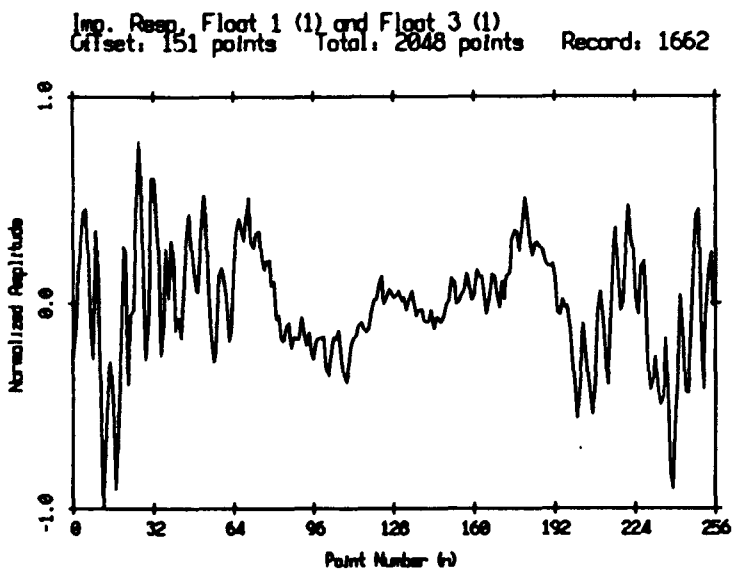
Imp. Resp. Float 1 (1) and Float 3 (1)
Offset: 151 points Total: 2048 points Record: 1662
Normalized Amplitude
1.0
0.0
-1.0
0
32
64
96
128
160
192
224
256
Point Number (n)

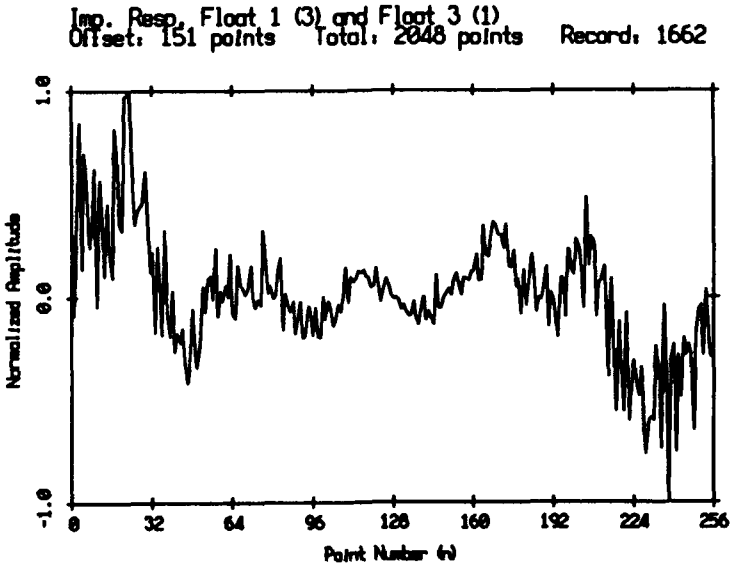
Imp. Resp. Float 1 (3) and Float 3 (1)
Offset: 151 points Total: 2048 points Record: 1662
Normalized Amplitude
1.0
0.0
-1.0
0
32
64
96
128
160
192
224
256
Point Number (n)

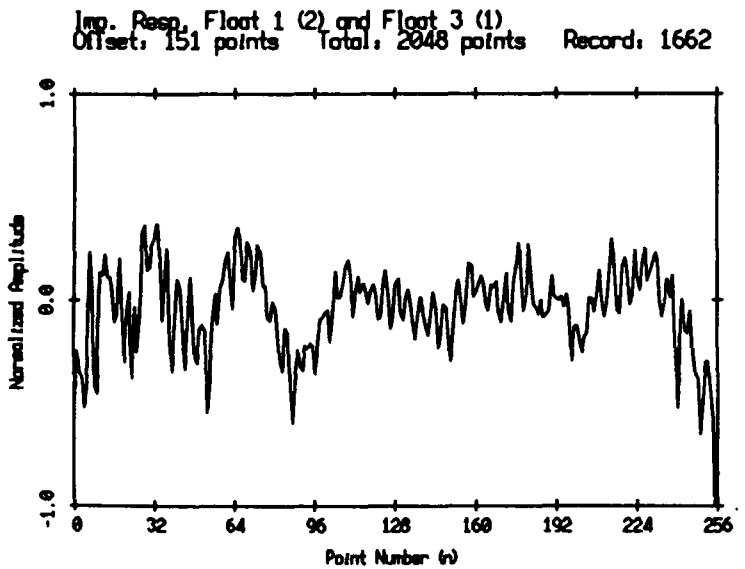
Imp. Resp. Float 1 (2) and Float 3 (1)
Offset: 151 points Total: 2048 points Record: 1662
Normalized Amplitude
1.0
0.0
-1.0
0
32
64
96
128
160
192
224
256
Point Number (n)

Figure V1.2

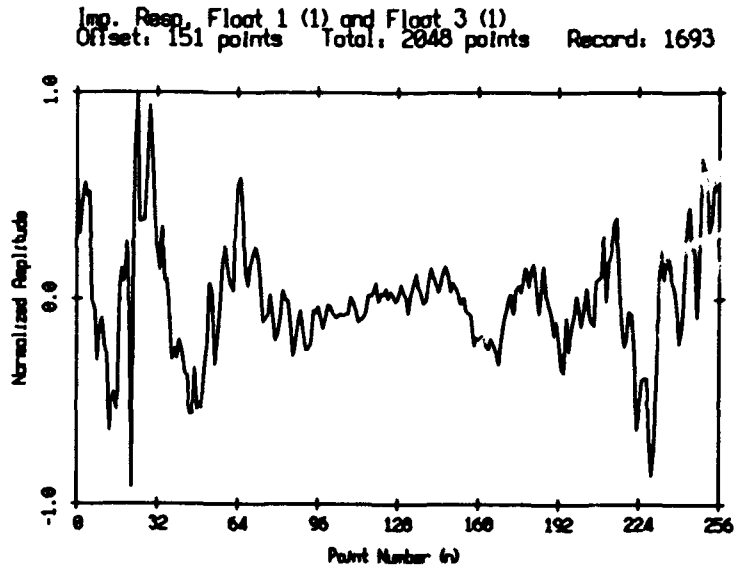
Imp. Resp. Float 1 (1) and Float 3 (1)
Offset: 151 points Total: 2048 points Record: 1693
Normalised Amplitude
1.0
0.0
-1.0
0
32
64
96
128
160
192
224
256
Point Number (n)

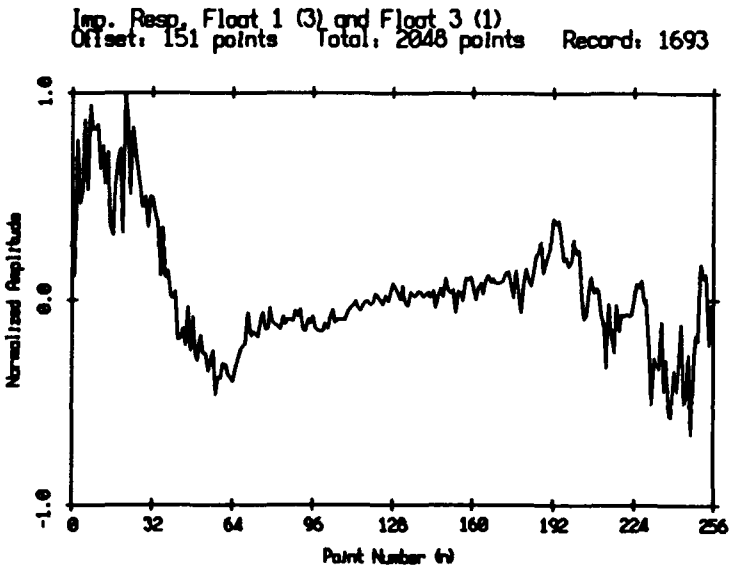
Imp. Resp. Float 1 (3) and Float 3 (1)
Offset: 151 points Total: 2048 points Record: 1693
Normalised Amplitude
1.0
0.0
-1.0
0
32
64
96
128
160
192
224
256
Point Number (n)

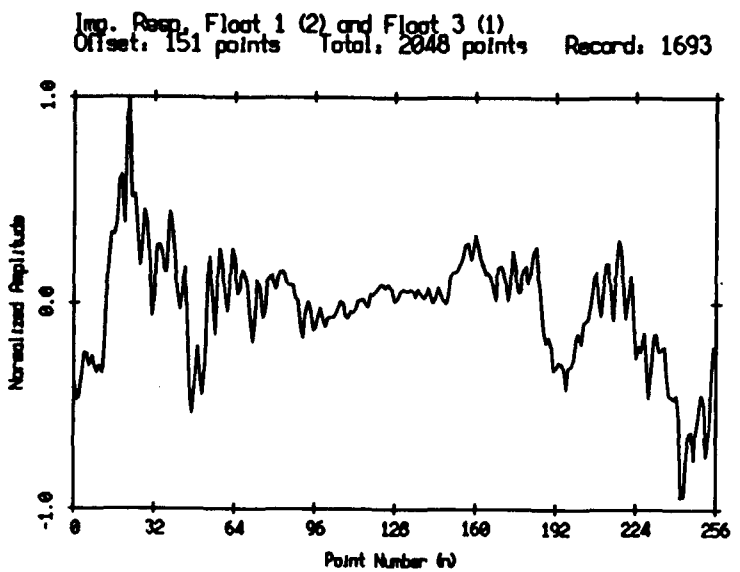
Imp. Resp. Float 1 (2) and Float 3 (1)
Offset: 151 points Total: 2048 points Record: 1693
Normalised Amplitude
1.0
0.0
-1.0
0
32
64
96
128
160
192
224
256
Point Number (n)

Figure VI.3

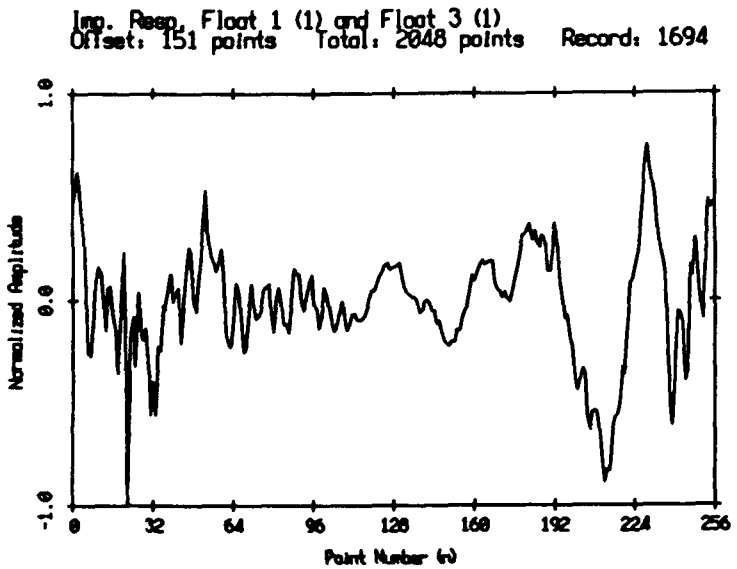
Imp. Resp. Float 1 (1) and Float 3 (1)
Offset: 151 points Total: 2048 points Record: 1694
Normalized Amplitude
1.0
0.0
-1.0
0
32
64
96
128
160
192
224
256
Point Number (n)

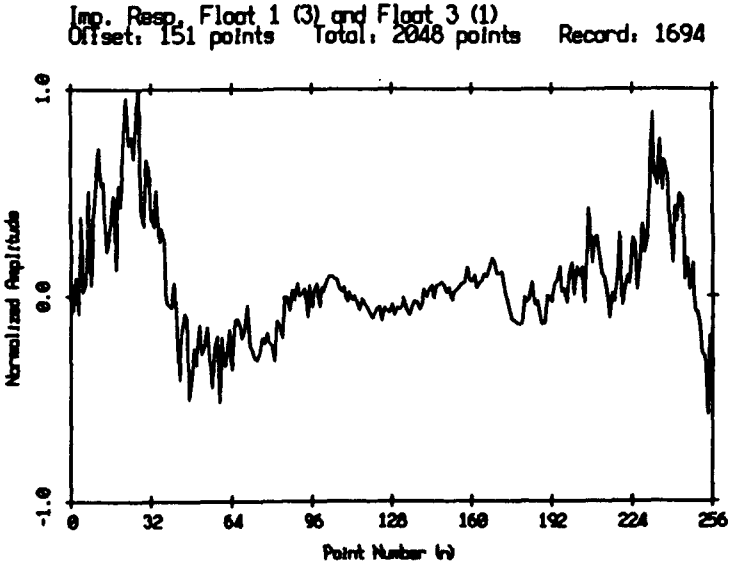
Imp. Resp. Float 1 (3) and Float 3 (1)
Offset: 151 points Total: 2048 points Record: 1694
Normalized Amplitude
1.0
0.0
-1.0
0
32
64
96
128
160
192
224
256
Point Number (n)

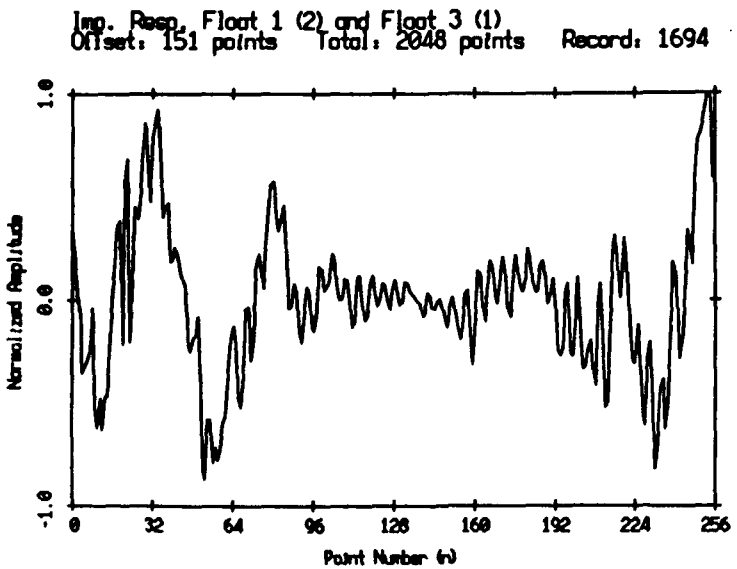
Imp. Resp. Float 1 (2) and Float 3 (1)
Offset: 151 points Total: 2048 points Record: 1694
Normalized Amplitude
1.0
0.0
-1.0
0
32
64
96
128
160
192
224
256
Point Number (n)

Figure VI.4

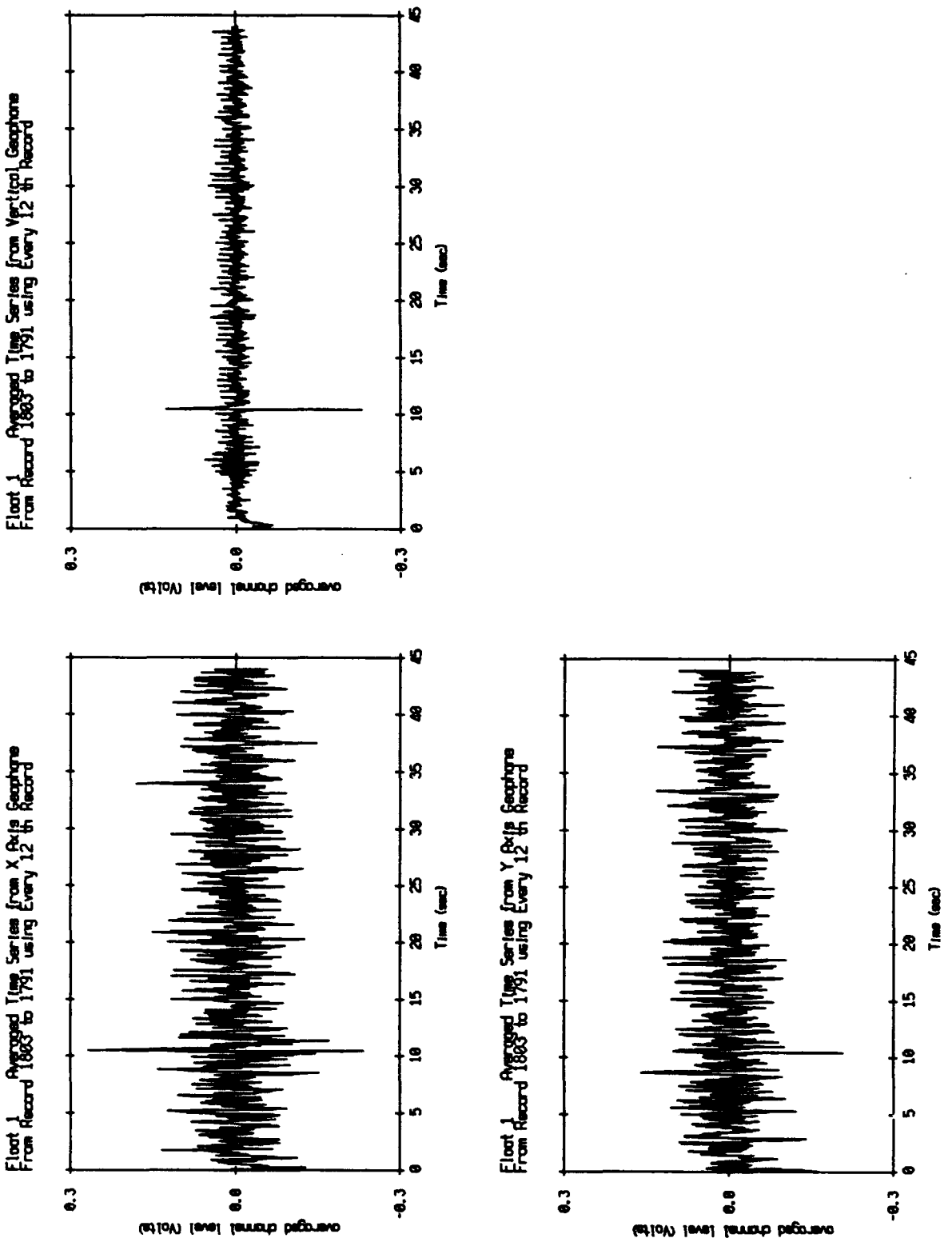
Float 1 Averaged Time Series from Vertical Geophone
From Record 1803 to 1791 using Every 12 th Record
averaged channel level (Volts)
Time (sec)
Float 1 Averaged Time Series from X Axis Geophone
From Record 1803 to 1791 using Every 12 th Record
averaged channel level (Volts)
Time (sec)
Float 1 Averaged Time Series from Y Axis Geophone
From Record 1803 to 1791 using Every 12 th Record
averaged channel level (Volts)
Time (sec)

Figure VI.5

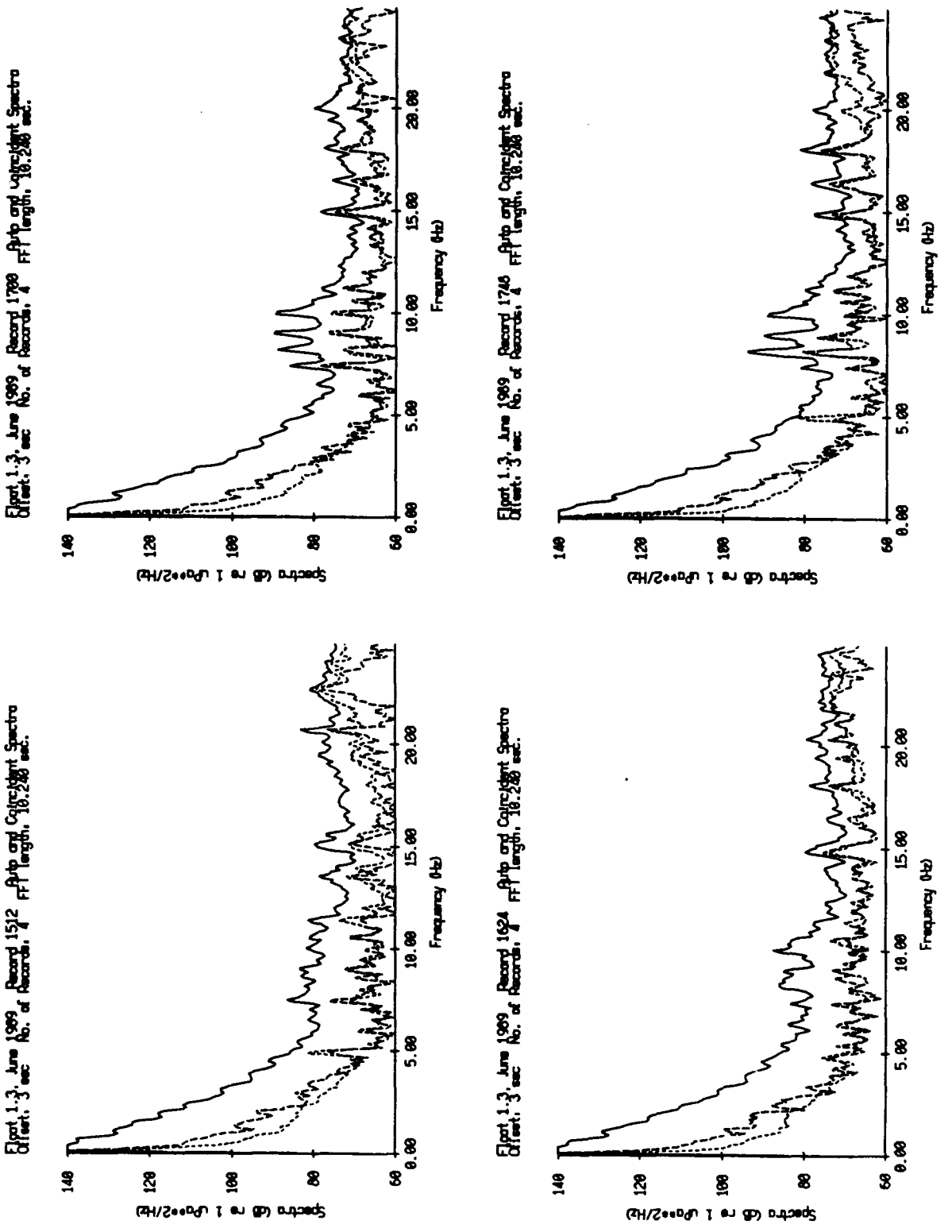
Figat 1.3, June 1989 Record 1512 Auto and Coincident Spectra
Offset: 3 sec No. of Records: 4 FFT length: 10.240 sec.
Figat 1.3, June 1989 Record 1700 Auto and Coincident Spectra
Offset: 3 sec No. of Records: 4 FFT length: 10.240 sec.
Figat 1.3, June 1989 Record 1624 Auto and Coincident Spectra
Offset: 3 sec No. of Records: 4 FFT length: 10.240 sec.
Figat 1.3, June 1989 Record 1748 Auto and Coincident Spectra
Offset: 3 sec No. of Records: 4 FFT length: 10.240 sec.
Spectra (dB re 1 uPa**2/Hz)
Frequency (Hz)
140
120
100
80
60
0.00
5.00
10.00
15.00
20.00

Figure VII.1

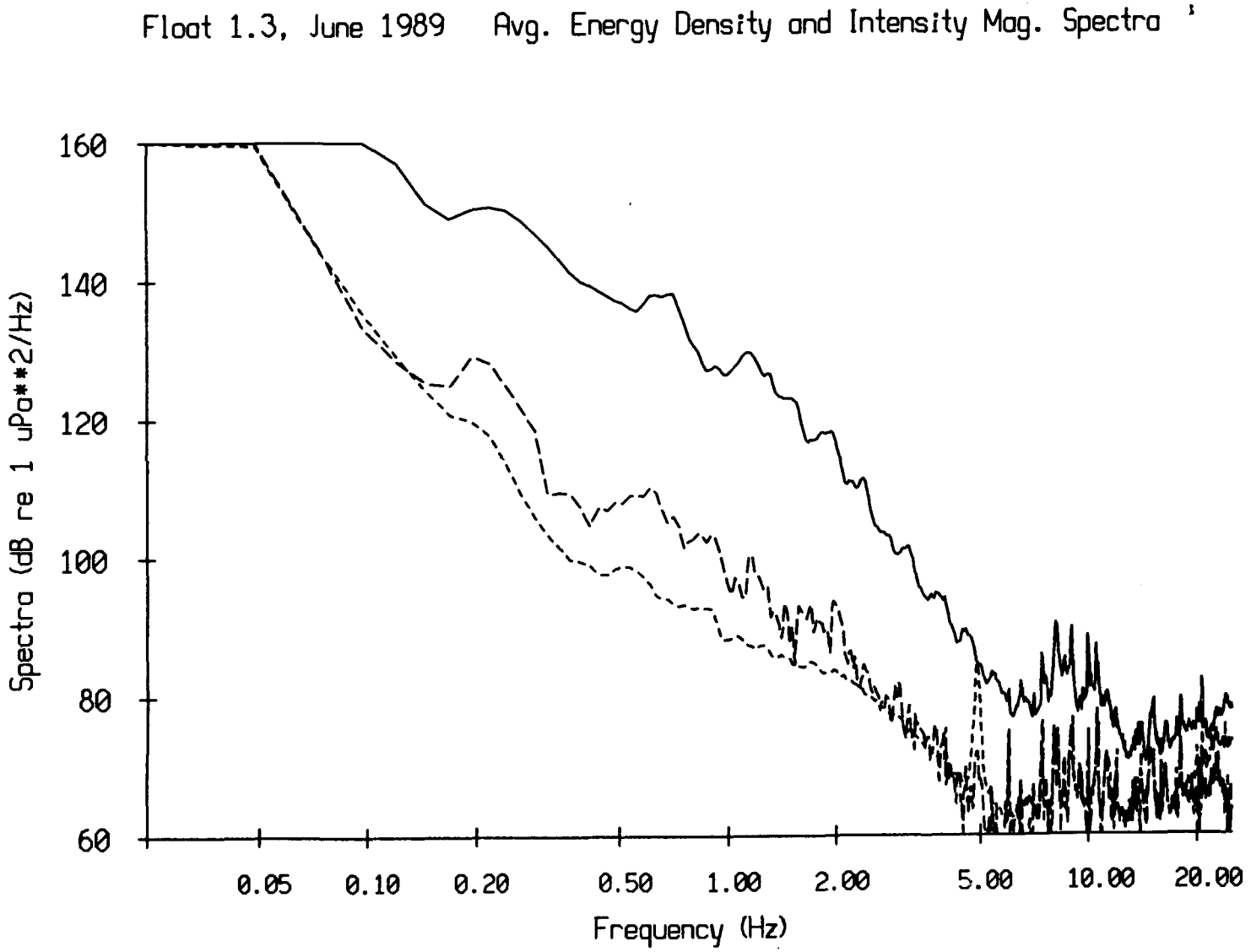
Float 1.3, June 1989 Avg. Energy Density and Intensity Mag. Spectra
Spectra (dB re 1 uPa**2/Hz)
160
140
120
100
80
60
0.05
0.10
0.20
0.50
1.00
2.00
5.00
10.00
20.00
Frequency (Hz)

Figure VII.2

Figure VII.3

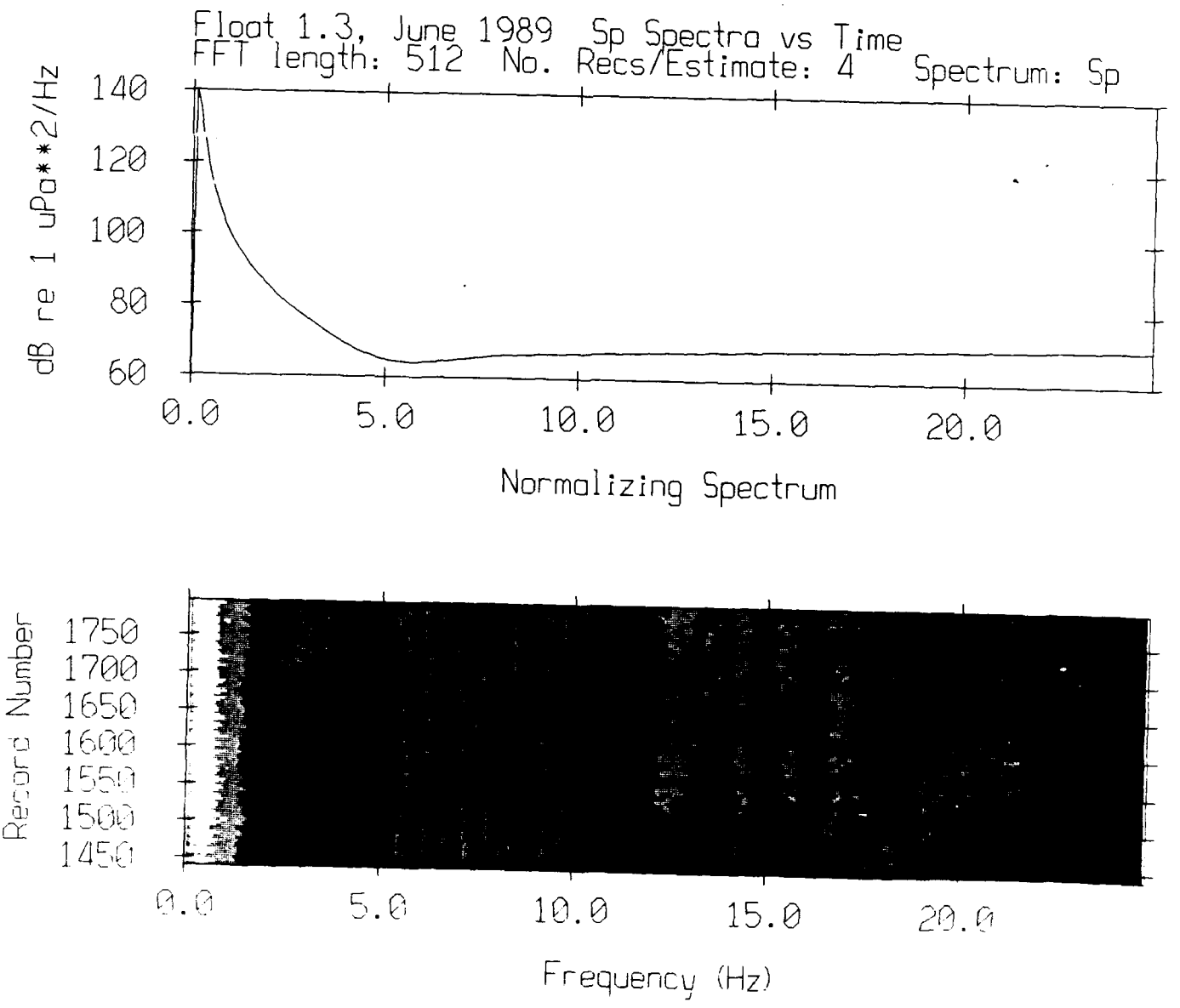
Float 1.3, June 1989 Sp Spectra vs Time
FFT length: 512 No. Recs/Estimate: 4 Spectrum: Sp
dB re 1 uPa**2/Hz
140
120
100
80
60
0.0
5.0
10.0
15.0
20.0
Normalizing Spectrum
Record Number
1750
1700
1650
1600
1550
1500
1450
0.0
5.0
10.0
15.0
20.0
Frequency (Hz)

Figure VII.4

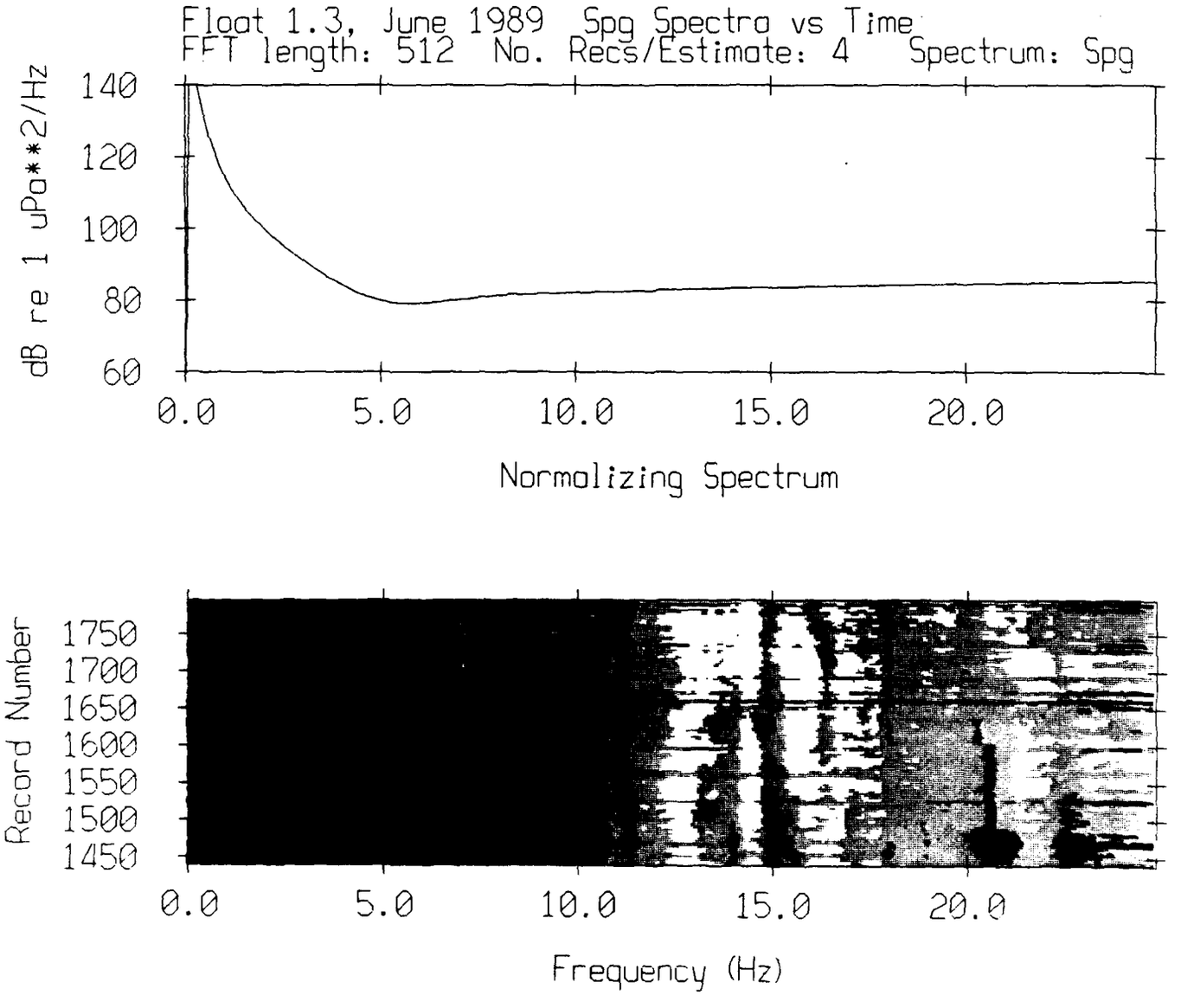
Float 1.3, June 1989 Spg Spectra vs Time
FFT length: 512 No. Recs/Estimate: 4 Spectrum: Spg
dB re 1 uPa**2/Hz
140
120
100
80
60
0.0
5.0
10.0
15.0
20.0
Normalizing Spectrum
Record Number
1750
1700
1650
1600
1550
1500
1450
0.0
5.0
10.0
15.0
20.0
Frequency (Hz)

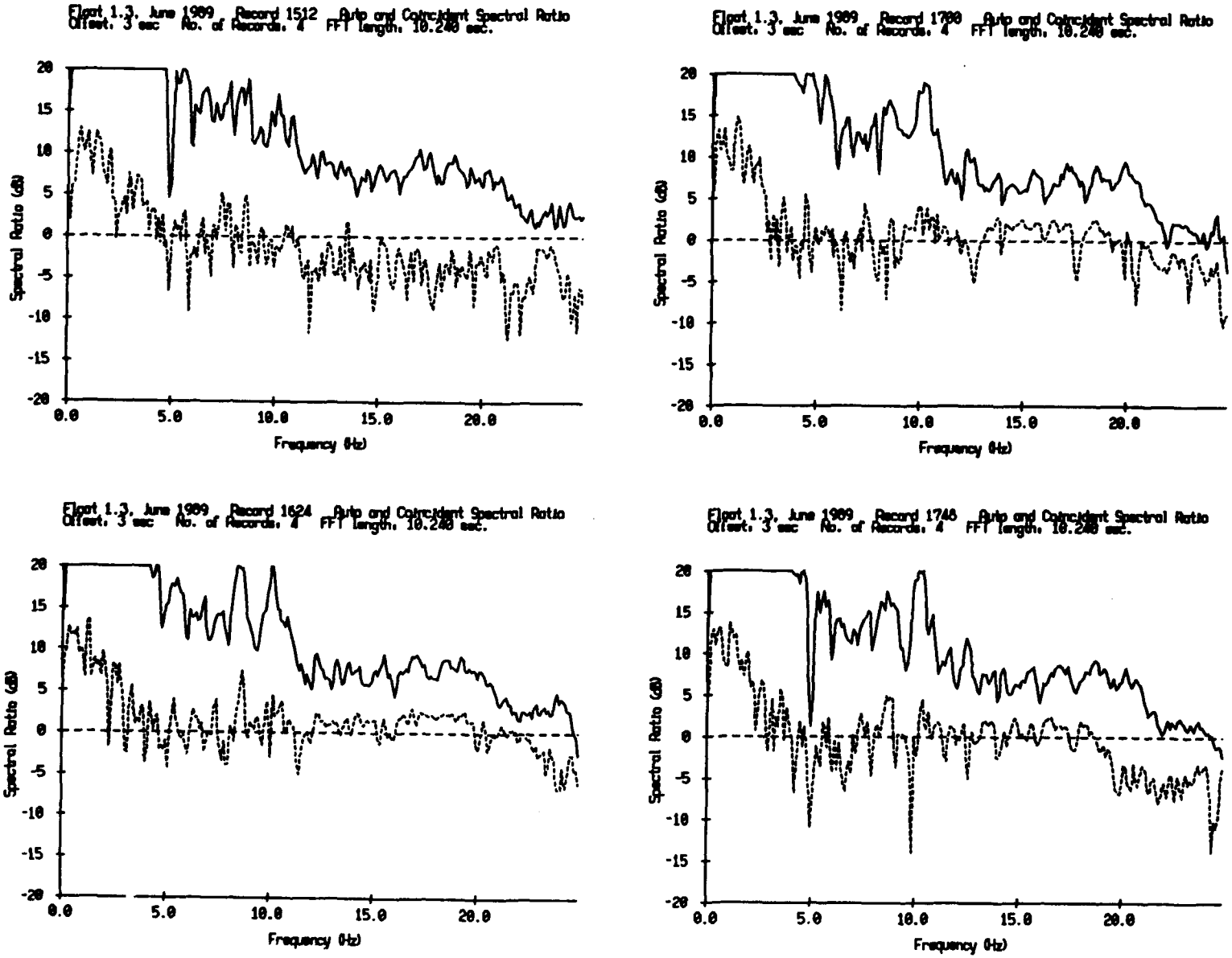
Float 1.3, June 1989 Record 1512 Auto and Coincident Spectral Ratio
Offset. 3 sec No. of Records. 4 FFT length. 10.240 sec.
Float 1.3, June 1989 Record 1700 Auto and Coincident Spectral Ratio
Offset. 3 sec No. of Records. 4 FFT length. 10.240 sec.
Float 1.3, June 1989 Record 1624 Auto and Coincident Spectral Ratio
Offset. 3 sec No. of Records. 4 FFT length. 10.240 sec.
Float 1.3, June 1989 Record 1748 Auto and Coincident Spectral Ratio
Offset. 3 sec No. of Records. 4 FFT length. 10.240 sec.
Spectral Ratio (dB)
Frequency (Hz)
20
15
10
5
0
-5
-10
-15
-20
0.0
5.0
10.0
15.0
20.0

Figure VII.5

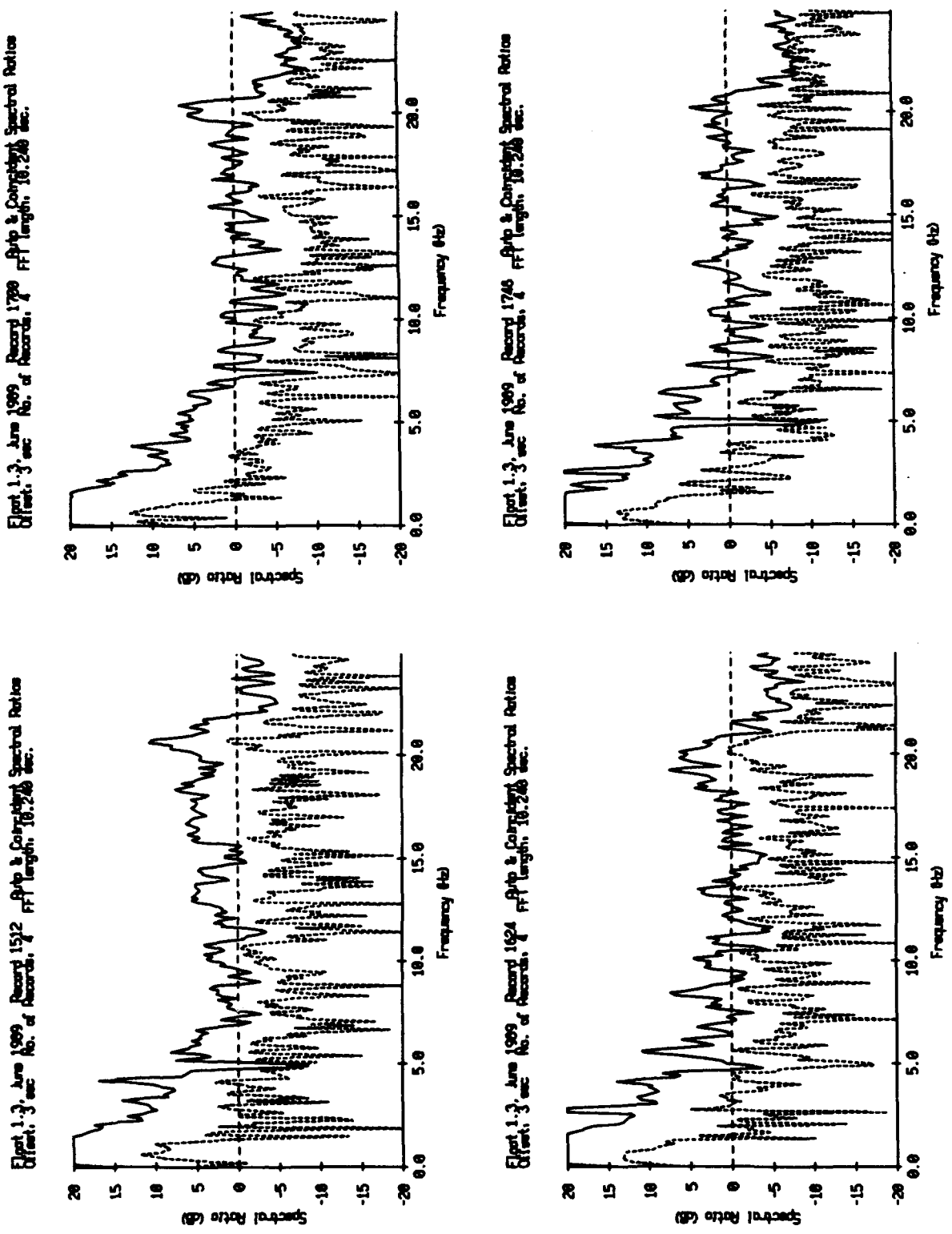
Spectral Ratio (dB)
Frequency (Hz)
20
15
10
5
0
-5
-10
-15
-20
0.0
5.0
10.0
15.0
20.0

Figure VII.6

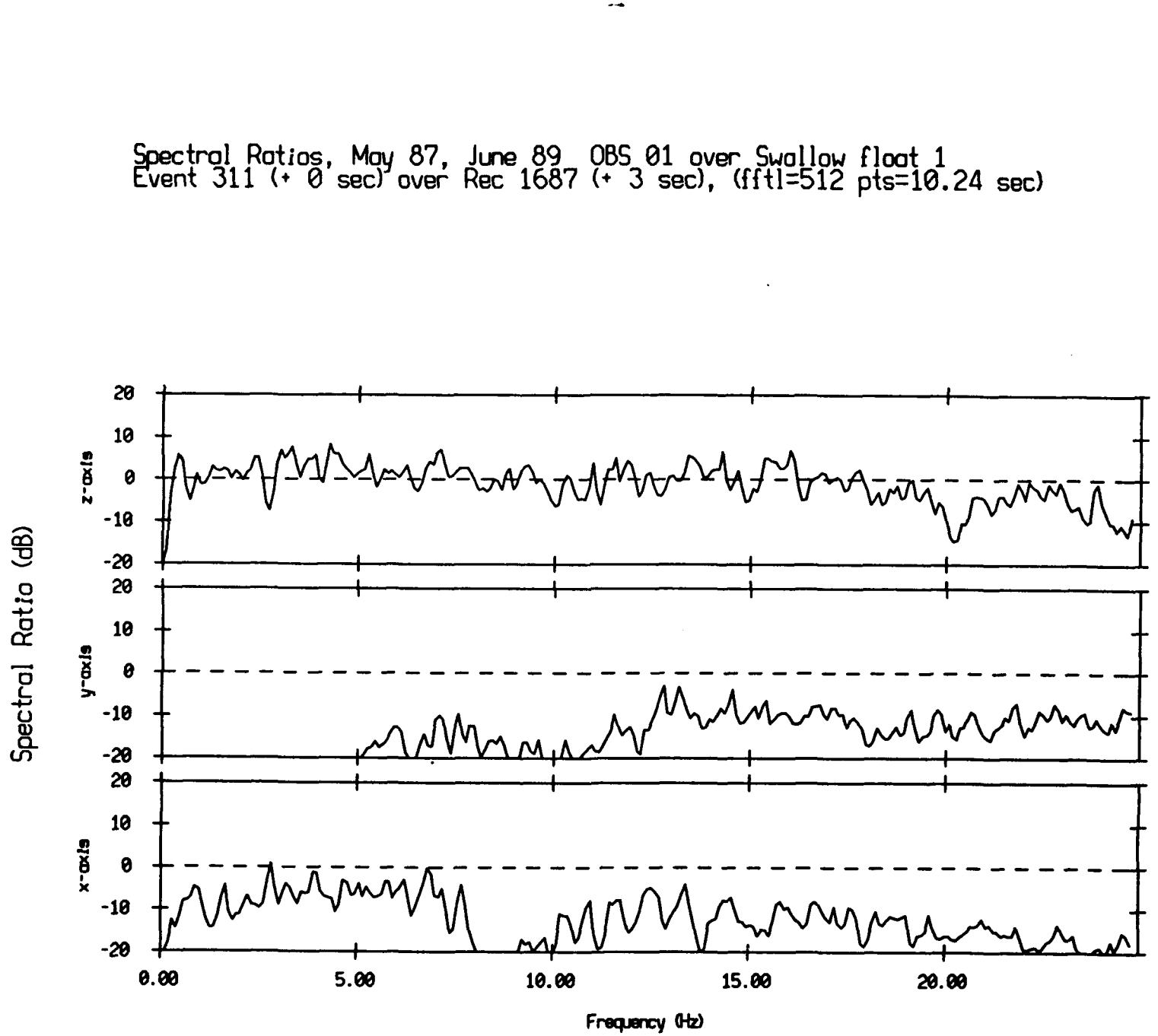
Spectral Ratios, May 87, June 89 OBS 01 over Swallow float 1
Event 311 (+ 0 sec) over Rec 1687 (+ 3 sec), (fftl=512 pts=10.24 sec)
Spectral Ratio (dB)
z-axis
y-axis
x-axis
20
10
0
-10
-20
0.00
5.00
10.00
15.00
20.00
Frequency (Hz)

Figure VII.7

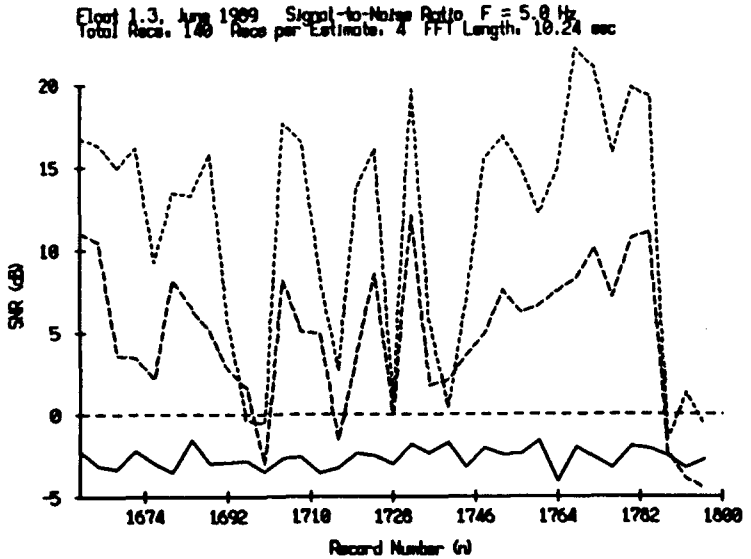
Float 1.3, June 1989 Signal-to-Noise Ratio F = 5.0 Hz
Total Recs. 140 Recs per Estimate. 4 FFT Length. 10.24 sec
SNR (dB)
20
15
10
5
0
-5
1674
1692
1710
1728
1746
1764
1782
1800
Record Number (n)

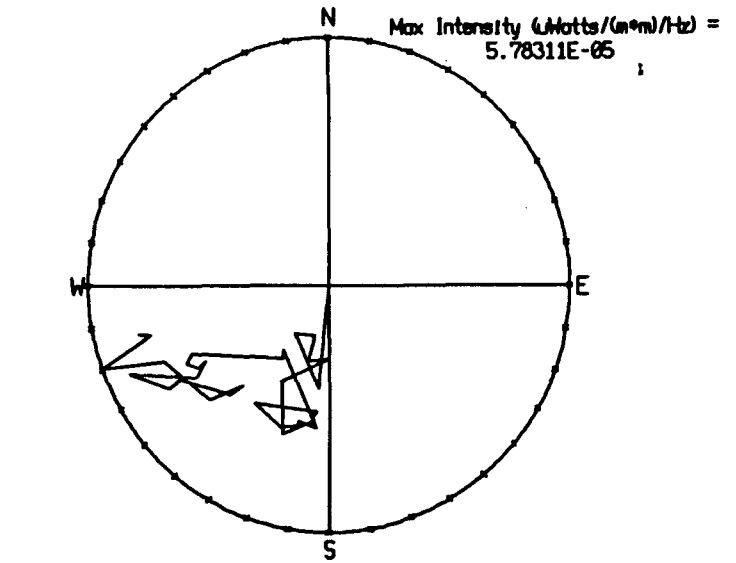
Float 1.3, June 1989 Horizontal Active Intensity F = 5.0 Hz
Start Record: 1660 Total Records: 140 Records per Vector: 4
Max Intensity (uWatts/(m*m)/Hz) =
5.78311E-05
N
W
E
S

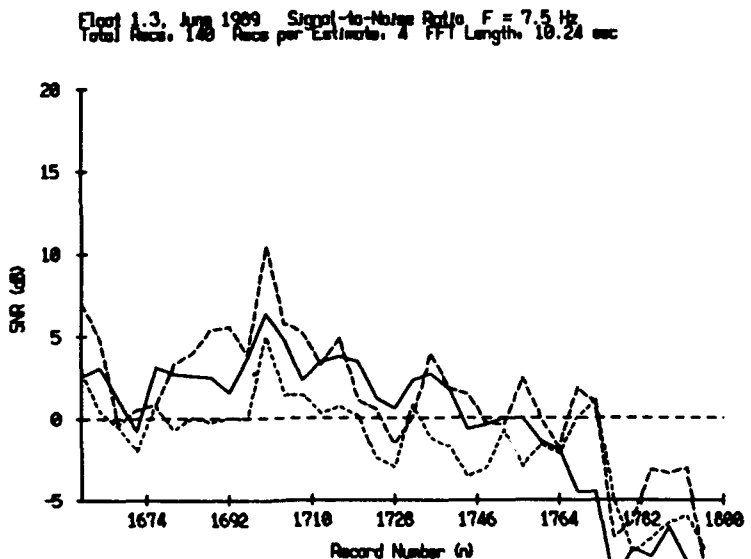
Float 1.3, June 1989 Signal-to-Noise Ratio F = 7.5 Hz
Total Recs. 140 Recs per Estimate. 4 FFT Length. 10.24 sec
SNR (dB)
20
15
10
5
0
-5
1674
1692
1710
1728
1746
1764
1782
1800
Record Number (n)

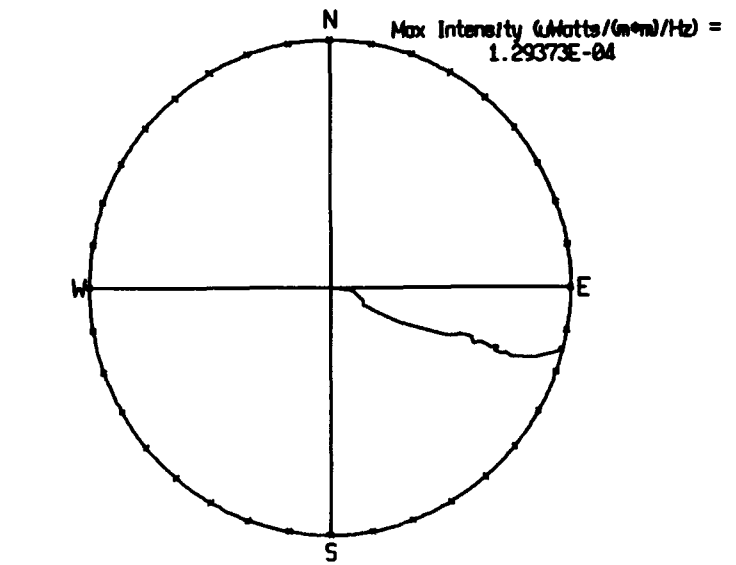
Float 1.3, June 1989 Horizontal Active Intensity F = 7.5 Hz
Start Record: 1660 Total Records: 140 Records per Vector: 4
Max Intensity (uWatts/(m*m)/Hz) =
1.29373E-04
N
W
E
S

Figure VII.8

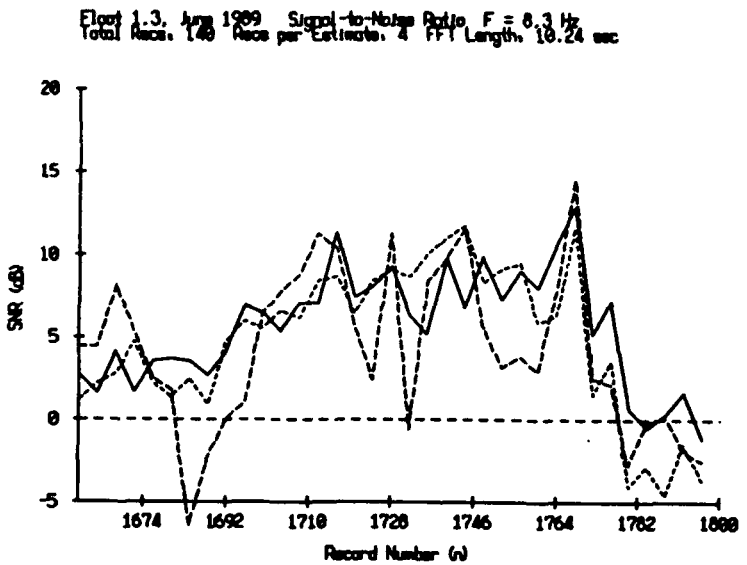
Float 1.3, June 1989 Signal-to-Noise Ratio F = 8.3 Hz
Total Recs: 140 Recs per Estimate: 4 FFT Length: 10.24 sec
SNR (dB)
20
15
10
5
0
-5
1674
1692
1710
1728
1746
1764
1782
1800
Record Number (n)

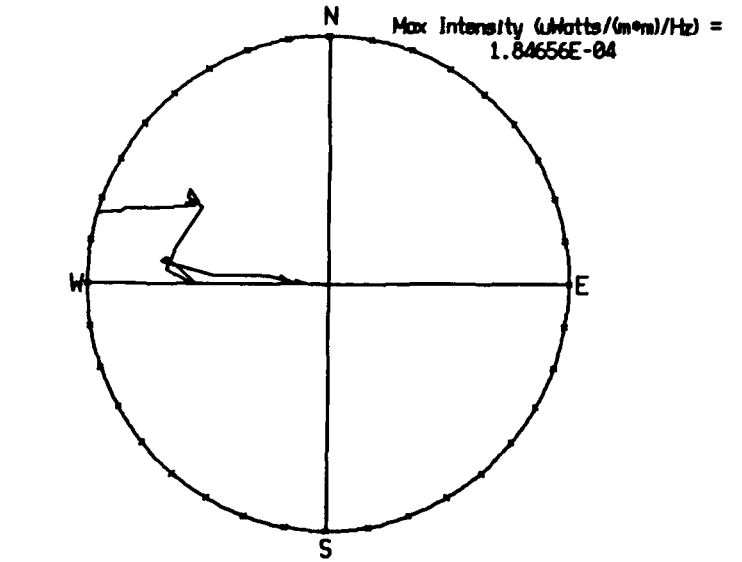
Float 1.3, June 1989 Horizontal Active Intensity F = 8.3 Hz
Start Record: 1660 Total Records: 140 Records per Vector: 4
Max Intensity (uWatts/(m*m)/Hz) =
1.84656E-04
N
W
E
S

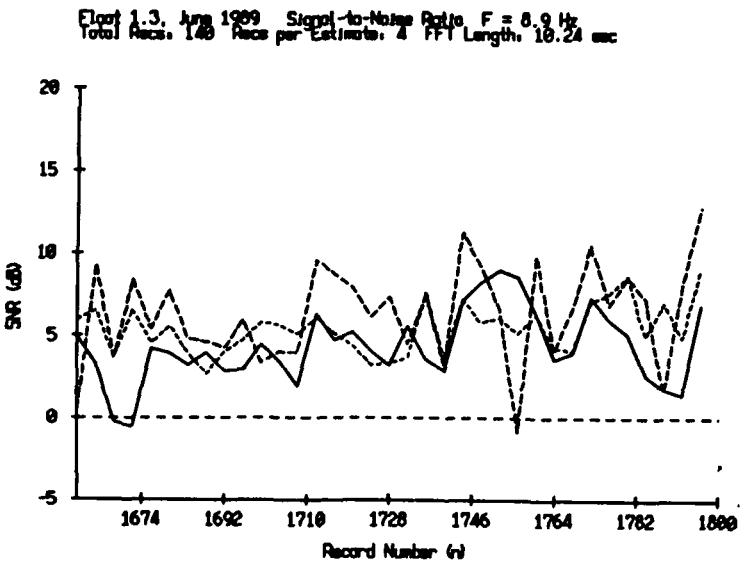
Float 1.3, June 1989 Signal-to-Noise Ratio F = 8.9 Hz
Total Recs: 140 Recs per Estimate: 4 FFT Length: 10.24 sec
SNR (dB)
20
15
10
5
0
-5
1674
1692
1710
1728
1746
1764
1782
1800
Record Number (n)

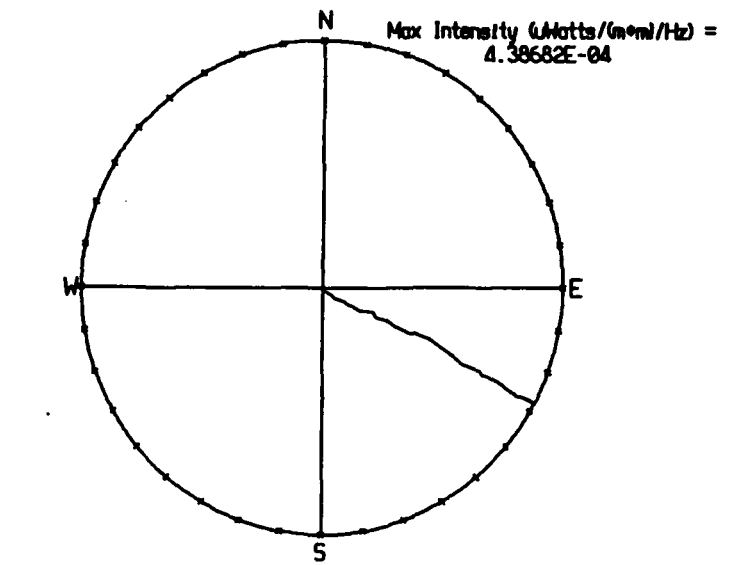
Float 1.3, June 1989 Horizontal Active Intensity F = 8.9 Hz
Start Record: 1660 Total Records: 140 Records per Vector: 4
Max Intensity (uWatts/(m*m)/Hz) =
4.38682E-04
N
W
E
S

Figure VII.9

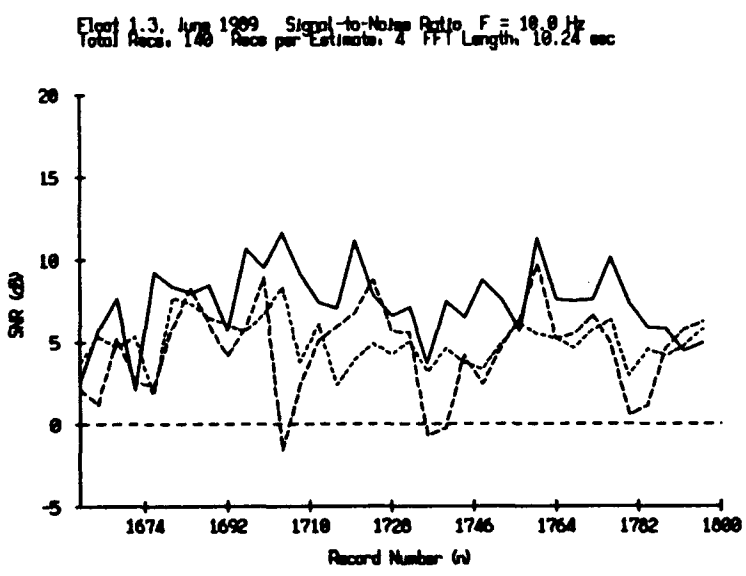

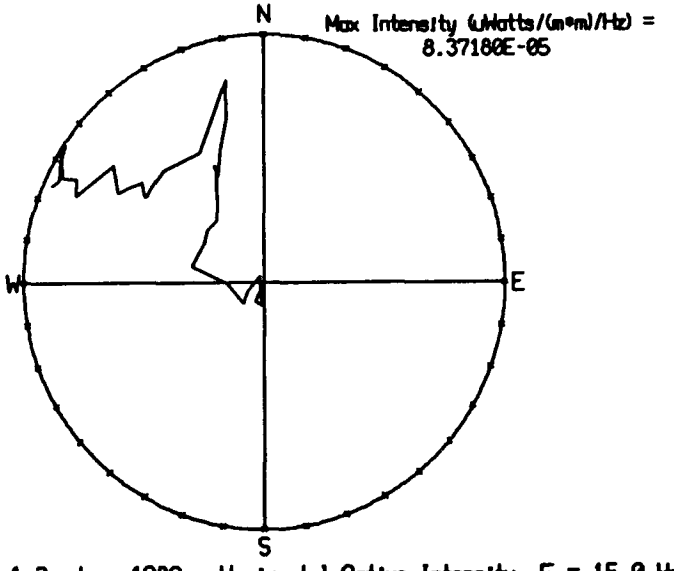

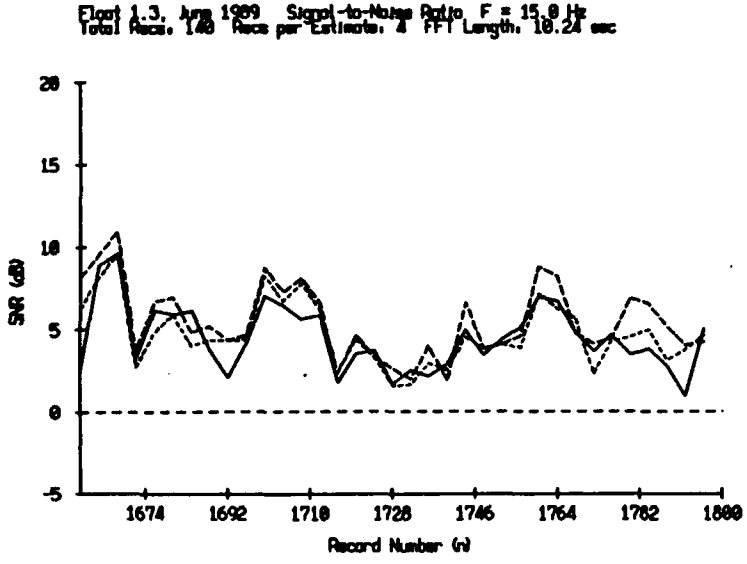

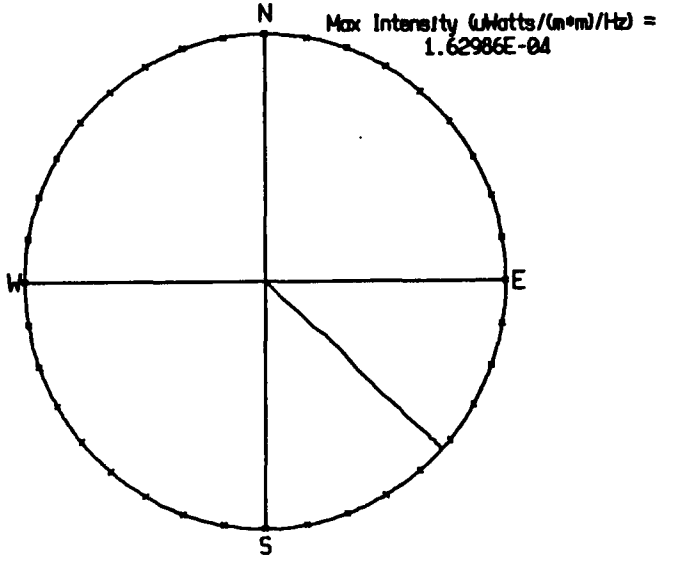

Figure VII.10

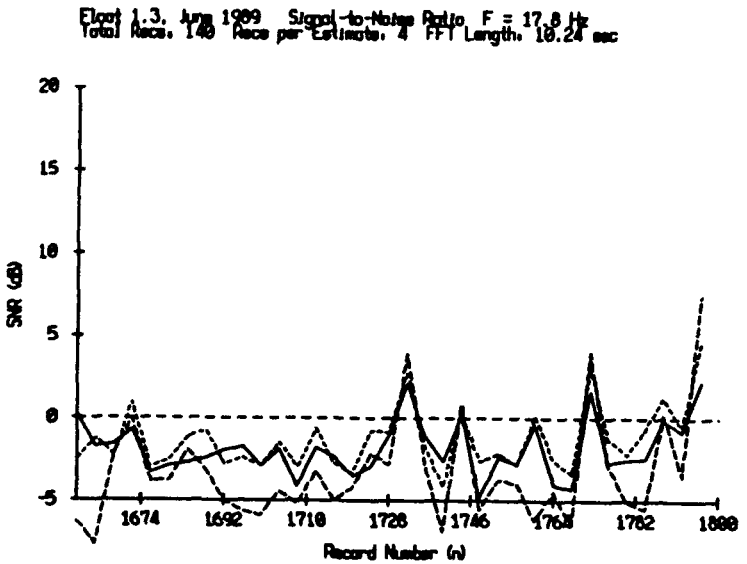

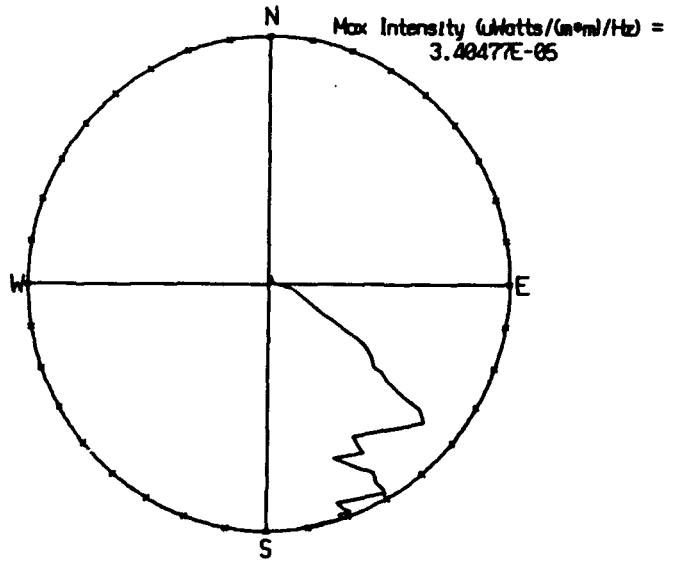

Figure VII.11

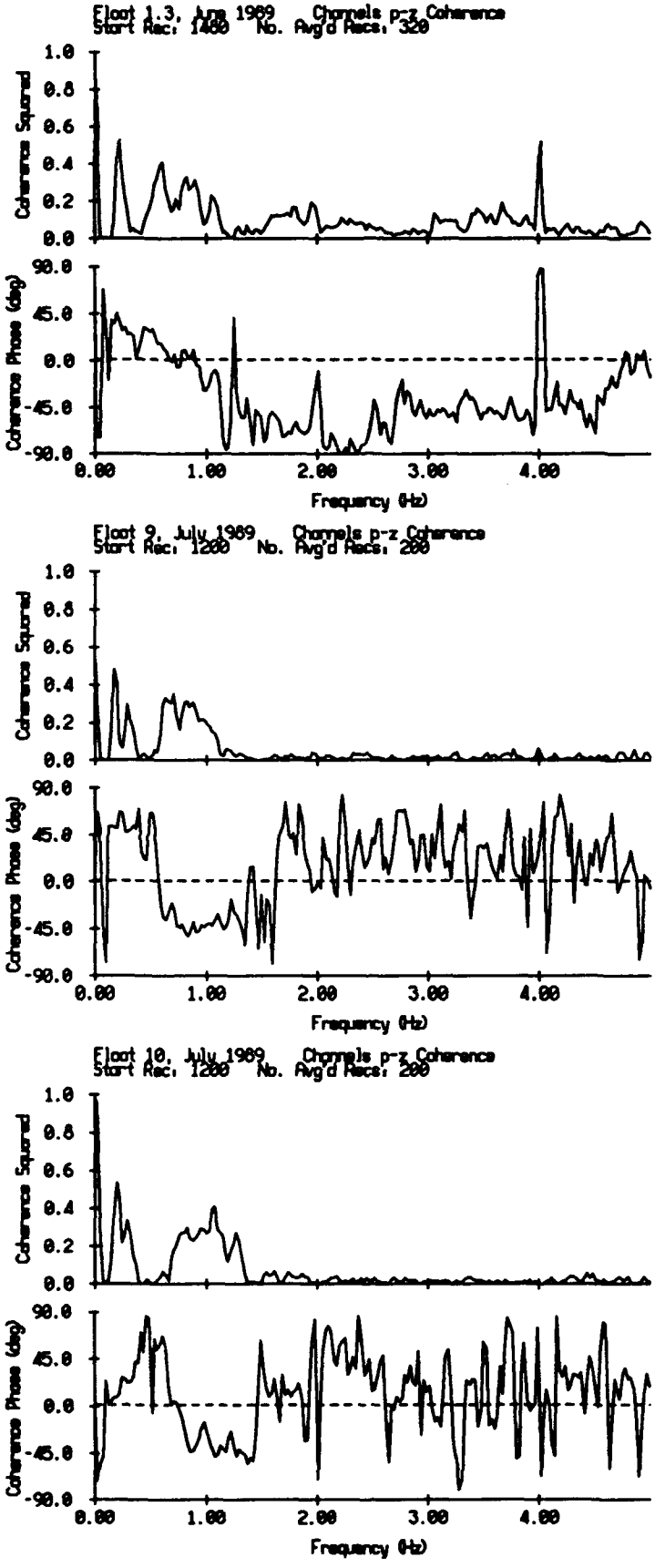

Figure VII.12

BLOCK DIAGRAM OF THE SWALLOW FLOAT INFRASONIC DATA ACQUISITION SYSTEM

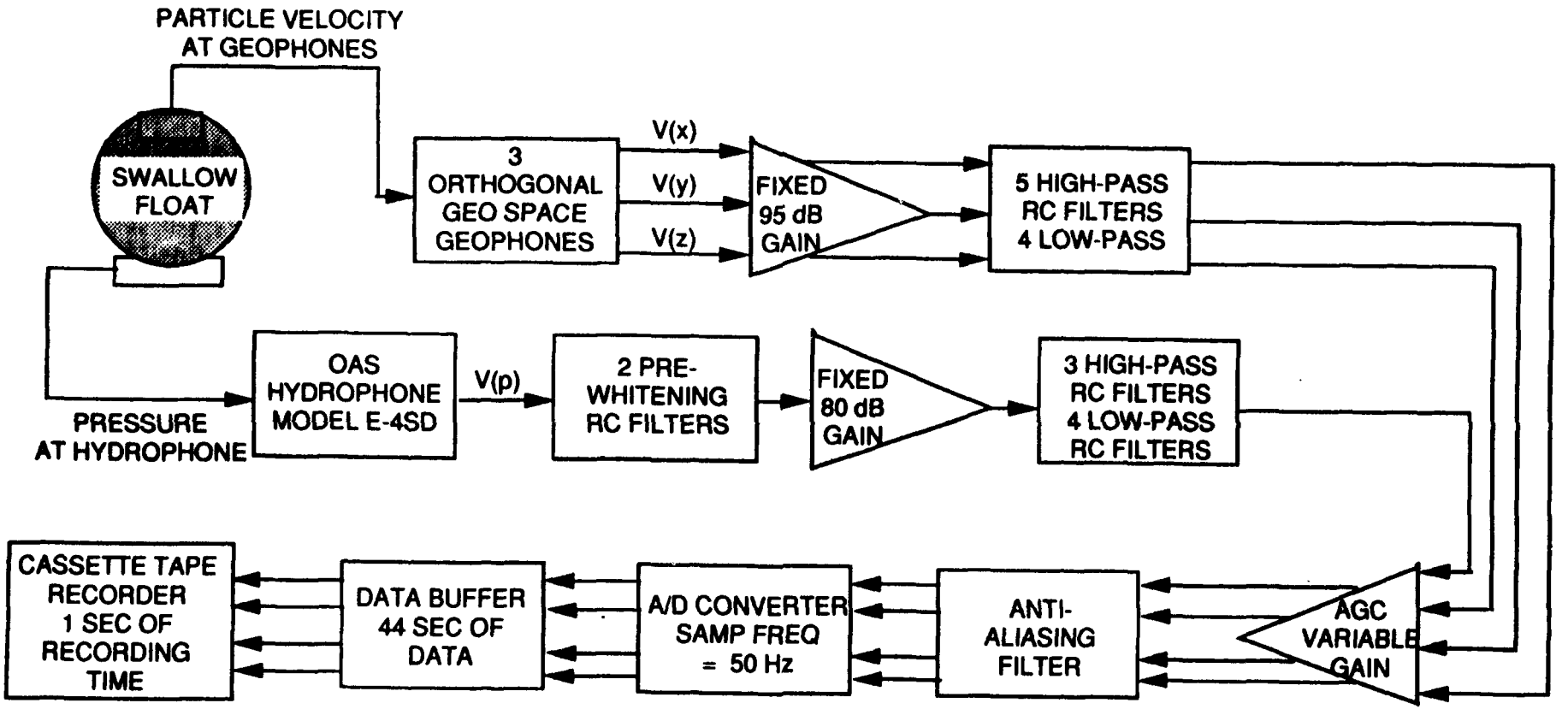

Figure A.1

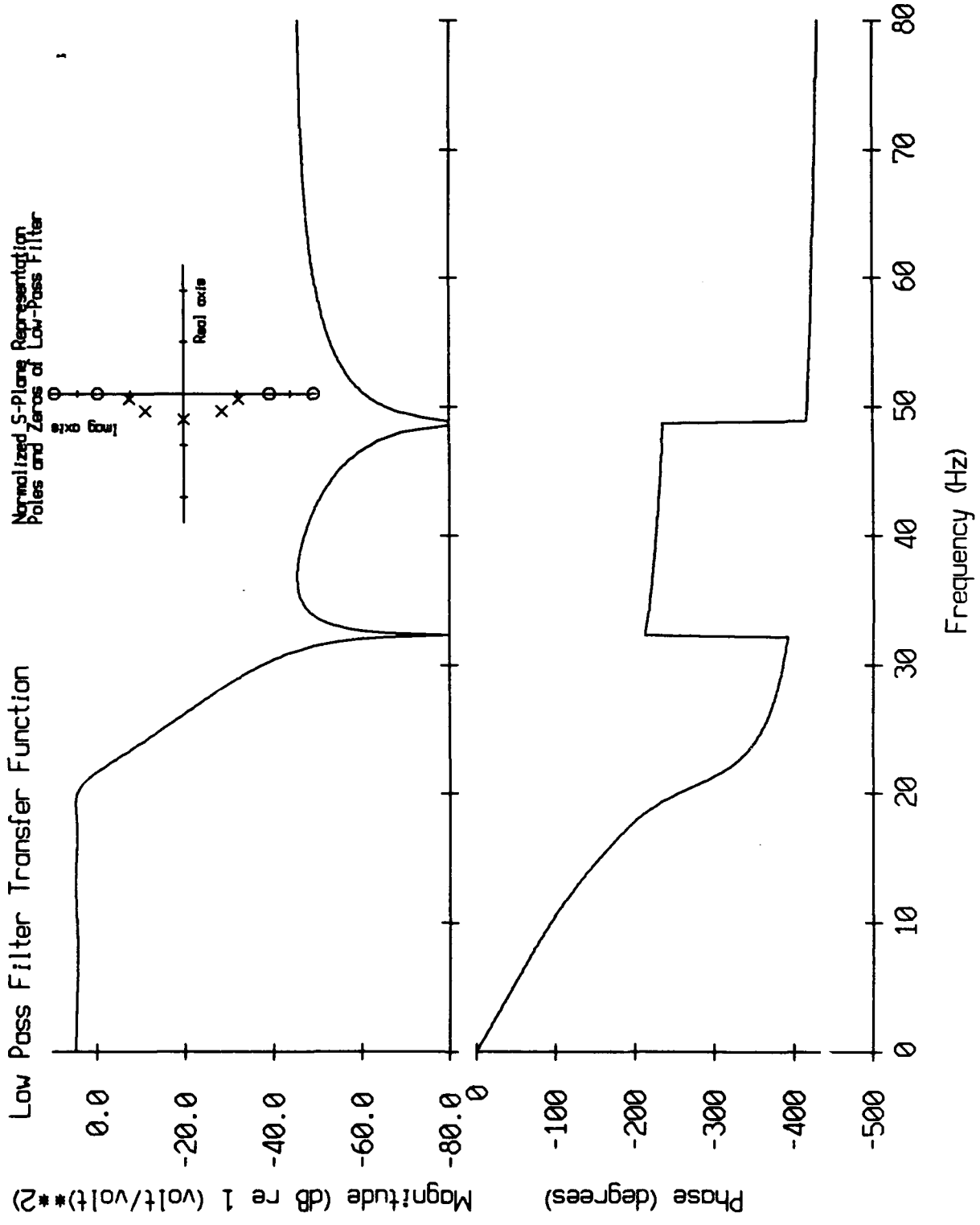
Low Pass Filter Transfer Function
Magnitude (dB re 1 (volt/volt)**2)
0.0
-20.0
-40.0
-60.0
-80.0
Phase (degrees)
0
-100
-200
-300
-400
-500
0
10
20
30
40
50
60
70
80
Frequency (Hz)
Normalized S-Plane Representation
Poles and Zeros of Low-Pass Filter
Real axis
Imag axis

Figure A.2

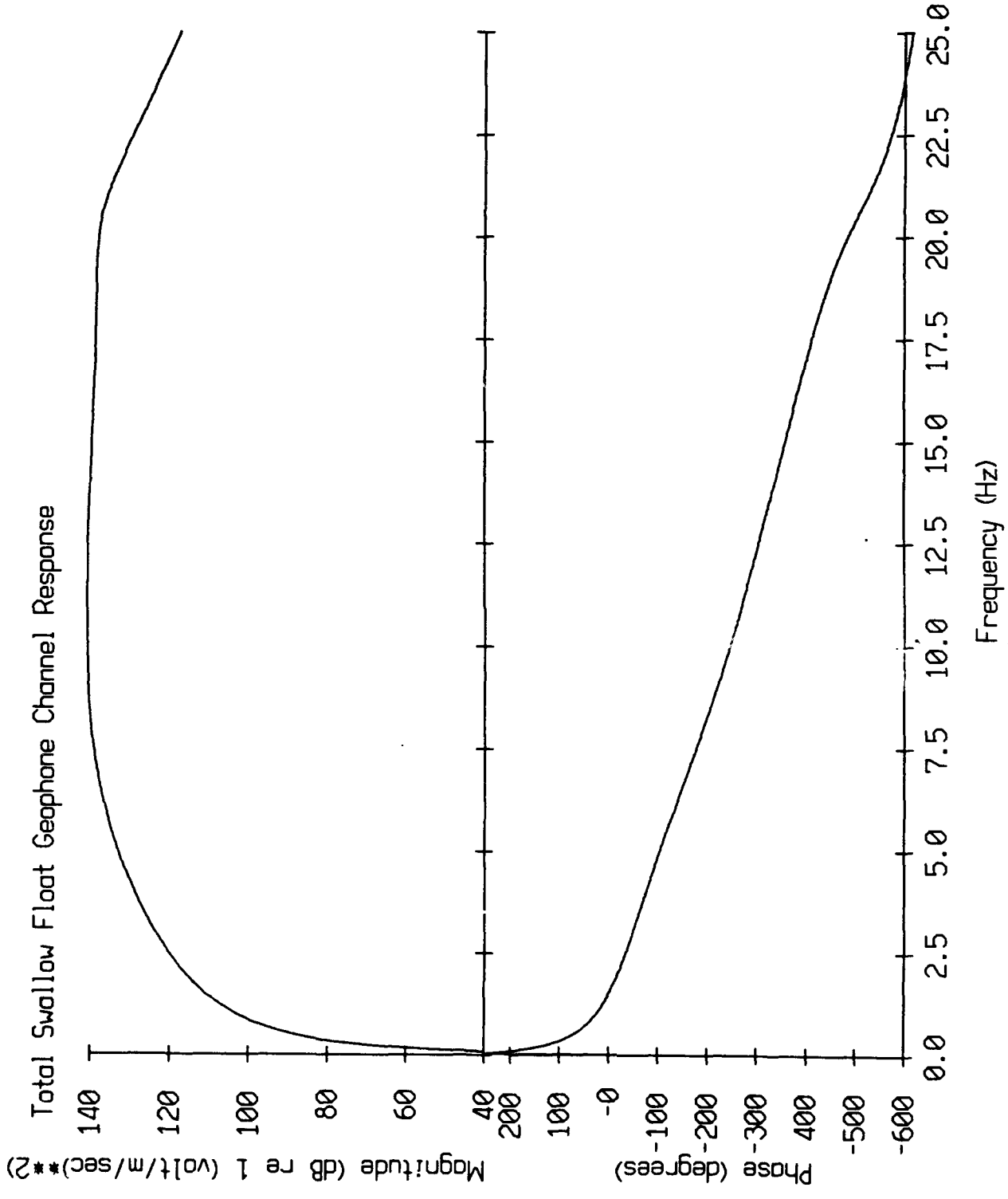
Total Swallow Float Geophone Channel Response
Magnitude (db re 1 (volt/m/sec)**2)
Phase (degrees)
Frequency (Hz)
140
120
100
80
60
40
200
100
-0
-100
-200
-300
400
-500
-600
0.0
2.5
5.0
7.5
10.0
12.5
15.0
17.5
20.0
22.5
25.0

Figure A.3

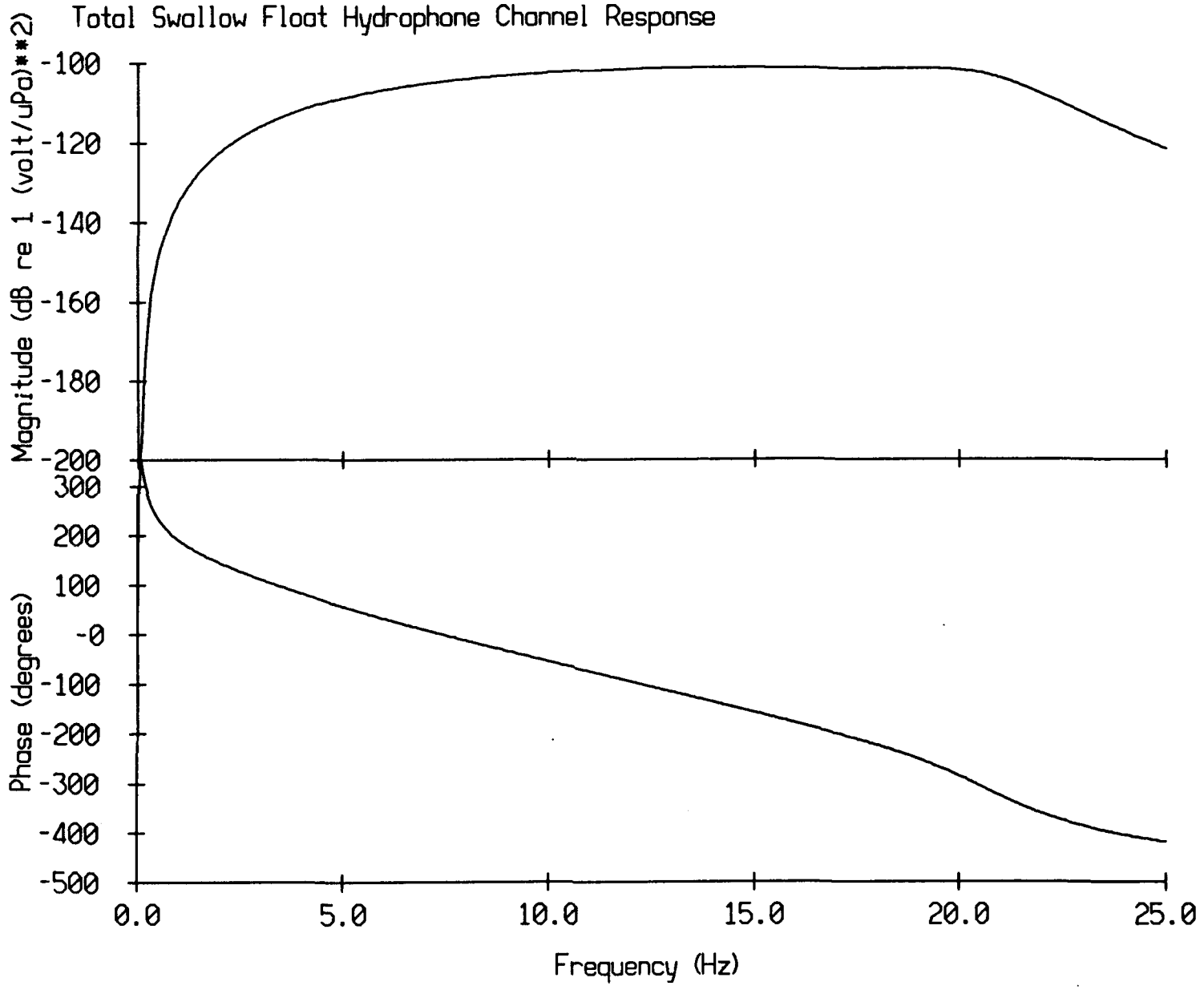
Total Swallow Float Hydrophone Channel Response
Magnitude (dB re 1 (volt/uPa)**2)
-100
-120
-140
-160
-180
-200
Phase (degrees)
300
200
100
-0
-100
-200
-300
-400
-500
0.0
5.0
10.0
15.0
20.0
25.0
Frequency (Hz)

Figure A.4